APPLICATION OF LINEARIZED FLOW THEORY TO AXIAL COMPRESSORS WITH ASYMMETRIC INLET FLOWS

Thesis by

Harvey N. Kreisberg

In Partial Fulfillment of the Requirements

for the Degree of

Mechanical Engineer

California Institute of Technology

Pasadena, California

1961

ACKNOWLEDGMENT

The author wishes to express appreciation for the assistance given by Dr. Frank E. Marble throughout the course of this research.

ABSTRACT

An analytical investigation was undertaken to determine the applicability of a two-dimensional linearized flow theory to axial compressors with severe asymmetric distortions in the approach flow.

Using the assumption of zero axial gap between blade rows, the simplified theory was applied to three compressor configurations: an expanded single stage, a normal single stage and a three-stage configuration. The three-stage configuration was analyzed for two values of the mean flow coefficient and at two radial positions.

The simplified theory was not adequate for describing experimentally determined total pressure profiles in an expanded single stage subjected to strong asymmetric inlet flows. The theory gave good agreement with experimental data for a normal single stage subjected to small asymmetric inlet disturbances. Application of the simplified theory to a three-stage compressor with severe peripheral distortions in the inlet flow showed that good agreement could be obtained between theoretical and experimental total pressure profiles. However, the loss coefficient required to attain this agreement resulted in theoretical predictions for other flow functions which were in error by as much as 50 per cent at the circumferential position corresponding to maximum flow distortion.

The present theory is capable of providing fair qualitative agreement between theory and experiment for axial compressors with severe asymmetric inlet flow distortions. However, this simplified theory does not simulate the flow processes in such compressors accurately enough to provide good quantitative agreement.

TABLE OF CONTENTS

I. INTRODUCTION

Performance analysis of axial flow compressors with severely distorted inlet flows is particularly important in the design of turbojet and turbofan engines. The axial compressor in a turbojet or turbofan engine may be subjected to entrance flow distortions caused by flow separation in the diffuser inlet during certain aerial maneuvers or by irregular ducting on the aircraft which may be necessitated by independent design criteria. It is important, therefore, to have the capability of quantitatively predicting compressor performance under these abnormal conditions.

Compressor inlet flow distortions can be divided into two general types. The distortion may be considered to be axially symmetric and vary in the radial direction only, or it may be considered to extend over a certain segment of the compressor circumference and have no variation in the radial direction. The latter occurs more commonly in aircraft applications and is the type of distortion which is the subject of this investigation.

An experimental investigation of axial compressors with small asymmetric inlet disturbances has been conducted, and a two-dimensional linearized flow theory has been developed to describe this type of flow. A detailed discussion of these experiments and the adequacy of the simplified theory has been published by Robert Katz (1). It was found that the simplified theory correctly described the flow processes which were experimentally determined for small inlet disturbances.

More recently, experiments were performed to determine axial compressor performance with strong peripheral distortions in the approach flow (2). These experiments were conducted by William H. Heiser, using

the same compressor employed in the earlier group of experiments reported in reference 1. As would be expected, a comparison of the experiments using small inlet distortions with those using strong inlet distortions revealed some changes in the flow process. Qualitatively, however, these differences did not seem to be of a gross nature. Similar circumferential displacement of the disturbed region downstream of the various blade rows and attenuation of the inlet disturbance through the three compressor stages were evident in both groups of experiments.

The possibility exists, therefore, that the simplified flow theory might be adequate to qualitatively describe compressor flows with strong peripheral disturbances. An estimate of the degree of accuracy obtainable with the simplified theory would give some indication as to the nature of the analytical refinements required to more accurately describe compressor flow with strong inlet distortions. The purpose of the present research is to establish the applicability of the linearized flow theory when strong flow distortions are present.

For completeness, a brief discussion of the two-dimensional linearized flow theory will be presented. Three separate compressor configurations are considered: an expanded single stage configuration, a normal single stage configuration and a three-stage configuration. In each case, certain flow parameters are calculated, using the simplified flow theory, and compared with the available experimental data. The test data for the expanded single stage and the three-stage configurations were obtained for strongly distorted inlet flows. The experimental data for the normal single stage configuration was obtained for an inlet flow with a small peripheral distortion.

II. THEORETICAL ANALYSIS OF COMPRESSOR WITH ASYMMETRIC INLET DISTURBANCE

2.1 Theoretical Model

The theory will be developed by considering a two-dimensional, isolated cascade located at the origin of the x' axis and extending from $-\pi r$ to πr along the y' axis. The flow field is confined to the infinite strip of width $2\pi r$, (figure 1). This two-dimensional flow field approximates the flow through an isolated cascade in a cylindrical duct of very high hub to tip ratio and infinite length. The x' coordinate is along the axis of the duct and the y' coordinate designates the circumferential direction. The asymmetric inlet distortion is assumed to be a small disturbance superimposed upon the known mean flow. The flow is assumed to be incompressible and inviscid.

2.2 Basic Equations

With these assumptions, the basic equations describing the flow are

$$\frac{\partial u'}{\partial x'} + \frac{\partial v'}{\partial y'} = 0 \tag{1}$$

$$u' \frac{\partial u'}{\partial x'} + v' \frac{\partial u'}{\partial y'} = - \frac{\partial}{\partial x'} \frac{p'}{\rho} \tag{2}$$

$$u' \frac{\partial v'}{\partial x'} + v' \frac{\partial v'}{\partial y'} = - \frac{\partial}{\partial y'} \frac{p'}{\rho} \tag{3}$$

The velocity and pressure terms may be written as

$$u' = U + u \tag{4}$$

$$v' = V + v \tag{5}$$

$$p' = P + p \tag{6}$$

where U, V and P are the mean components of u', v' and p' and u, v and p are the perturbation components. The quantities U, V and P define the known mean flow and have constant values upstream and downstream of the blade row. The variable quantities u, v and p define the perturbation

to the mean flow and have zero average values.

Substituting equations 4, 5 and 6 into equations 1, 2 and 3, linearizing the resultant equations and rearranging the terms, it can be shown that the following expressions result:

$$\frac{\partial}{\partial y'}(Uv - Vu) = \frac{\partial}{\partial x'}\frac{p}{\rho} \tag{7}$$

$$\frac{\partial}{\partial x'}(Uv - Vu) = -\frac{\partial}{\partial y'}\frac{p}{\rho} \tag{8}$$

$$\left(U\frac{\partial}{\partial x'} + V\frac{\partial}{\partial y'}\right)\left(\frac{p}{\rho} + Uu + Vv\right) = 0 \tag{9}$$

Introducing the definitions

$$\Theta = Uv - Vu \tag{10}$$

$$\mathcal{P} = \frac{p}{\rho} \tag{11}$$

$$H = \frac{p}{\rho} + Uu + Vv \tag{12}$$

$$x = \frac{x'}{r} \tag{13}$$

$$y = \frac{y'}{r} \tag{14}$$

equations 7, 8 and 9 can be written

$$\frac{\partial\Theta}{\partial y} = \frac{\partial\mathcal{P}}{\partial x} \tag{15}$$

$$\frac{\partial\Theta}{\partial x} = -\frac{\partial\mathcal{P}}{\partial y} \tag{16}$$

$$\left(U\frac{\partial}{\partial x} + V\frac{\partial}{\partial y}\right)H = 0 \tag{17}$$

The quantity H is proportional to the perturbation total pressure, $\mathcal{P}$ is proportional to the perturbation static pressure and Θ is proportional to the perturbed flow angle. It will be noted that equations 15 and 16 are the Couchy-Riemann conditions. Therefore, $\mathcal{P}$ and Θ are conjugate harmonic functions and must satisfy the two-dimensional Laplace equation.

2.3 General Solution

Equations 15, 16 and 17 describe the flow upstream and downstream of the cascade. The cascade, at the origin of the x' axis, divides the flow into two regions of different mean flows. Let subscript 1 refer to conditions upstream of the cascade and subscript 2 to conditions downstream of the cascade. The boundary conditions are

$$\lim_{x \to -\infty} \rho_1 (x,y) = \lim_{x \to -\infty} \Theta_1 (x,y) = 0 \tag{18}$$

$$\lim_{x \to \infty} \rho_2 (x,y) = \lim_{x \to \infty} \Theta_2 (x,y) = 0 \tag{19}$$

$$f_n (x,y) = f_n (x, y + 2\pi) \tag{20}$$

In the construction of the general solutions for H, ρ and Θ, it is assumed that H_1 is known and that it can be represented by a Fourier series. Therefore, assume that H_1 is given by

$$H_1 = \sum_{n=1}^{\infty} a_{1_n} \cos n\left(y - x \frac{V_1}{U}\right) + b_{1_n} \sin n\left(y - x \frac{V_1}{U}\right) \tag{21}$$

It can be determined that H is a function of $y - x \frac{V_1}{U}$ from equation 17. A solution for Θ_1 which satisfies the Laplace equation and the boundary condition is

$$\Theta_1 = \sum_{n=1}^{\infty} (c_{1_n} \cos ny + d_{1_n} \sin ny) e^{nx} \tag{22}$$

Having assumed a form of solution for Θ_1, it then follows from the Couchy Riemann conditions that

$$\rho_1 = \sum_{n=1}^{\infty} (d_{1_n} \cos ny - c_{1_n} \sin ny) e^{nx} \tag{23}$$

Similarly the functions downstream of the cascade are

$$H_2 = \sum_{n=1}^{\infty} a_{2_n} \cos n\left(y - x\frac{V_2}{U}\right) + b_{2_n} \sin n\left(y - x\frac{V_2}{U}\right) \tag{24}$$

$$\Theta_2 = \sum_{n=1}^{\infty} (c_{2_n} \cos ny + d_{2_n} \sin ny)e^{-nx} \tag{25}$$

$$\rho_2 = \sum_{n=1}^{\infty} (-d_{2_n} \cos ny + c_{2_n} \sin ny)e^{-nx} \tag{26}$$

Equations 21 through 26 are the general solutions for the functions H_1, Θ_1, ρ_1, H_2, Θ_2 and ρ_2.

2.4 Matching Conditions

Having constructed the general form of the solution for the functions upstream and downstream of the blade row, it is necessary to construct a set of matching conditions across the blade row in order to relate the downstream functions to the upstream functions.

2.4.1 Rotor Blade Row

Three matching conditions across the blade row can be established by making use of the continuity equation, a relation for the downstream flow angle in terms of the upstream flow angle and the Bernoulli equation.

The continuity equation requires that

$$u_1 (0,y) = u_2 (0,y) \tag{27}$$

It will be assumed that the downstream flow angle is known as a function of the upstream angle from cascade tests. Then a curve such as the one shown in figure 3 would be available and the slope of this curve,

δ_r, could be established at the mean operating point. Then, for small perturbations

$$\Delta\beta_2 = \delta_r \Delta\beta_1 \tag{28}$$

The Bernoulli equation for the flow through a rotor is

$$p_1' + \frac{1}{2}\rho\left[u_1'^2 + (v_1' - \omega r)^2\right] = p_2' + \frac{1}{2}\rho\left[u_2'^2 + (v_2' - \omega r)^2\right] + \frac{1}{2}\rho\, u_1'^2 L_r (\tan\beta_1) \tag{29}$$

The L_r is a loss coefficient referred to the upstream axial velocity and is a function of the tangent of the relative inlet angle. For the purposes of this investigation, a linear loss representation, shown schematically in figure 4, was used. The loss coefficient at the perturbed operating point can then be approximated by the expression

$$L_r\left[\tan(\beta_1 + \Delta\beta_1)\right] = L_r\left[\tan\beta_1\right] + \Delta\beta_1 \sec^2\beta_1 L_r'\left[\tan\beta_1\right] \tag{30}$$

where $L_r\left[\tan\beta_1\right]$ is the loss coefficient at the mean operating point and $L_r'\left[\tan\beta_1\right]$ is the slope of the curve at the mean operating point.

The Bernoulli equation for the mean flow is

$$P_1 + \frac{1}{2}\rho\left[U^2 + (V_1 - \omega r)^2\right] = P_2 + \frac{1}{2}\rho\left[U^2 + (V_2 - \omega r)^2\right] + \frac{1}{2}\rho\, U^2 L_r \tag{31}$$

Substituting equations 4, 5, 6, and 30 into equation 29 and subtracting equation 31 from the result, yields the Bernoulli equation for the perturbed flow

$$\frac{p_1}{\rho} + Uu_1 + (V_1 - \omega r)\, v_1 = \frac{p_2}{\rho} + Uu_2 + (V_2 - \omega r)\, v_2 + UL_r u_1 + U^2 \sec^2 \beta_1 \frac{L'_r}{2} \Delta\beta_1 \qquad (32)$$

which is the third matching condition. The three matching conditions can be written in terms of the variables H, $\mathcal{P}$ and Θ as follows:

$$H_2 + \left(\frac{\cos \theta_1}{\cos \theta_2}\right)^2 \tan \theta_1\, \Theta_1 + \left(\frac{\cos \theta_1}{\cos \theta_2}\right)^2 \mathcal{P}_1 - \tan \theta_2\, \Theta_2 - \mathcal{P}_2 = \left(\frac{\cos \theta_1}{\cos \theta_2}\right)^2 H_1 \qquad (33)$$

$$\left[\delta_r \frac{\cos^2 \beta_1}{\cos^2 \beta_2} + \frac{\cos^2 \theta_1 \tan \theta_1}{\varphi}\left(1 - \delta_r \frac{\cos^2 \beta_1}{\cos^2 \beta_2}\right)\right]\Theta_1 + \left[\frac{\cos^2 \theta_1}{\varphi}\left(1 - \delta_r \frac{\cos^2 \beta_1}{\cos^2 \beta_2}\right)\right]\mathcal{P}_1 - \Theta_2 = \left[\frac{\cos \theta_1}{\varphi}\left(1 - \delta_r \frac{\cos^2 \beta_1}{\cos^2 \beta_2}\right)\right] H_1 \qquad (34)$$

$$H_2 + \left[\frac{1}{\varphi} - \frac{L'_r}{2} + \frac{\cos^2 \theta_1 \tan \theta_1}{\varphi}\left(\tan \theta_2 - \tan \theta_1 + \frac{L'_r}{2} - \varphi L_r\right)\right]\Theta_1 + \left[\frac{\cos^2 \theta_1}{\varphi}\left(\tan \theta_2 - \tan \theta_1 + \frac{L'_r}{2} - \varphi L_r\right)\right]\mathcal{P}_1 - \frac{1}{\varphi}\Theta_2 = \left[1 + \frac{\cos^2 \theta_1}{\varphi}\left(\tan \theta_2 - \tan \theta_1 + \frac{L'_r}{2} - \varphi L_r\right)\right] H_1 \qquad (35)$$

Assuming that H_1 is known, we have three equations and five unknowns. At this point we can make use of the Hilbert transform which shall be defined by

$$f_n^*(x,y) = \frac{1}{2\pi} \int_{-\pi}^{\pi} f_n(x,\eta) \cot\left(\frac{y-\eta}{2}\right) d\eta \tag{36}$$

where $f_n^*(x,y)$ indicates the Hilbert transform of $f_n(x,y)$. It can be shown that

$$\rho_1^*(x,y) = \Theta_1(x,y) \tag{37}$$

$$\Theta_1^*(x,y) = -\rho_1(x,y) \tag{38}$$

$$\rho_2^*(x,y) = -\Theta_2(x,y) \tag{39}$$

$$\Theta_2^*(x,y) = \rho_2(x,y) \tag{40}$$

$$\left[H_1(x,y)\right]^* = H_1^*(x,y) \tag{41}$$

$$\left[H_2(x,y)\right]^* = H_2^*(x,y) \tag{42}$$

Substituting equations 37 through 42 into equations 33 through 35, the following relationships result:

$$H_2^* + \left(\frac{\cos\theta_1}{\cos\theta_2}\right)^2 \Theta_1 - \left(\frac{\cos\theta_1}{\cos\theta_2}\right)^2 \tan\theta_1 \rho_1 + \Theta_2 - \tan\theta_2 \rho_2 = \left(\frac{\cos\theta_1}{\cos\theta_2}\right)^2 H_1^* \tag{43}$$

$$\left[\frac{\cos^2\theta_1}{\varphi}\left(1 - \delta_r \frac{\cos^2\beta_1}{\cos^2\beta_2}\right)\right]\Theta_1 - \left[\delta_r \frac{\cos^2\beta_1}{\cos^2\beta_2} + \frac{\cos^2\theta_1 \tan\theta_1}{\varphi}\left(1 - \delta_r \frac{\cos^2\beta_1}{\cos^2\beta_2}\right)\right]\rho_1 - \rho_2 = \left[\frac{\cos^2\theta_1}{\varphi}\left(1 - \delta_r \frac{\cos^2\beta_1}{\cos^2\beta_2}\right)\right] H_1^* \tag{44}$$

$$H_2^* + \left[\frac{\cos^2\theta_1}{\varphi}\left(\tan\theta_2 - \tan\theta_1 + \frac{L_r'}{2} - \varphi L_r\right)\right]\Theta_1$$

$$- \left[\frac{1}{\varphi} - \frac{L_r'}{2} + \frac{\cos^2\theta_1 \tan\theta_1}{\varphi}\left(\tan\theta_2 - \tan\theta_1 + \frac{L_r'}{2} - \varphi L_r\right)\right]\mathcal{P}_1 - \frac{1}{\varphi}\mathcal{P}_2$$

$$= \left[1 + \frac{\cos^2\theta_1}{\varphi}\left(\tan\theta_2 - \tan\theta_1 + \frac{L_r'}{2} - \varphi L_r\right)\right] H_1^* \qquad (45)$$

We now have six unknowns, $\Theta_1, \mathcal{P}_1, \Theta_2, \mathcal{P}_2, H_2$ and H_2^*, and six equations. H_1 and H_1^* are known.

2.4.2 Stationary Blade Row

The matching conditions across a stationary blade row are obtained by an analysis completely analogous to that given in the preceding section for a rotating blade row. In terms of the variables Θ, $\mathcal{P}$ and H, the matching conditions are

$$H_2 + \left(\frac{\cos\theta_1}{\cos\theta_2}\right)^2 \tan\theta_1\,\Theta_1 + \left(\frac{\cos\theta_1}{\cos\theta_2}\right)^2 \mathcal{P}_1 - \tan\theta_2\,\Theta_2 - \mathcal{P}_2$$

$$= \left(\frac{\cos\theta_1}{\cos\theta_2}\right)^2 H_1 \qquad (46)$$

$$\delta_s \left(\frac{\cos\theta_1}{\cos\theta_2}\right)^2 \Theta_1 - \Theta_2 = 0 \qquad (47)$$

$$H_2 + \left[\frac{L_s'}{2} - \cos^2\theta_1 \tan\theta_1 L_s\right]\Theta_1 - \left[\cos^2\theta_1 L_s\right]\mathcal{P}_1$$

$$= \left[1 - \cos^2\theta_1 L_s\right] H_1 \qquad (48)$$

$$H_2^* + \left(\frac{\cos\theta_1}{\cos\theta_2}\right)^2 \Theta_1 - \left(\frac{\cos\theta_1}{\cos\theta_2}\right)^2 \tan\theta_1 \mathcal{P}_1 + \Theta_2 - \tan\theta_2 \mathcal{P}_2$$

$$= \left(\frac{\cos\theta_1}{\cos\theta_2}\right)^2 H_1^* \quad (49)$$

$$- \delta_s \left(\frac{\cos\theta_1}{\cos\theta_2}\right)^2 \mathcal{P}_1 - \mathcal{P}_2 = 0 \quad (50)$$

$$H_2^* - \left[\cos^2\theta_1 L_s\right] \Theta_1 - \left[\frac{L_s'}{2} - \cos^2\theta_1 \tan\theta_1 L_s\right] \mathcal{P}_1$$

$$= \left[1 - \cos^2\theta_1 L_s\right] H_1^* \quad (51)$$

2.5 Zero Axial Gap Approximation

It will prove convenient, in the analysis that follows, to write the matching equations in matrix form. The following notation will be used:

Subscript	Axial Position
0	directly upstream of inlet vanes
1	directly downstream of inlet vanes
2	directly upstream of rotor
3	directly downstream of rotor
4	directly upstream of stator
5	directly downstream of stator

In each case, the matching equations have been solved in terms of H and H* upstream of the respective blade rows. In matrix form, the matching equations for the three blade rows become:

Inlet Vanes

$$\begin{bmatrix} 1 & 0 & \lambda_7 & -\lambda_6 & 0 & 0 \\ 0 & 1 & -\lambda_6 & -\lambda_7 & 0 & 0 \\ 1 & 0 & \lambda_3 & \lambda_1 & -\lambda_4 & -1 \\ 0 & 1 & \lambda_1 & -\lambda_3 & 1 & -\lambda_4 \\ 0 & 0 & \lambda_5 & 0 & -1 & 0 \\ 0 & 0 & 0 & -\lambda_5 & 0 & -1 \end{bmatrix} \begin{bmatrix} H_1 \\ H_1^* \\ \Theta_o \\ \rho_o \\ \Theta_1 \\ \rho_1 \end{bmatrix} = \begin{bmatrix} (1-\lambda_6)\, H_o \\ (1-\lambda_6)\, H_o^* \\ \lambda_1 H_o \\ \lambda_1 H_o^* \\ 0 \\ 0 \end{bmatrix}$$

Rotor

$$\begin{bmatrix} 1 & 0 & \mu_6 & \mu_7 & -\mu_8 & 0 \\ 0 & 1 & \mu_7 & -\mu_6 & 0 & -\mu_8 \\ 1 & 0 & \mu_1 & \mu_2 & -\mu_3 & -1 \\ 0 & 1 & \mu_2 & -\mu_1 & 1 & -\mu_3 \\ 0 & 0 & \mu_4 & \mu_5 & -1 & 0 \\ 0 & 0 & \mu_5 & -\mu_4 & 0 & -1 \end{bmatrix} \begin{bmatrix} H_3 \\ H_3^* \\ \Theta_2 \\ \rho_2 \\ \Theta_3 \\ \rho_3 \end{bmatrix} = \begin{bmatrix} (1+\mu_7)\, H_2 \\ (1+\mu_7)\, H_2^* \\ \mu_2 H_2 \\ \mu_2 H_2^* \\ \mu_5 H_2 \\ \mu_5 H_2^* \end{bmatrix}$$

Stator

$$\begin{bmatrix} 1 & 0 & \nu_7 & -\nu_6 & 0 & 0 \\ 0 & 1 & -\nu_6 & -\nu_7 & 0 & 0 \\ 1 & 0 & \nu_3 & \nu_1 & -\nu_4 & -1 \\ 0 & 1 & \nu_1 & -\nu_3 & 1 & -\nu_4 \\ 0 & 0 & \nu_5 & 0 & -1 & 0 \\ 0 & 0 & 0 & -\nu_5 & 0 & -1 \end{bmatrix} \begin{bmatrix} H_5 \\ H_5^* \\ \Theta_4 \\ \rho_4 \\ \Theta_5 \\ \rho_5 \end{bmatrix} = \begin{bmatrix} (1-\nu_6)\, H_4 \\ (1-\nu_6)\, H_4^* \\ \nu_1 H_4 \\ \nu_1 H_4^* \\ 0 \\ 0 \end{bmatrix}$$

The constants in the preceding matrices are defined as follows:

$$\lambda_1 = \left(\frac{\cos\theta_o}{\cos\theta_1}\right)^2 \qquad \lambda_4 = \tan\theta_1$$

$$\lambda_2 = \tan\theta_o \qquad \lambda_5 = \delta_v\lambda_1$$

$$\lambda_3 = \lambda_1\lambda_2 \qquad \lambda_6 = \cos^2\theta_o\, L_v$$

$$\lambda_7 = \frac{L'_v}{2} - \lambda_2\lambda_6$$

$$\mu_1 = \left(\frac{\cos\theta_2}{\cos\theta_3}\right)^2 \tan\theta_2$$

$$\mu_2 = \left(\frac{\cos\theta_2}{\cos\theta_3}\right)^2$$

$$\mu_3 = \tan\theta_3$$

$$\mu_4 = \delta_r \frac{\cos^2\beta_2}{\cos^2\beta_3} + \frac{\cos^2\theta_2\tan\theta_2}{\varphi}\left(1 - \delta_r\frac{\cos^2\beta_2}{\cos^2\beta_3}\right)$$

$$\mu_5 = \frac{\cos^2\theta_2}{\varphi}\left(1 - \delta_r\frac{\cos^2\beta_2}{\cos^2\beta_3}\right)$$

$$\mu_6 = \frac{1}{\varphi} - \frac{L'_r}{2} + \frac{\cos^2\theta_2\tan\theta_2}{\varphi}\left(\tan\theta_3 - \tan\theta_2 + \frac{L'_r}{2} - \varphi L_r\right)$$

$$\mu_7 = \frac{\cos^2\theta_2}{\varphi}\left(\tan\theta_3 - \tan\theta_2 + \frac{L'_r}{2} - \varphi L_r\right)$$

$$\mu_8 = \frac{1}{\varphi}$$

$$\nu_1 = \left(\frac{\cos\theta_4}{\cos\theta_5}\right)^2 \qquad \nu_3 = \nu_1\nu_2$$

$$\nu_2 = \tan\theta_4 \qquad \nu_4 = \tan\theta_5$$

$$\nu_5 = \delta_s \, \nu_1 \qquad\qquad \nu_6 = \cos^2 \theta_4 \, L_s$$

$$\nu_7 = \frac{L'_s}{2} - \nu_2 \nu_6$$

Simplifying the coefficient matrices and finding the inverses we have the following:

Inlet Vanes

$$\begin{bmatrix} H_1 \\ H_1^* \\ \Theta_o \\ \rho_o \\ \Theta_1 \\ \rho_1 \end{bmatrix} = \begin{bmatrix} 1 & 0 & \lambda_{11} & -\lambda_{12} & 0 & 0 \\ 0 & 1 & \lambda_{12} & \lambda_{11} & 0 & 0 \\ 0 & 0 & \lambda_{13} & \lambda_{14} & 0 & 0 \\ 0 & 0 & \lambda_{14} & -\lambda_{13} & 0 & 0 \\ 0 & 0 & \lambda_{15} & -\lambda_{16} & 1 & 0 \\ 0 & 0 & \lambda_{16} & \lambda_{15} & 0 & 1 \end{bmatrix} \begin{bmatrix} (1-\lambda_6) H_o \\ (1-\lambda_6) H_o^* \\ -\lambda_{10} H_o \\ -\lambda_{10} H_o^* \\ 0 \\ 0 \end{bmatrix}$$

where

$$\lambda_8 = \lambda_3 - \lambda_7 - \lambda_4 \lambda_5$$

$$\lambda_9 = \lambda_1 + \lambda_5 + \lambda_6$$

$$\lambda_{10} = 1 - \lambda_1 - \lambda_6$$

$$\lambda_{11} = (\lambda_6 \lambda_9 - \lambda_7 \lambda_8) / (\lambda_8^2 + \lambda_9^2)$$

$$\lambda_{12} = (\lambda_6 \lambda_8 + \lambda_7 \lambda_9) / (\lambda_8^2 + \lambda_9^2)$$

$$\lambda_{13} = \lambda_8 / (\lambda_8^2 + \lambda_9^2)$$

$$\lambda_{14} = \lambda_9 / (\lambda_8^2 + \lambda_9^2)$$

$$\lambda_{15} = \lambda_5 \lambda_8 / (\lambda_8^2 + \lambda_9^2)$$

$$\lambda_{16} = -\lambda_5 \lambda_9 / (\lambda_8^2 + \lambda_9^2)$$

Rotor

$$\begin{bmatrix} H_3 \\ H_3^* \\ \Theta_2 \\ P_2 \\ \Theta_3 \\ P_3 \end{bmatrix} = \begin{bmatrix} 1 & 0 & \mu_{14} & -\mu_{15} & 0 & 0 \\ 0 & 1 & \mu_{15} & \mu_{14} & 0 & 0 \\ 0 & 0 & \mu_{16} & \mu_{17} & 0 & 0 \\ 0 & 0 & \mu_{17} & -\mu_{16} & 0 & 0 \\ 0 & 0 & \mu_{18} & -\mu_{19} & 1 & 0 \\ 0 & 0 & \mu_{19} & \mu_{18} & 0 & 1 \end{bmatrix} \begin{bmatrix} (1+\mu_{10})\, H_2 \\ (1+\mu_{10})\, H_2^* \\ -\mu_{13} H_2 - \mu_5 H_2^* \\ \mu_5 H_2 - \mu_{13} H_2^* \\ -\mu_5 H_2 \\ -\mu_5 H_2^* \end{bmatrix}$$

where

$$\mu_9 = \mu_6 - \mu_4 \mu_8$$

$$\mu_{10} = \mu_7 - \mu_5 \mu_8$$

$$\mu_{11} = \mu_1 - \mu_6 - \mu_5 + \mu_4 (\mu_8 - \mu_3)$$

$$\mu_{12} = \mu_2 - \mu_7 + \mu_4 + \mu_5 (\mu_8 - \mu_3)$$

$$\mu_{13} = 1 + \mu_7 - \mu_2 - \mu_5 (\mu_8 - \mu_3)$$

$$\mu_{14} = -(\mu_9 \mu_{11} + \mu_{10} \mu_{12}) / (\mu_{11}^2 + \mu_{12}^2)$$

$$\mu_{15} = (\mu_9 \mu_{12} - \mu_{10} \mu_{11}) / (\mu_{11}^2 + \mu_{12}^2)$$

$$\mu_{16} = \mu_{11} / (\mu_{11}^2 + \mu_{12}^2)$$

$$\mu_{17} = \mu_{12} / (\mu_{11}^2 + \mu_{12}^2)$$

$$\mu_{18} = (\mu_4 \mu_{11} + \mu_5 \mu_{12}) / (\mu_{11}^2 + \mu_{12}^2)$$

$$\mu_{19} = -(\mu_4 \mu_{12} - \mu_5 \mu_{11}) / (\mu_{11}^2 + \mu_{12}^2)$$

Stator

$$\begin{bmatrix} H_5 \\ H_5^* \\ \Theta_4 \\ \rho_4 \\ \Theta_5 \\ \rho_5 \end{bmatrix} = \begin{bmatrix} 1 & 0 & \nu_{11} & -\nu_{12} & 0 & 0 \\ 0 & 1 & \nu_{12} & \nu_{11} & 0 & 0 \\ 0 & 0 & \nu_{13} & \nu_{14} & 0 & 0 \\ 0 & 0 & \nu_{14} & -\nu_{13} & 0 & 0 \\ 0 & 0 & \nu_{15} & -\nu_{16} & 1 & 0 \\ 0 & 0 & \nu_{16} & \nu_{15} & 0 & 1 \end{bmatrix} \begin{bmatrix} (1-\nu_6)\, H_4 \\ (1-\nu_6)\, H_4^* \\ -\nu_{10} H_4 \\ -\nu_{10} H_4^* \\ 0 \\ 0 \end{bmatrix}$$

where

$$\nu_8 = \nu_3 - \nu_7 - \nu_4 \nu_5$$

$$\nu_9 = \nu_1 + \nu_5 + \nu_6$$

$$\nu_{10} = 1 - \nu_1 - \nu_6$$

$$\nu_{11} = (\nu_6 \nu_9 - \nu_7 \nu_8) / (\nu_8^2 + \nu_9^2)$$

$$\nu_{12} = (\nu_6 \nu_8 + \nu_7 \nu_9) / (\nu_8^2 + \nu_9^2)$$

$$\nu_{13} = \nu_8 / (\nu_8^2 + \nu_9^2)$$

$$\nu_{14} = \nu_9 / (\nu_8^2 + \nu_9^2)$$

$$\nu_{15} = \nu_5 \nu_8 / (\nu_8^2 + \nu_9^2)$$

$$\nu_{16} = -\nu_5 \nu_9 / (\nu_8^2 + \nu_9^2)$$

The introduction of the zero axial gap approximation at this point in the analysis greatly simplifies the task of computing functions downstream of a compressor stage, given the total pressure distribution upstream of the stage. Hand calculations would be extremely prohibitive if this approximation were not made. It is assumed, therefore, that the variation of the functions between blade rows can be neglected and that

effectively a zero axial gap exists between blade rows. This is equivalent to the statement that functions with subscript 1 are equal to functions with subscript 2, and functions with subscript 3 are equal to functions with subscript 4. The following notation will now be adopted and used throughout the remainder of the analysis:

Subscript	Axial Position
0	upstream of inlet vanes
1	between inlet vanes and first rotor
2	between first rotor and first stator
3	between first stator and second rotor
etc.	

2.6 Analytical Expressions for Functions to Be Compared with Experimental Data

2.6.1 Total Pressure Coefficient

The total pressure coefficient, ψ, is given by the expression

$$\psi = \frac{P_t - P_a}{\frac{1}{2}\rho\,(\omega r_t)^2} \tag{52}$$

The total pressure, P_t, can then be written as

$$P_t = p' + \frac{1}{2}\rho\,(u'^2 + v'^2) \tag{53}$$

Substituting equations 4, 5 and 6 into equation 53, the expression for the total pressure becomes

$$P_t = P + p + \frac{1}{2}\rho\left[(U + u)^2 + (V + v)^2\right] \tag{54}$$

Expanding and linearizing equation 54 and making use of the definition of H, gives the following expression:

$$P_t = P + \frac{1}{2}\rho\,(U^2 + V^2) + \rho H \tag{55}$$

Therefore,

$$\psi = \frac{P + \frac{1}{2}\rho\,(U^2 + V^2) - P_a}{\frac{1}{2}\rho\,(\omega r_t)^2} + \frac{H}{\frac{1}{2}\,(\omega r_t)^2} = \Psi + \frac{H}{\frac{1}{2}\,(\omega r_t)^2} \tag{56}$$

where Ψ is the mean total pressure coefficient. Let i refer to the particular axial position being investigated (i.e., i = 0, 1, 2, ---); then the total pressure coefficient at axial position i is given by

$$\psi_i = \Psi_i + \frac{H_i}{\frac{1}{2}\,(\omega r_t)^2} \tag{57}$$

But H_i can be solved for in terms of H_o and H_o^*, the solution being of the form

$$H_i = \gamma_m H_o + \gamma_n H_o^* \tag{58}$$

where γ_m and γ_n are constants. Substituting equation 58 into equation 57 and using the fact that $H_o = \frac{1}{2}\,(\omega r_t)^2 \psi_o$ and $H_o^* = \frac{1}{2}\,(\omega r_t)^2 \psi_o^*$, the following expression results:

$$\psi_i = \Psi_i + \gamma_m \psi_o + \gamma_n \psi_o^*$$

Let

$$\psi_1 = \Psi_1 + \gamma_1 \psi_o + \gamma_2 \psi_o^*$$

$$\psi_2 = \Psi_2 + \gamma_3 \psi_0 + \gamma_4 \psi_o^*$$

$$\psi_3 = \Psi_3 + \gamma_5 \psi_o + \gamma_6 \psi_o^*$$

The quantities $\Psi_1, \Psi_2, \Psi_3, \psi_o$ and ψ_o^* are assumed to be known. The six constants are equivalent to the following expressions if the zero axial gap approximation is used.

$$\gamma_1 = 1 - \lambda_6 - \lambda_{10}\,\lambda_{11}$$

$$\gamma_2 = \lambda_{10}\,\lambda_{12}$$

$$\gamma_3 = (1 - \lambda_6 - \lambda_{10}\lambda_{11})(1 + \mu_{10} - \mu_{13}\mu_{14} - \mu_5\mu_{15}) - (\lambda_{10}\lambda_{12})(\mu_{13}\mu_{15} - \mu_5\mu_{14})$$

$$\gamma_4 = (1 - \lambda_6 - \lambda_{10}\lambda_{11})(\mu_{13}\mu_{15} - \mu_5\mu_{14}) + (\lambda_{10}\lambda_{12})(1 + \mu_{10} - \mu_{13}\mu_{14} - \mu_5\mu_{15})$$

$$\gamma_5 = (1 - \lambda_6 - \lambda_{10}\lambda_{11})\left[(1 - \nu_6 - \nu_{10}\nu_{11})(1 + \mu_{10} - \mu_{13}\mu_{14} - \mu_5\mu_{15}) + (\nu_{10}\nu_{12})(\mu_5\mu_{14} - \mu_{13}\mu_{15})\right] - (\lambda_{10}\lambda_{12})\left[(1 - \nu_6 - \nu_{10}\nu_{11})(\mu_{13}\mu_{15} - \mu_5\mu_{14}) + (\nu_{10}\nu_{12})(1 + \mu_{10} - \mu_5\mu_{15} - \mu_{13}\mu_{14})\right]$$

$$\gamma_6 = (1 - \lambda_6 - \lambda_{10}\lambda_{11})\left[(1 - \nu_6 - \nu_{10}\nu_{11})(\mu_{13}\mu_{15} - \mu_5\mu_{14}) + (\nu_{10}\nu_{12})(1 + \mu_{10} - \mu_5\mu_{15} - \mu_{13}\mu_{14})\right] + (\lambda_{10}\lambda_{12})\left[(1 - \nu_6 - \nu_{10}\nu_{11})(1 + \mu_{10} - \mu_{13}\mu_{14} - \mu_5\mu_{15}) + (\nu_{10}\nu_{12})(\mu_5\mu_{14} - \mu_{13}\mu_{15})\right]$$

2.6.2 Relative Rotor Inlet Angle

One of the parameters which is helpful in determining the validity of applying the simplified flow theory to strongly disturbed compressor flows is the magnitude of the change in relative rotor inlet angle ($\Delta\beta_1$), caused by the disturbed flow pattern.

Combining equations 10, 12, 27 and 32, the following expression can be derived:

$$H_2 - H_1 = \frac{\omega r}{U}(\Theta_2 - \Theta_1) + uU\left[\frac{\omega r}{U}(\tan\theta_2 - \tan\theta_1) - L_r\right] - U^2 \sec^2\beta_1 \frac{L'_r}{2}\Delta\beta_1 \qquad (59)$$

The produce uU is eliminated by using the relationship

$$\Delta\beta_1 = - \frac{\cos^2 \beta_1}{U^2} \left[\Theta_1 + \frac{uU}{\varphi} \right] \tag{60}$$

Combining equations 59 and 60, and rearranging the terms, the following expression for $\Delta\beta_1$ results:

$$\Delta\beta_1 = \frac{H_1 - H_2 + \frac{1}{\varphi}\Theta_2 - (\tan\theta_2 - \tan\theta_1 - \varphi L_r + \frac{1}{\varphi})\Theta_1}{U^2 \sec^2\beta_1 \left(\tan\theta_2 - \tan\theta_1 - \varphi L_r + \frac{L'_r}{2}\right)} \tag{61}$$

Equation 61 can be put in a more convenient form by using the relationships

$$\frac{H_1}{\frac{1}{2}(\omega r_t)^2} = \gamma_1 \psi_o + \gamma_2 \psi_o^* \tag{62}$$

$$\frac{H_2}{\frac{1}{2}(\omega r_t)^2} = \gamma_3 \psi_o + \gamma_4 \psi_o^* \tag{63}$$

$$\frac{\Theta_1}{\frac{1}{2}(\omega r_t)^2} = \gamma_7 \psi_o + \gamma_8 \psi_o^* \tag{64}$$

$$\frac{\Theta_2}{\frac{1}{2}(\omega r_t)^2} = \gamma_9 \psi_o + \gamma_{10} \psi_o^* \tag{65}$$

The constants γ_1, γ_2, γ_3 and γ_4 have already been defined. The constants γ_7, γ_8, γ_9 and γ_{10} are given by the following expressions:

$$\gamma_7 = - \lambda_{10} \lambda_{15}$$

$$\gamma_8 = \lambda_{10} \lambda_{16}$$

$$\gamma_9 = - (1 - \lambda_6 - \lambda_{10} \lambda_{11})(\mu_{13} \mu_{18} + \mu_5 \mu_{19} + \mu_5) - (\lambda_{10} \lambda_{12})(\mu_{13} \mu_{19} - \mu_5 \mu_{18})$$

$$\gamma_{10} = (1 - \lambda_6 - \lambda_{10}\lambda_{11})(\mu_{13}\mu_{19} - \mu_5\mu_{18}) - (\lambda_{10}\lambda_{12})(\mu_{13}\mu_{18} + \mu_5\mu_{19} + \mu_5)$$

For convenience, define two additional constants, C_1 and C_2 as follows:

$$C_1 = \tan\theta_2 - \tan\theta_1 - \varphi L_r + \frac{1}{\varphi}$$

$$C_2 = 2(\Phi)^2 \sec^2\beta_1 \left(\tan\theta_2 - \tan\theta_1 - \varphi L_r + \frac{L'_r}{2}\right)$$

The expression for $\Delta\beta_1$ can now be written in the following form:

$$\Delta\beta_1 = \frac{\gamma_1\psi_o + \gamma_2\psi_o^* - \gamma_3\psi_o - \gamma_4\psi_o^* + \frac{1}{\varphi}(\gamma_9\psi_o + \gamma_{10}\psi_o^*) - C_1(\gamma_7\psi_o + \gamma_8\psi_o^*)}{C_2} \tag{66}$$

2.6.3 Loss Coefficient

The loss coefficient, L_r, is approximated by the expression

$$L_r\left[\tan(\beta_1 + \Delta\beta_1)\right] = L_r\left[\tan\beta_1\right] + L'_r \sec^2\beta_1 \Delta\beta_1 \tag{67}$$

where $L_r\left[\tan(\beta_1 + \Delta\beta_1)\right]$ is the local value of the loss coefficient, $L_r\left[\tan\beta_1\right]$ is the mean value and

$$L'_r = \frac{d\, L_r\left[\tan\beta_1\right]}{d\tan\beta_1}$$

All terms appearing in equation 67 are known or assumed, with the exception of $\Delta\beta_1$ which is calculated as a function of circumferential angle using equation 66.

2.6.4 Rotor Work

Due to the distorted inlet flow, the blade forces are composed of a mean value plus a variable component. The variable force parallel to the blade row is given by

$$F_y = (\rho)(S)\left[\Theta_1 - \Theta_2 + 2\cos^2\theta_1\,(\tan\theta_1 - \tan\theta_2)(H_1 - \mathcal{P}_1 - \tan\theta_1\,\Theta_1)\right] \qquad (68)$$

where S is the distance between blades and a unit dimension in the radial direction is implied. The increment of work done by the rotor per unit time as a result of the disturbed flow would then be given by

$$\Delta W_{rotor} = (\rho)(S)(r\omega)\left[\Theta_1 - \Theta_2 + 2\cos^2\theta_1\,(\tan\theta_1 - \tan\theta_2)(H_1 - \mathcal{P}_1 - \tan\theta_1\,\Theta_1)\right] \qquad (69)$$

where $r\omega$ is the average rotor speed over the small increment of length in the radial direction being considered.

Defining the constant C_3 as

$$C_3 = 2\cos^2\theta_1\,(\tan\theta_1 - \tan\theta_2)$$

and using the relationship

$$\frac{\mathcal{P}_1}{\frac{1}{2}(\omega r_t)^2} = -\gamma_8\psi_o + \gamma_7\psi_o^*$$

equation 69 may be written in the form

$$\frac{\Delta W_{Rotor}}{\frac{1}{2}(\omega r_t)^2(\rho)(S)(r\omega)} = \gamma_7\psi_o + \gamma_8\psi_o^* - \gamma_9\psi_o - \gamma_{10}\psi_o^* + C_3\left[\gamma_1\psi_o + \gamma_2\psi_o^* + \gamma_8\psi_o - \gamma_7\psi_o^* - \tan\theta_1\,(\gamma_7\psi_o + \gamma_8\psi_o^*)\right] \qquad (70)$$

2.6.5 Perturbation Flow Coefficient

Solving for the perturbation axial velocity from equation 60, it is found that

$$u = -\varphi\left[\frac{U\,\Delta\beta_1}{\cos^2\beta_1} + \frac{\Theta_1}{U}\right] \tag{71}$$

The perturbation flow coefficient is defined as

$$\phi = \frac{u}{\omega r_t} \tag{72}$$

Dividing equation 71 by ωr_t and using the definition of the mean flow coefficient, it follows that

$$\phi_1 = -\varphi\left[\frac{\Phi\Delta\beta_1}{\cos^2\beta_1} + \frac{1}{2\Phi}\frac{\Theta_1}{\frac{1}{2}(\omega r_t)^2}\right] \tag{73}$$

Substituting equation 64 into equation 73, the resultant expression for the perturbation flow coefficient is

$$\phi_1 = -\varphi\left[\frac{\Phi}{\cos^2\beta_1}\Delta\beta_1 + \frac{1}{2\Phi}\left(\gamma_7\psi_o + \gamma_8\psi_o^*\right)\right] \tag{74}$$

where, as before, $\Delta\beta_1$ is calculated as a function of circumferential angle using equation 66.

III. EXPERIMENTAL EQUIPMENT AND PROCEDURES

For convenience, a brief description of the test compressor and the method for obtaining asymmetric inlet flows is given below. More detailed discussions are given in references 1, 2 and 3.

Three sources of experimental data were used by the author, and each of these three sources made use of the large, slow-speed, three-stage axial compressor of the Turbomachinery Laboratory, California Institute of Technology. The compressor blades are removable so that a variety of configurations can be investigated. In its normal configuration, the compressor consists of a row of inlet vanes, three stages of rotor and stator blades and two rows of stationary straightening vanes located downstream of the last stage. There are thirty blades per rotor row and thirty-two blades per stator row. The compressor has a constant outer diameter of thirty-six inches and a constant hub to tip ratio of 0.6. A schematic drawing of the compressor is shown in figure 5. Air enters the compressor through a bellmouth whose inlet area is about twenty-one times as large as the area of the compressor annulus. The compressor is driven by a dynamometer from the downstream end. After flowing through the two straightening vanes, the flow is turned upward and discharged through an adjustable orifice.

The compressor is designed to permit measurements at several circumferential positions upstream and downstream of each blade row. The rotational speed can be adjusted to an accuracy of 2 rpm in 1000 rpm by using a revolution counter and timer. The flow rate through the compressor was obtained by calibrating a band of static pressure taps downstream of the bellmouth inlet. This flow rate measurement should be accurate to within 1 per cent.

Total pressure measurements were made by means of a conventional shielded impact tube carried on a remotely controlled carriage. Pressures were detected by a high response Statham strain-gage pressure pickup. The strain-gage unit was calibrated against a conventional micromanometer.

Small asymmetric inlet disturbances were produced by partially blocking a portion of the inlet flow with a series of superimposed screens. These screens were uniform in the radial direction and extended circumferentially over approximately one quarter of the inlet area. A similar technique was used to obtain more severe asymmetric inlet disturbances. In this case a ninety-degree section of the inlet area was blocked by using three layers of fine screen covered in the center by a sixty-degree segment of cardboard. In each case, the edges of the blockage screens were feathered off to suppress the development of vortices. In order to more easily obtain circumferential surveys, the measuring probe was held fixed, and the blockage screen was rotated. To accomplish this, the screens were mounted on a wire framework about 8 inches ahead of the inlet vane row, and the angular position of this wire framework was externally controlled by a pair of selsyn motors. A schematic drawing showing the installation of the blockage screen is given in figure 6, and a schematic drawing showing the blockage screen positioning device is given in figure 7.

IV. COMPARISON OF THEORETICAL RESULTS WITH EXPERIMENTAL DATA

4.1 General Analytical Procedures

All calculations were based on the zero axial gap approximation and, in each case considered, all functions were calculated as a function of circumferential angle using the experimental total pressure coefficient upstream of the inlet vanes as the known variable. The following sections list the assumed mean flow parameters and the resultant analytical expressions for the various compressor configurations, mean flow coefficients and radial distances investigated. The values of all the constants appearing in the matching equations are tabulated in the appendix, pp. 95 - 99. Values of mean flow parameters were taken from reference 3 for the particular mean flow coefficient and radial position under investigation. The experimental total pressure coefficients were approximated by Fourier series containing twenty-one terms. The corresponding Hilbert transforms of the total pressure coefficients were obtained by using the relationships

$$(\cos ny)^* = \sin ny$$

$$(\sin ny)^* = -\cos ny$$

$$(\text{constant})^* = 0$$

The criterion which was used to establish the loss coefficients, L, and the slopes of the loss coefficient curves, L', was the experimentally determined total pressure coefficient at the particular axial position under investigation. Various combinations of L and L' were tried, and that combination of L and L' which gave the best agreement between theoretical and experimental total pressure coefficients was selected. The values of L and L' determined in this manner were then used in the

analytical expressions for the other flow functions which were investigated. Depending on the severity of the inlet flow distortion, the flow processes may or may not be adequately described by the linearized two-dimensional theory with a zero axial gap approximation. In addition to listing the mean flow parameters and the analytical expressions, the following sections also contain discussions of the adequacy of the simplified theory for each of the six flow cases investigated.

4.2 Expanded Single Stage, $\Phi = 0.35$, $\xi = 0.9$

A schematic drawing of the expanded single stage, showing the survey planes at which measurements were taken, is presented in figure 8. Total pressure coefficient as a function of circumferential angle was experimentally determined directly upstream and directly downstream of the inlet vanes, second rotor and third stator. The axial spacing between rotor and stator centerlines in this configuration is 7.625 inches, or 1.059 blade lengths. Figure 9 shows the experimentally determined total pressure coefficient and the Fourier representation which was used to approximate it. Figure 9 also shows the Hilbert transform which corresponds to this Fourier series.

The experimental data for this configuration is reported in reference 2. The peripheral disturbance upstream of the inlet vanes is reasonably strong, although not as severe as the distortion to which the three-stage configuration is subjected. The following mean flow parameters were used:

$$\theta_o = 0^\circ \qquad \delta_v = 0.6$$

$$\theta_1 = \theta_3 = 16^\circ \qquad L_v = 0.2$$

$$\theta_4 = \theta_6 = 47^\circ \qquad L_v' = 1.0$$

$\theta_7 = 25°$ $\quad$ $\delta_r = 0.6$

$\beta_1 = \beta_3 = 68°$ $\quad$ $L_r = 0.3$

$\beta_4 = \beta_6 = 54°$ $\quad$ $L_r' = 1.0, 2.0, 3.0$

$\Psi_4 = \Psi_6 = 0.200$ $\quad$ $\delta_s = 0$

$\Psi_7 = 0.200$ $\quad$ $L_s = 0$

$\varphi = 0.389$ $\quad$ $L_s' = 0$

Three values are listed for L_r' due to the fact that this was the only configuration where the analytical expressions proved inadequate to approximate the experimental data. The three values of L_r' illustrate that no value of L_r' exists which will give reasonable analytical results. Because of this, the following functions were the only ones investigated for this particular configuration:

$$\psi_1 = \psi_3 = 0.849\,\psi_o - 0.056\,\psi_o^*$$

$$\psi_4 = \psi_6 = 0.200 - 0.096\psi_o - 0.584\psi_o^* \text{ for } L_r' = 1.0$$

$$\psi_4 = \psi_6 = 0.200 + 0.297\psi_o - 0.508\psi_o^* \text{ for } L_r' = 2.0$$

$$\psi_4 = \psi_6 = 0.200 + 0.715\psi_o + 0.062\psi_o^* \text{ for } L_r' = 3.0$$

The simplified flow theory is able to give excellent agreement with the experimental results at station 1 (figure 10) and fair agreement at station 3 (figure 11). The slight contraction of the disturbed region at station 1 is predicted quite well by the theoretical results. Because of the zero axial gap approximation, the theory does not take into account the changes which occur between blade rows; hence, it fails to predict the widening of the disturbed region seen in figure 11. The experimental flow coefficients at stations 4 and 6 are shown in figure 12.

It was not possible to obtain agreement between theory and experiment at station 4. Had the theory been able to give good agreement with the experimental results at station 4, it would not have been able to predict the significant changes which are seen to occur between stations 4 and 6. Because of the severity of the flow distortion, the dip in the theoretical pressure coefficient at the trailing edge of the disturbed region and the peak at the leading edge, which were present to a lesser degree in the theoretical results shown in figure 76 of reference 1, are seen in figure 12 to be greatly magnified, resulting in gross disagreement between theory and experiment. Theoretical total pressure profiles are shown for three different values of L_r', which is the prime factor affecting the shape of the theoretical curves downstream of the rotor.

This particular configuration was subjected to an asymmetric inlet flow distortion which was approximately twice as severe as the one used by Katz in reference 1. Katz was able to show good agreement between theory and experiment for the small inlet distortion which he investigated. The strong distortion investigated here has evidently given rise to flow processes which exceed the limitations of the simplified flow theory.

4.3 Normal Single Stage, $\Phi = 0.4$, $\bar{\xi} = 0.8$

A schematic drawing of the normal single stage configuration is shown in figure 13. This configuration consists of the inlet vanes, first rotor row and first stator row. The asymmetric inlet distortion, the Fourier series used to represent it and the corresponding Hilbert transform are shown in figure 14. The asymmetric distortion imposed on the flow for this configuration was relatively small; however, there are two reasons for including it in this analysis. First, it allows one to

compare the analytical results for a normal single stage configuration with the results for the expanded single stage and three-stage configurations. Second, it shows that the flow processes resulting from a relatively small asymmetric inlet distortion are adequately described by the simplified theory and hence do not exceed the limitations imposed by the linearization of the basic equations. This will be seen to be in contrast with the results for extremely severe inlet flow distortions. The experimental data for this configuration is reported in reference 1. No experimental data was available for the normal single stage configuration with strong peripheral inlet distortions. The following mean flow parameters were used:

$\theta_0 = 0°$	$\delta_v = 0$
$\theta_1 = 20°$	$L_v = 0$
$\theta_2 = 47°$	$L_v' = 0$
$\theta_3 = 25°$	$\delta_r = 0.6$
$\beta_1 = 59°$	$L_r = 0.2$
$\beta_2 = 42°$	$L_r' = 0.9$
$\Psi_3 = 0.330$	$\delta_s = 0.6$
$\varphi = 0.500$	$L_s = 0.2$
	$L_s' = 0.9$

Using these mean flow parameters, the following analytical expressions result:

$$\psi_3 = 0.330 + 0.416\psi_o - 0.333\psi_o^*$$

$$\Delta\beta_1 = -0.492\psi_o + 0.284\psi_o^*$$

$$L_r = 0.200 + 3.393\ \Delta\beta_1$$

$$\frac{\Delta W_{Rotor}}{\frac{1}{2}(\omega r_t)^2(\rho)(S)(r\omega)} = -0.641\psi_o + 0.035\psi_o^*$$

$$\phi_1 = -0.754\ \Delta\beta_1$$

The theoretical and experimental total pressure coefficients at station 3 are shown in figure 15. It will be noted that the dip in total pressure at the trailing edge of the disturbed region and the peak at the leading edge are still present, although to a much lesser degree than was noted for the more severe inlet distortion in the preceding case. Reasonably good agreement is achieved between theory and experiment, although it is clear that the present theory is incapable of predicting small, localized losses approximately one blade spacing in width. Figure 16 shows the amount by which the relative rotor inlet angle changes as predicted by the simplified theory. The mean value of the relative rotor inlet angle is 59°, and the maximum value as predicted by theory would be approximately 70°. This would occur at a circumferential angle of about 52° which is where the inlet flow is most severely depressed. Figure 17 shows the variation of the rotor loss coefficient, L_r, as a function of circumferential angle. It is significant that the rotor loss coefficient always remains positive, because a negative loss coefficient would indicate that the assumptions inherent in the linearization of the basic equations are no longer valid. It will be seen that the rotor loss coefficients, calculated for the three-stage configuration with severe inlet distortions, do not remain positive throughout the disturbed region.

4.4 Three-Stage Configuration

Four flow cases were investigated with this particular configuration since it is the three-stage configuration which most closely simulates the operation of normal multiple stage axial compressors. A schematic drawing of the three-stage configuration showing the location of the survey planes is given in figure 20. Figures 21 through 28 pertain to a mean flow coefficient of 0.4 and a dimensionless radius of 0.8. Figures 29 through 36 are for a mean flow coefficient of 0.4 and a dimensionless radius of 0.9. Figures 37 through 44 and 45 through 52 refer to dimensionless radii of 0.8 and 0.9 respectively with both groups having the same mean flow coefficient of 0.45. The experimental data for these four cases is reported in reference 2. In each of these cases, the peripheral inlet flow distortion was extremely severe. The mean flow parameters and the resulting analytical expressions are listed separately for the four combinations of mean flow coefficient and radial position investigated.

$\Phi = 0.40, \quad \xi = 0.8$

$\theta_o = 0°$	$\delta_v = 0.6$
$\theta_1 = 20°$	$L_v = 0.3$
$\theta_2 = 47°$	$L'_v = 1.5$
$\theta_3 = 25°$	$\delta_r = 0.6$
$\beta_1 = 59°$	$L_r = 0.4$
$\beta_2 = 42°$	$L'_r = 1.7$
$\Psi_2 = 0.200$	$\delta_s = 0$
$\Psi_3 = 0.200$	$L_s = 0$

$\varphi = 0.500$ $\qquad$ $L_s' = 0$

$\psi_1 = 0.809\psi_o - 0.102\psi_o^*$

$\psi_2 = 0.200 + 0.538\psi_o - 0.258\psi_o^*$

$\psi_3 = 0.200 + 0.538\psi_o - 0.258\psi_o^*$

$\Delta\beta_1 = -0.287\psi_o - 0.304\psi_o^*$

$L_r = 0.400 + 6.409\ \Delta\beta_1$

$$\frac{\Delta W_{Rotor}}{\frac{1}{2}(\omega r_t)^2(\rho)(S)(r\omega)} = -0.795\psi_o + 0.410\psi_o^*$$

$\phi_1 = -0.754\ \Delta\beta_1 + 0.034\psi_o - 0.072\psi_o^*$

$\underline{\Phi = 0.40,\ \xi = 0.9}$

$\theta_o = 0°$	$\delta_v = 0.6$
$\theta_1 = 16°$	$L_v = 0.5$
$\theta_2 = 43°$	$L_v' = 1.5$
$\theta_3 = 22°$	$\delta_r = 0.6$
$\beta_1 = 63°$	$L_r = 0.5$
$\beta_2 = 51°$	$L_r' = 2.0$
$\Psi_2 = 0.180$	$\delta_s = 0$
$\Psi_3 = 0.180$	$L_s = 0$
$\varphi = 0.444$	$L_s' = 0$

$\psi_1 = 0.681\psi_o - 0.120\psi_o^*$

$\psi_2 = 0.180 + 0.399\psi_o - 0.283\psi_o^*$

$\psi_3 = 0.180 + 0.399\psi_o - 0.283\psi_o^*$

$$\Delta\beta_1 = -0.215\psi_o - 0.261\psi_o^*$$

$$L_r = 0.500 + 9.704\,\Delta\beta_1$$

$$\frac{\Delta W_{Rotor}}{\frac{1}{2}(\omega r_t)^2(\rho)(S)(r\omega)} = -0.657\psi_o + 0.421\psi_o^*$$

$$\phi_1 = -0.863\,\Delta\beta_1 + 0.034\psi_o - 0.080\psi_o^*$$

$\underline{\Phi = 0.45,\ \mathfrak{S} = 0.8}$

$\theta_o = 0°$	$\delta_v = 0.6$
$\theta_1 = 20°$	$L_v = 0.3$
$\theta_2 = 43°$	$L'_v = 1.5$
$\theta_3 = 23°$	$\delta_r = 0.6$
$\beta_1 = 55°$	$L_r = 0.4$
$\beta_2 = 40°$	$L'_r = 1.5$
$\Psi_2 = 0.200$	$\delta_s = 0$
$\Psi_3 = 0.200$	$L_s = 0$
$\varphi = 0.563$	$L'_s = 0$

$$\psi_1 = 0.809\psi_o - 0.102\psi_o^*$$

$$\psi_2 = 0.200 + 0.588\psi_o - 0.207\psi_o^*$$

$$\psi_3 = 0.200 + 0.588\psi_o - 0.207\psi_o^*$$

$$\Delta\beta_1 = -0.323\psi_o - 0.283\psi_o^*$$

$$L_r = 0.400 + 4.559\,\Delta\beta_1$$

$$\frac{\Delta W_{Rotor}}{\frac{1}{2}(\omega r_t)^2(\rho)(S)(r\omega)} = -0.606\psi_o + 0.341\psi_o^*$$

$$\phi_1 = -0.770\,\Delta\beta_1 + 0.034\psi_o - 0.072\psi_o^*$$

$\Phi = 0.45, \quad \mathfrak{S} = 0.9$

$\theta_o = 0°$	$\delta_v = 0.6$
$\theta_1 = 16°$	$L_v = 0.3$
$\theta_2 = 38°$	$L_v' = 1.5$
$\theta_3 = 21°$	$\delta_r = 0.6$
$\beta_1 = 60°$	$L_r = 0.4$
$\beta_2 = 50°$	$L_r' = 2.0$
$\Psi_2 = 0.200$	$\delta_s = 0$
$\Psi_3 = 0.200$	$L_s = 0$
$\varphi = 0.500$	$L_s' = 0$

$$\psi_1 = 0.800\psi_o - 0.095\psi_o^*$$

$$\psi_2 = 0.200 + 0.690\psi_o - 0.139\psi_o^*$$

$$\psi_3 = 0.200 + 0.690\psi_o - 0.139\psi_o^*$$

$$\Delta\beta_1 = -0.255\psi_o - 0.371\psi_o^*$$

$$L_r = 0.400 + 8.0\,\Delta\beta_1$$

$$\frac{\Delta W_{Rotor}}{\frac{1}{2}(\omega r_t)^2(\rho)(S)(r\omega)} = -0.506\psi_o + 0.467\psi_o^*$$

$$\phi_1 = -0.900\,\Delta\beta_1 + 0.026\psi_o - 0.056\psi_o^*$$

Figure 21 shows the extremely severe asymmetric inlet distortion to which the three-stage configuration was subjected, along with the Fourier series approximation to it and the corresponding Hilbert transform. Figure 22 gives a comparison between the theoretical and experimental

total pressure profiles downstream of the inlet vanes. The slight contraction in the disturbed region is reasonably well predicted by the theory. In figures 23 and 24, the experimental total pressure coefficients have been shifted circumferentially in a direction opposite to the rotor motion in order to cause the centers of the disturbed regions downstream to coincide with the center of the inlet disturbance. This was done so that the adequacy of the simplified theory could be more easily determined. The theory is clearly incapable of predicting circumferential displacement of the disturbed region. Figures 23 and 24 both demonstrate good agreement between theory and experiment although, as before, small localized losses approximately one blade spacing in width cannot be predicted. The mean value of the relative rotor inlet angle was 59°. Therefore, using the theoretical curve shown in figure 25, the maximum predicted value for the relative rotor inlet angle in the disturbed region would be approximately 98°. This is clearly impossible. However, with an inlet flow distortion as severe as the one imposed in this case, a very appreciable decrease in magnitude of axial velocity would be experienced in the disturbed region and very high relative rotor inlet angles would result. No experimental data was available to indicate what this angle should have been, but an indication of the order of magnitude of the error involved in this calculation can be obtained by reconsidering the normal single stage configuration examined earlier. In that case, it appeared that the flow processes did not violate the assumptions made in the simplified flow theory and hence the theoretical results for the normal single stage configuration are probably reasonably accurate. Assuming, therefore, that the maximum relative rotor inlet angle of 70° calculated for the normal single stage

configuration is reasonably correct, it follows that the corresponding angle in the present case should lie between 70° and 90°. It should be larger than 70° because the axial velocity is smaller for the more severe inlet disturbance observed for the three-stage configuration, and it must be less than 90°. Therefore, we know that the predicted angle is in error for the three-stage configuration, but that the error is of the order of 15° or 20°. This means that the maximum error in $\Delta\beta_1$ is probably less than 50 per cent. The rotor loss coefficient is shown in figure 26. The fact that this coefficient assumes negative values between 0° and 30° indicates that the flow processes induced by the severe inlet distortion do not completely satisfy the assumptions inherent in the simplified analytical treatment which was used. This is seen to be in contrast with the results for the normal single stage configuration with small asymmetric inlet distortions.

The results for different mean flow coefficients and different dimensionless radii were essentially the same as for the case discussed above. Agreement between experimental and analytical total pressure coefficients was not as good for the higher flow coefficient. It was stated in reference 2 that the inlet total pressure distribution was substantially the same for mean flow coefficients of 0.40 and 0.45; hence, the same inlet total pressure distribution was used for both mean flow coefficients in the present calculations. Part of the disagreement between theory and experiment at the higher flow coefficient may therefore be due to slight variations in the inlet total pressure distributions at the higher mean flow coefficient.

V. CONCLUSIONS

1) Based on the results obtained for the normal single stage configuration, it is concluded that the theory, as it has been presented, is adequate for predicting performance of axial flow compressors with normal blade row spacing and small asymmetric inlet flows. The inlet distortion which was used to investigate this particular configuration was small enough so that the flow processes were adequately simulated by the mathematical model inherent in the linearized two-dimensional theory.

2) The results for the three-stage configuration indicate that the simplified flow theory can adequately describe total pressure profiles of axial compressors which are subjected to strong asymmetric inlet flow distortions. The loss coefficients required to obtain these predictions, however, appear to be extremely high. Also, some of the theoretical results for this configuration are known to be physically impossible. It is concluded, therefore, that the present theory is capable of providing fair qualitative agreement between theory and experiment for axial compressors with severe asymmetric inlet flow distortions but does not simulate the flow processes in such compressors accurately enough to provide good quantitative agreement.

3) The two-dimensional linearized flow theory with the zero axial gap approximation is not adequate to describe the flow processes in an expanded single stage configuration subjected to severe asymmetric inlet distortions. Changes in the experimental functions between blade rows cannot be predicted, and the total pressure profile downstream of the rotor is such that it cannot be predicted by this theory.

4) It is necessary to make a simplifying assumption, such as the zero axial gap approximation, to facilitate hand calculation of several flow

functions. If the complexity of the mathematical operations was increased beyond that required for the present analysis, the calculations would have to be done by a computer.

VI. SYMBOLS

a	Constant
b	Constant
c	Constant
d	Constant
f_n	Function
H	Perturbation total pressure $= \frac{p}{\rho} + Uu + Vv$
k	Constant
L	Total pressure loss coefficient
L'	Slope of the total pressure loss coefficient curve
n	Wave number
p	Perturbation static pressure
p'	Static pressure
P	Mean static pressure
P_a	Atmospheric pressure
P_t	Total pressure
$\mathcal{P}$	Harmonic pressure function $= \frac{p}{\rho}$
r	Radius
r_h	Hub radius
r_t	Tip radius
S	Blade spacing
u	Perturbation axial velocity
u'	Axial velocity
U	Mean axial velocity
v	Perturbation tangential velocity
v'	Tangential velocity
V	Mean tangential velocity

x	Dimensionless axial coordinate $= \frac{x'}{r}$
x'	Axial coordinate
y	Dimensionless tangential coordinate $= \frac{y'}{r}$
y'	Tangential coordinate
β	Relative flow angle
γ	Constant
δ	Slope of leaving vs inlet angle curve
Δ	Incremental change
θ	Flow angle
Θ	Angle perturbation function = Uv - Vu
λ	Constant
μ	Constant
ν	Constant
ξ	Dimensionless radius $= \frac{r}{r_t}$
ρ	Fluid density
φ	Flow coefficient $= \frac{U}{\omega r}$
ϕ	Perturbation flow coefficient $= \frac{u}{\omega r_t}$
Φ	Mean flow coefficient $= \frac{U}{\omega r_t}$
ψ	Total pressure coefficient $= \frac{P_t - P_a}{\frac{1}{2}\rho (\omega r_t)^2}$
Ψ	Mean total pressure coefficient
ω	Rotational speed of the rotor

Subscripts

1, 2, 3, ...	Flow region
r	Rotor
s	Stator
v	Inlet vanes

Superscript

*	Denotes Hilbert transform of function

VII. REFERENCES

1. Katz, R., "Performance of Axial Compressors with Asymmetric Inlet Flows," Daniel and Florence Guggenheim Jet Propulsion Center, California Institute of Technology, Pasadena, California, prepared under Contract No. AF 18(600)-178, U. S. Air Force, Office of Scientific Research, Air Research and Development Command, (1958).

2. Marble, F. E. and Heiser, W. H., "Some Preliminary Experiments Concerning the Effects of Strongly Distorted Inlet Flow on the Performance of an Axial Compressor," Daniel and Florence Guggenheim Jet Propulsion Center, California Institute of Technology, Pasadena, California, prepared under Contract No. AF 49(638)-497, U. S. Air Force, Office of Scientific Research, Air Research and Development Command, (1960).

3. Bowen, J. T., Sabersky, R. H., and Rannie, W. D., "Theoretical and Experimental Investigations of Axial Flow Compressors," Mechanical Engineering Laboratory, California Institute of Technology, Pasadena, California, prepared under Navy Contract N6-ORI-102, Task Order IV, Summary Report, (1949).

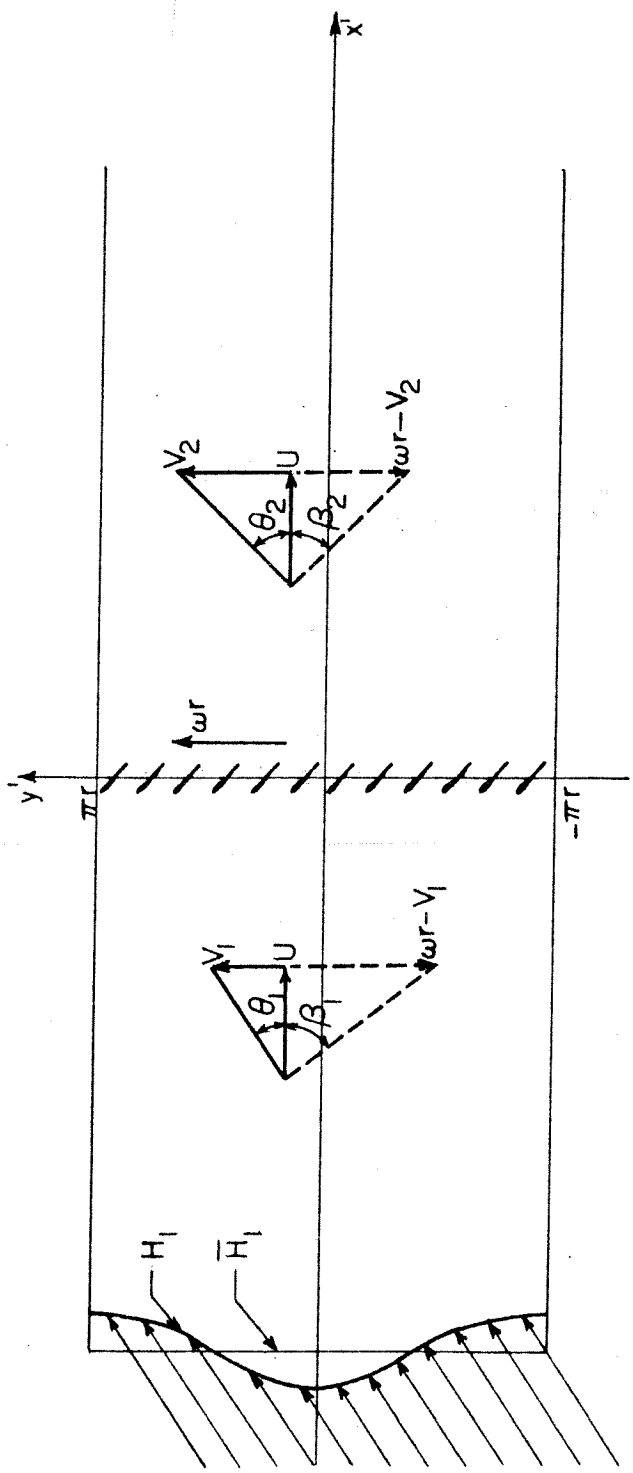

Fig. 1. Isolated Rotor Blade Row with an Inlet Distortion.

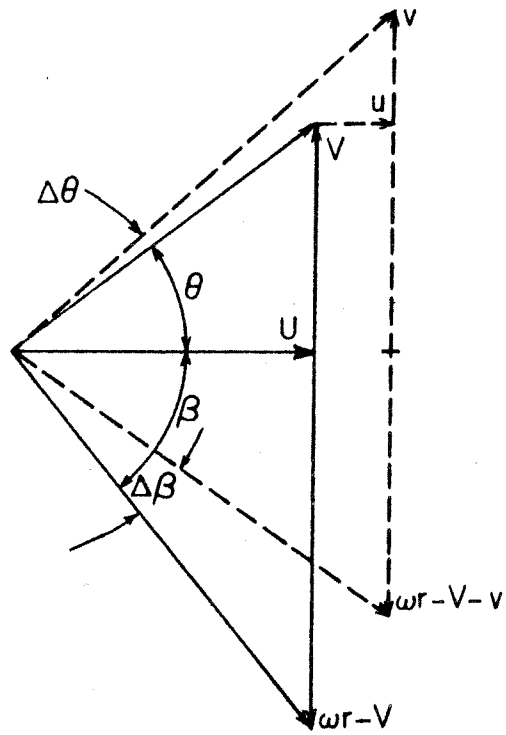

Fig. 2. Mean and Perturbation Flow Angles.

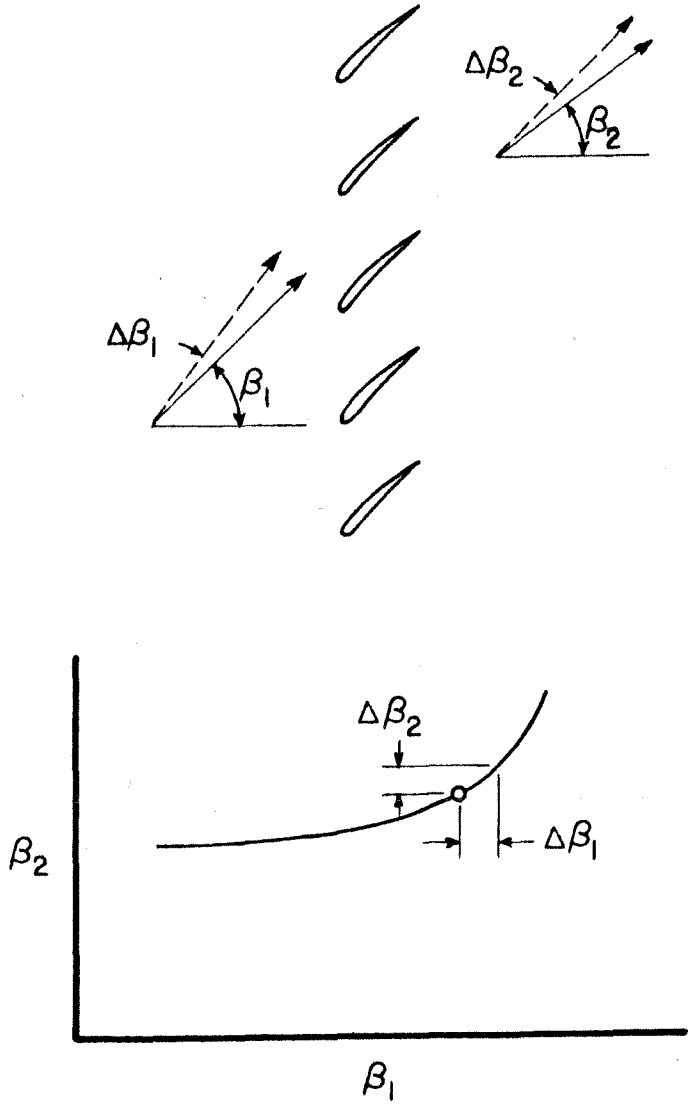

Fig. 3. Flow Angles at a Blade Row.

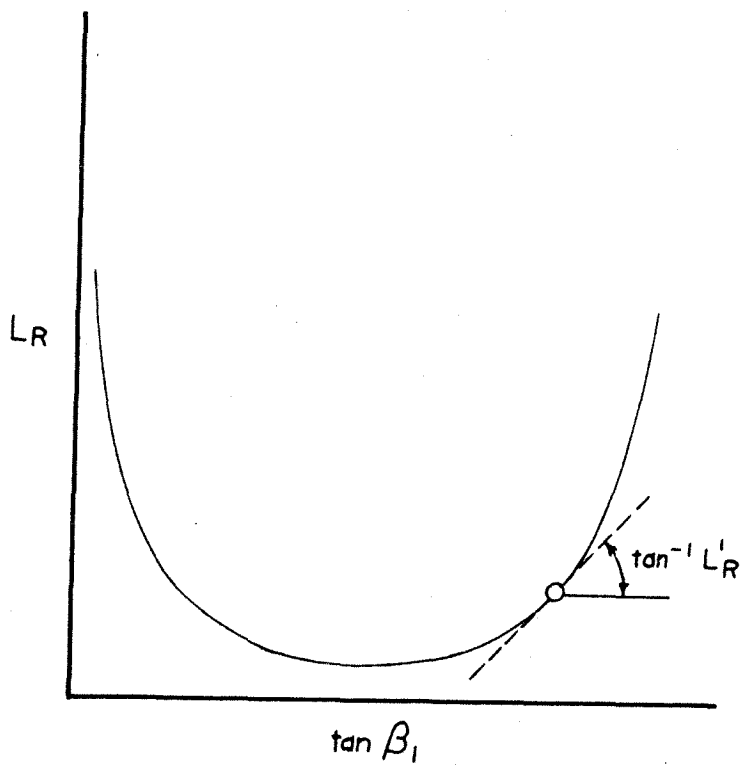

Fig. 4. Linear Loss Coefficient

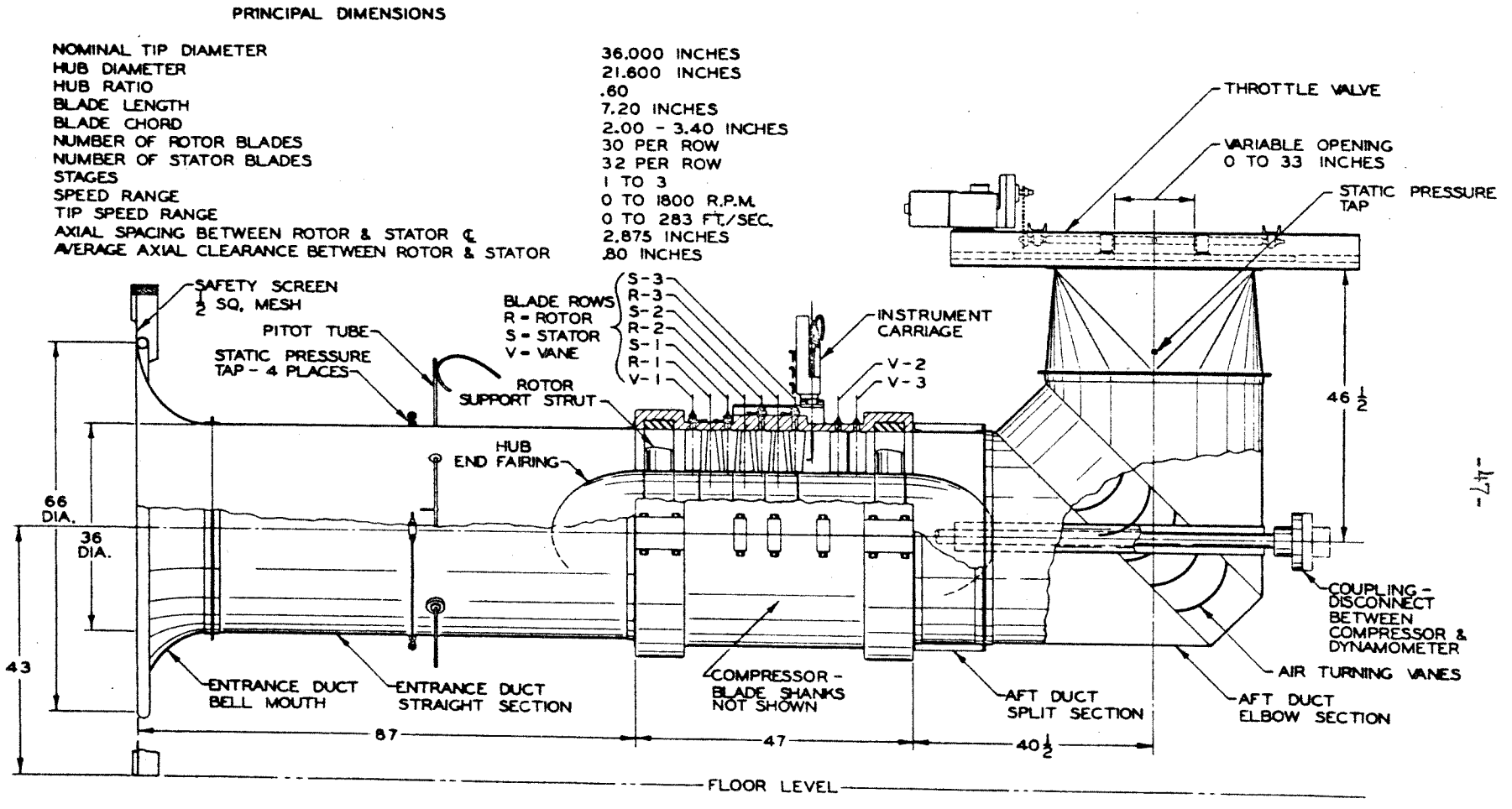

Fig. 5. Axial-Flow Compressor.

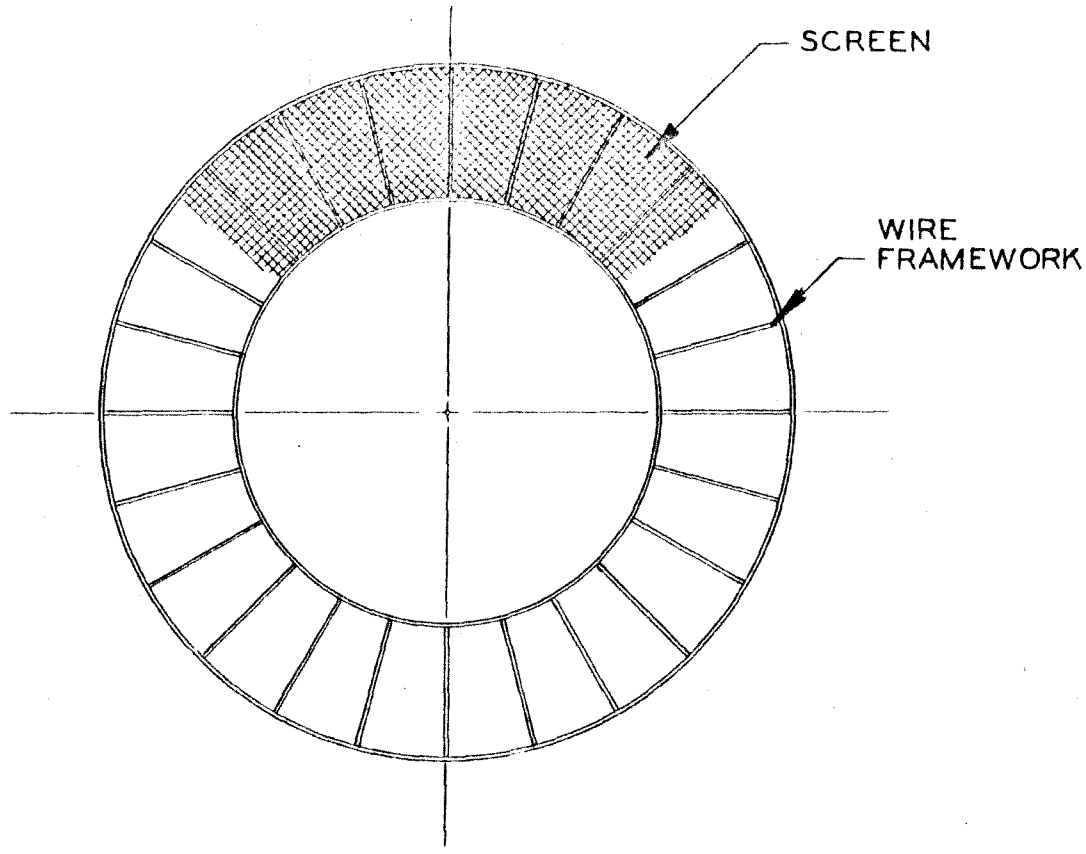

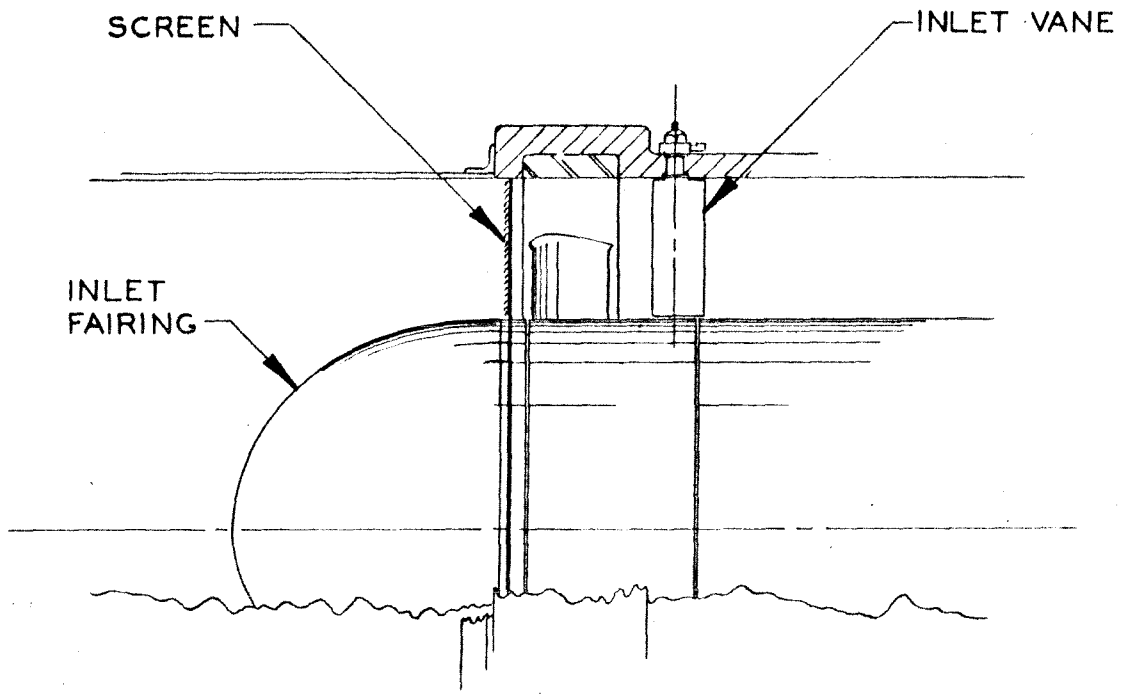

Fig. 6. Blockage Screen.

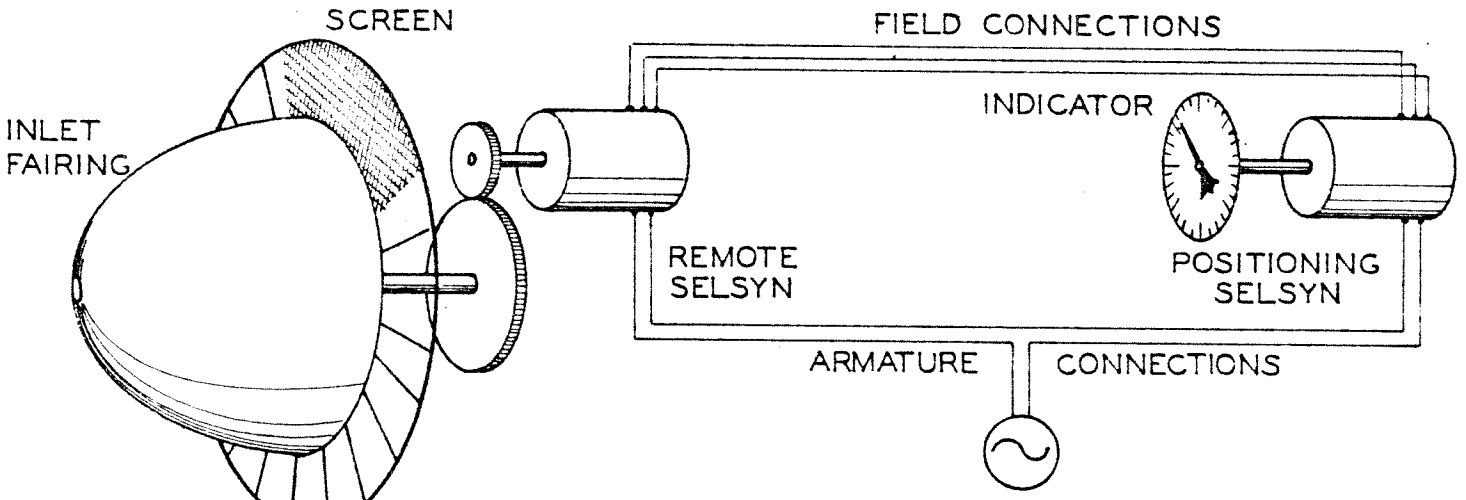

Fig. 7. Schematic Drawing of Screen Positioning Device.

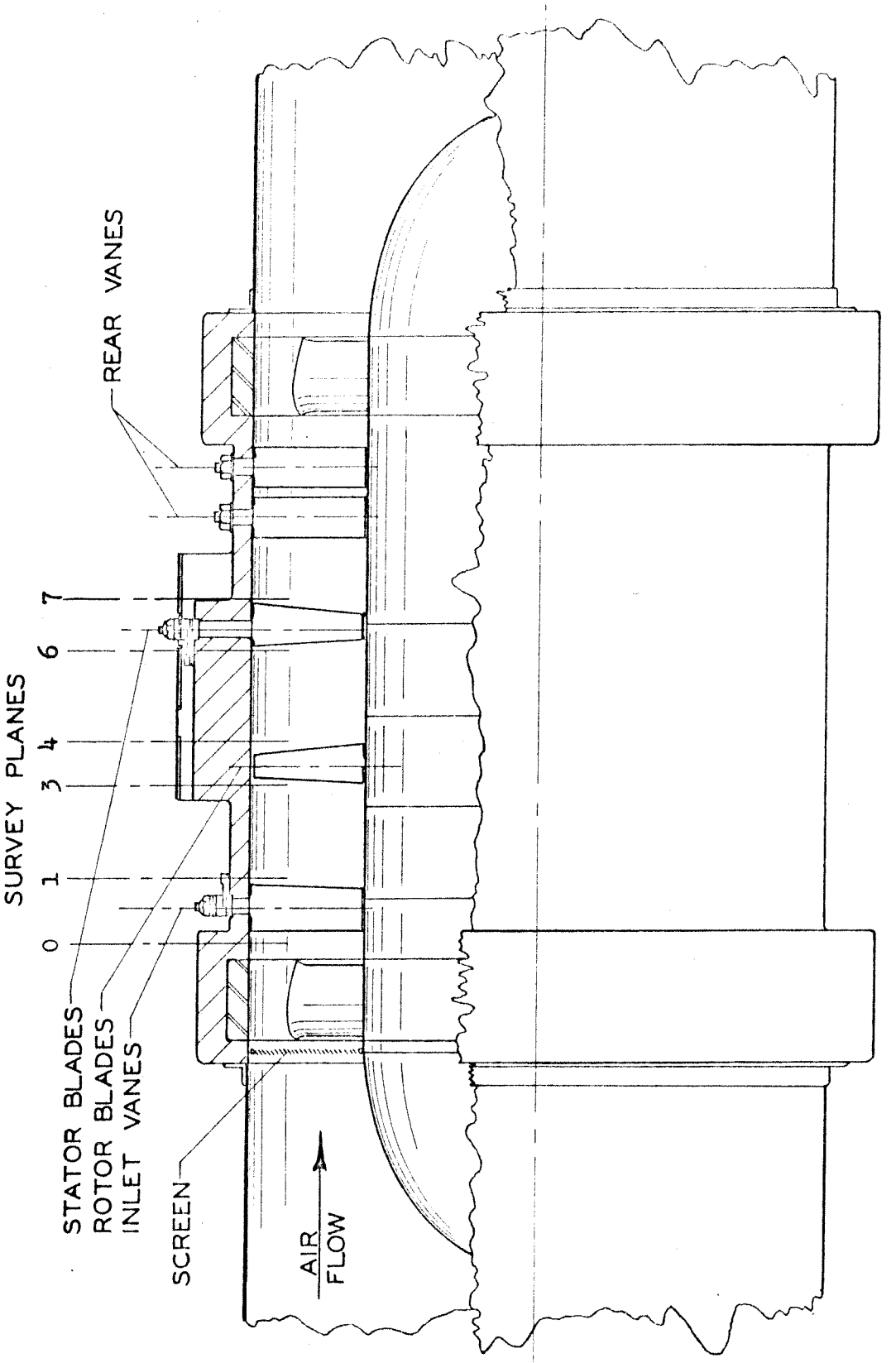

Fig. 8. Expanded Single Stage Configuration.

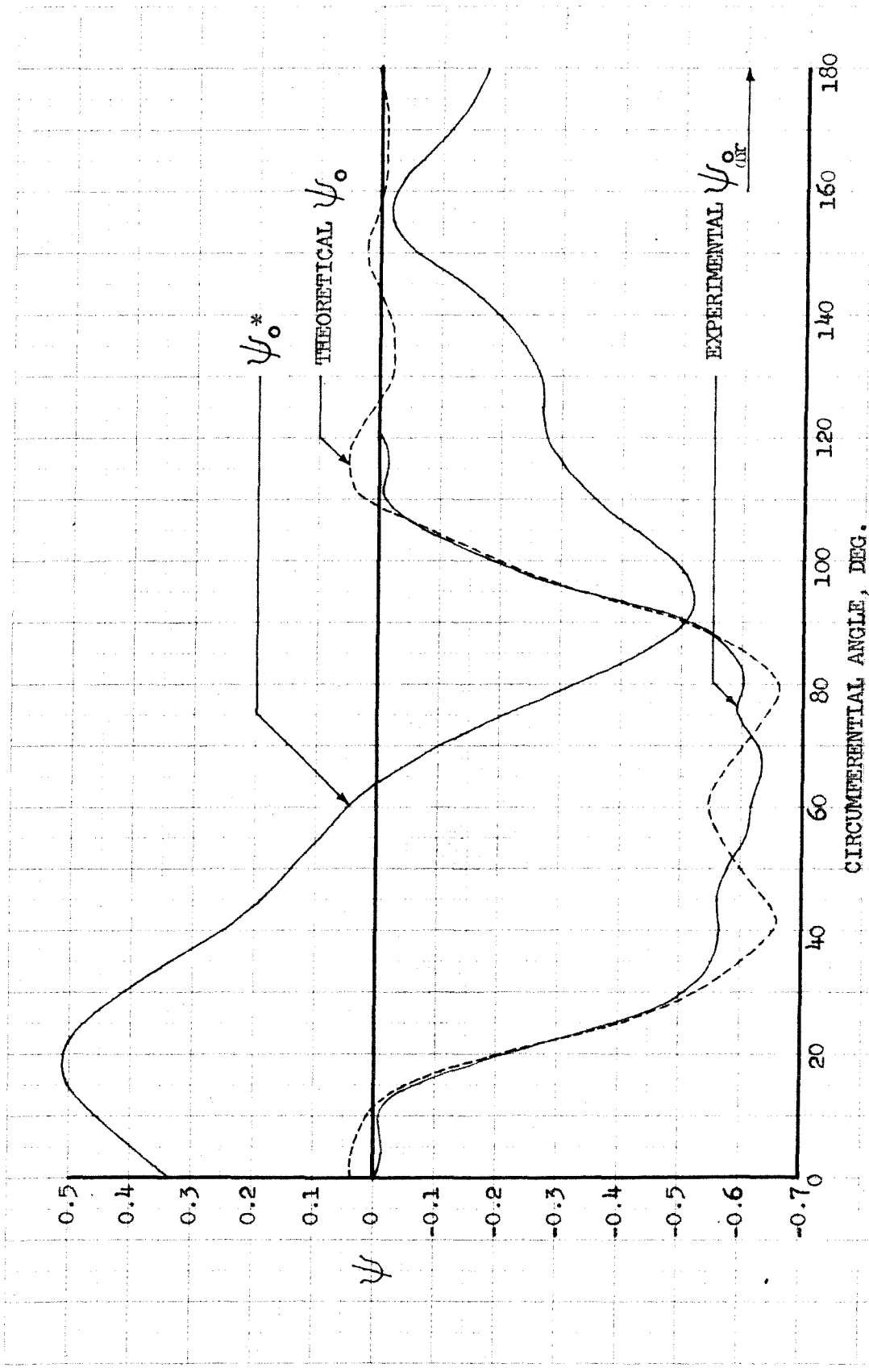

Fig. 9. Total Pressure Coefficient vs. Circumferential Angle. Expanded Single Stage Configuration, Station 0. $\Phi = 0.35$, $\overline{\omega} = 0.9$

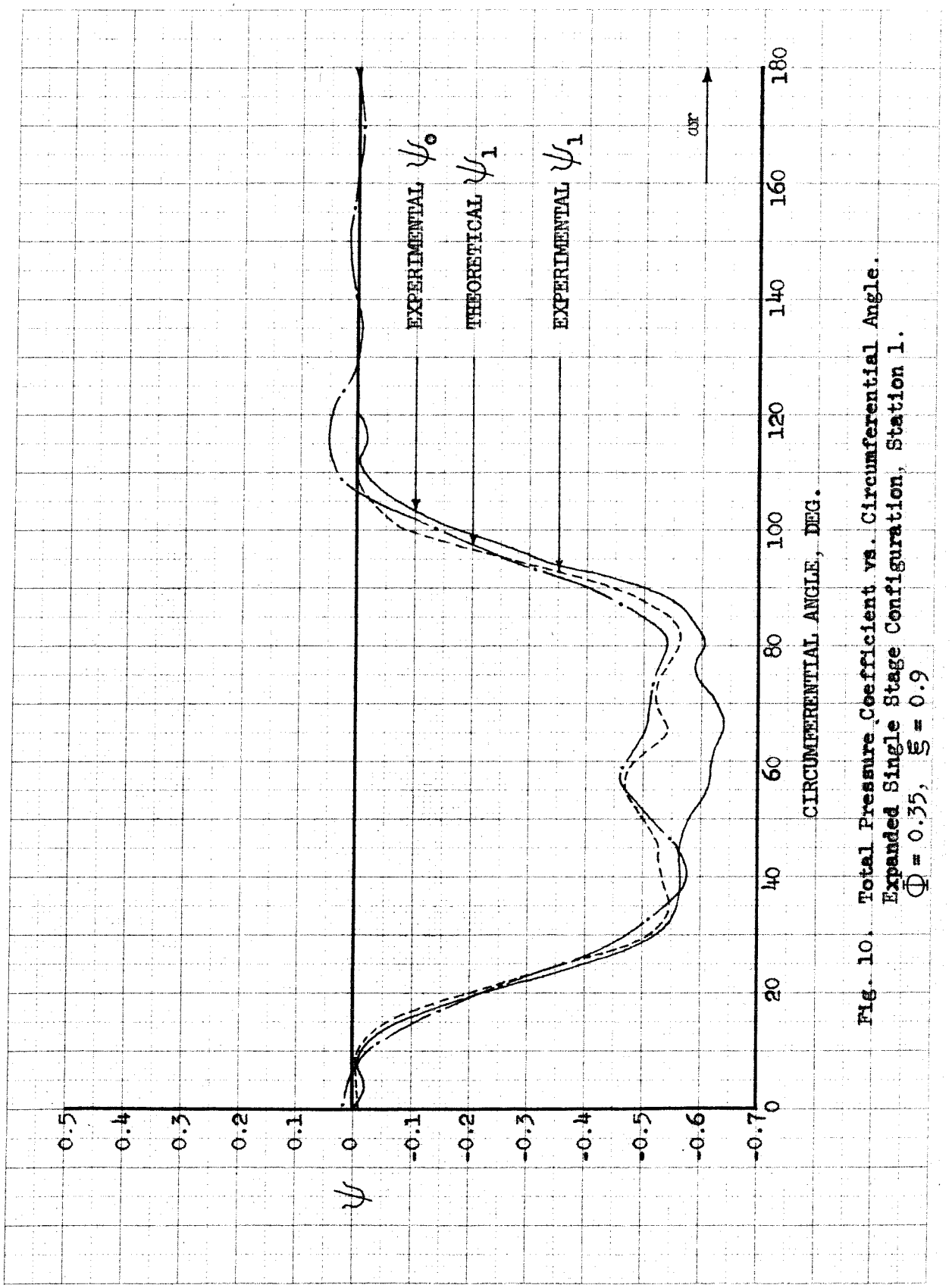

Fig. 10. Total Pressure Coefficient vs. Circumferential Angle.
Expanded Single Stage Configuration, Station 1.
$\Phi = 0.35$, $\bar{\varepsilon} = 0.9$

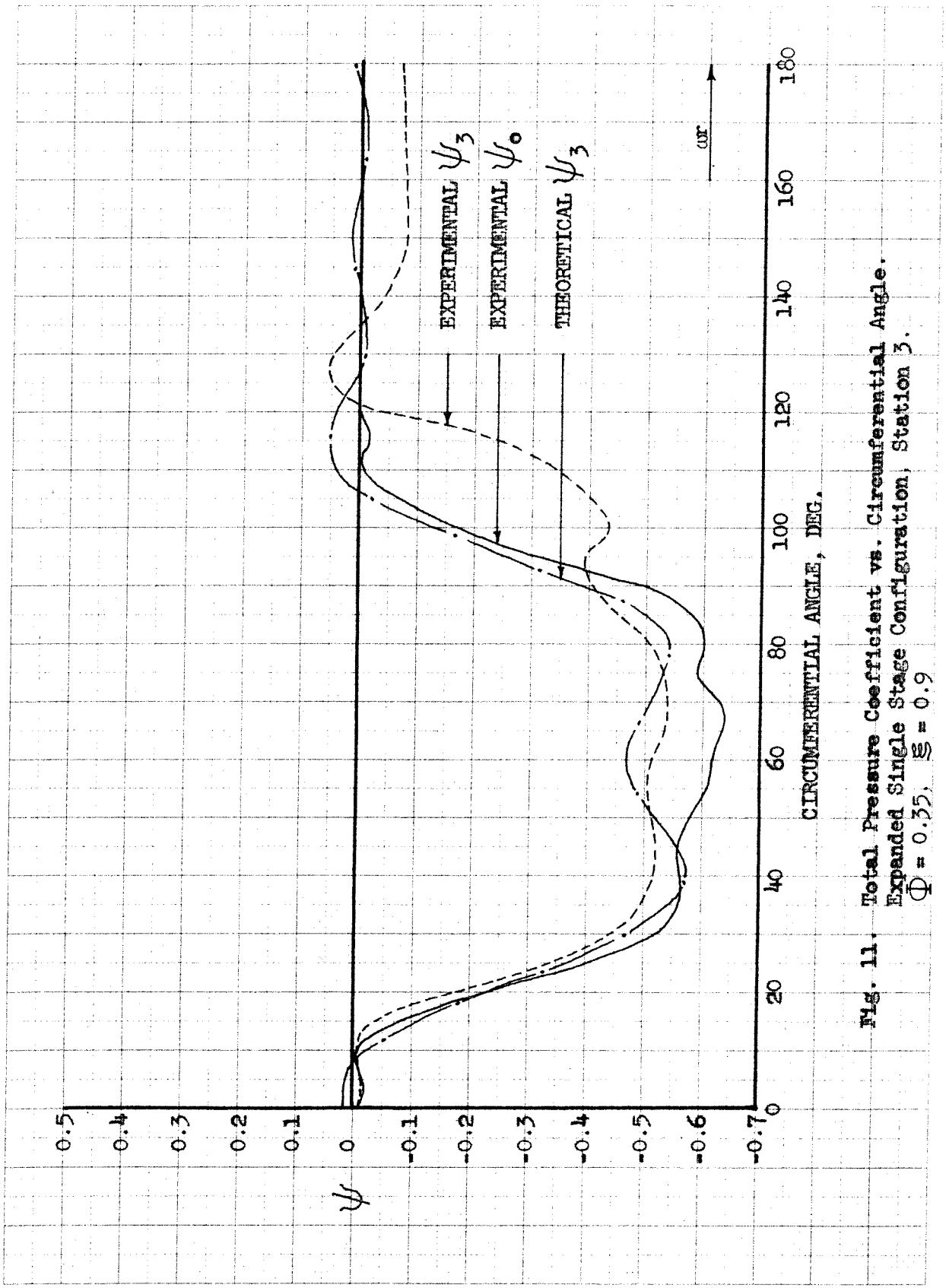

Fig. 11. Total Pressure Coefficient vs. Circumferential Angle.
Expanded Single Stage Configuration, Station 3.
$\Phi = 0.35$, $\mathbb{S} = 0.9$

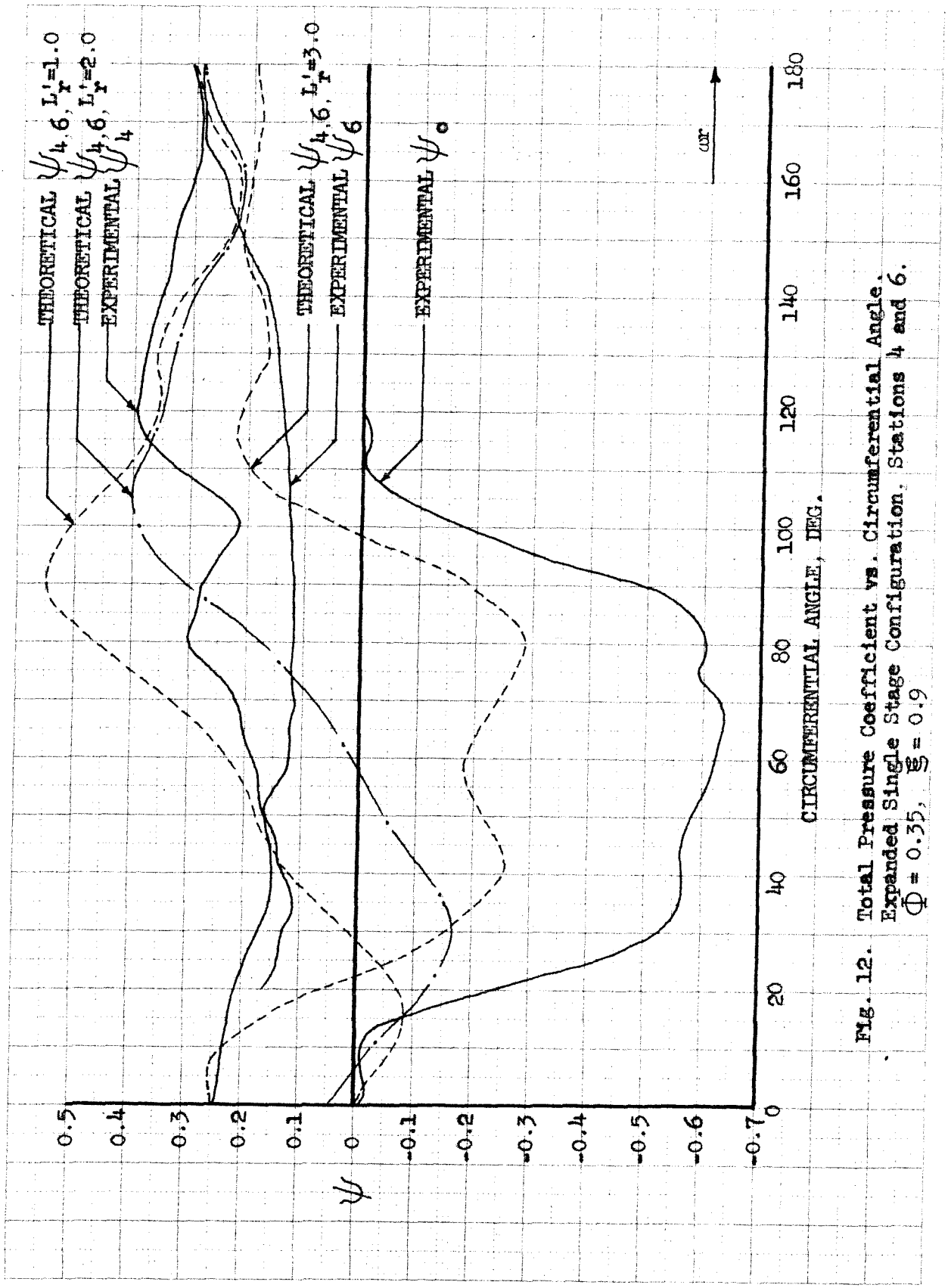

Fig. 12. Total Pressure Coefficient vs. Circumferential Angle. Expanded Single Stage Configuration, Stations 4 and 6. Φ = 0.35, $\overline{\mathrm{g}}$ = 0.9

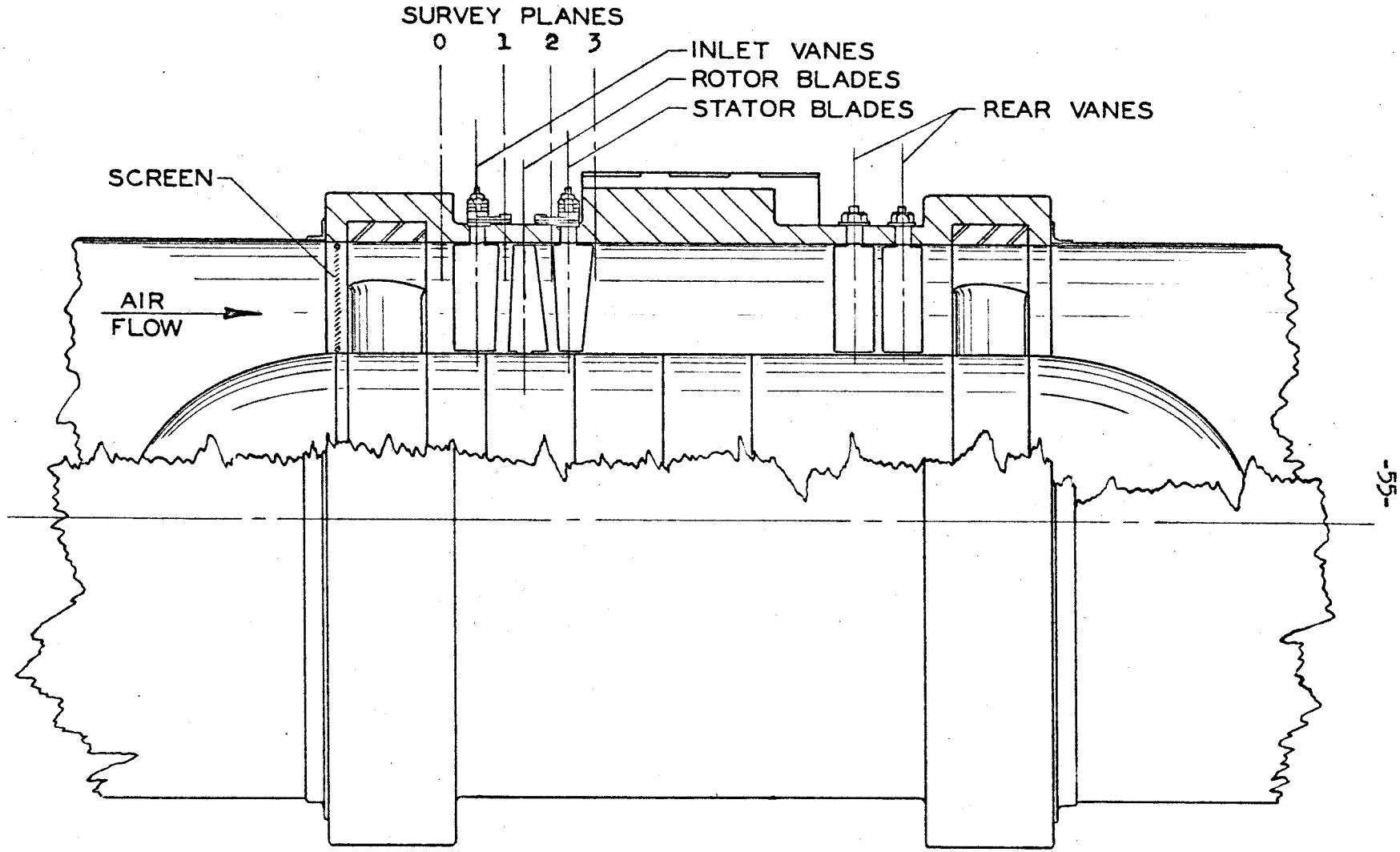

Fig. 13. Normal Single Stage Configuration.

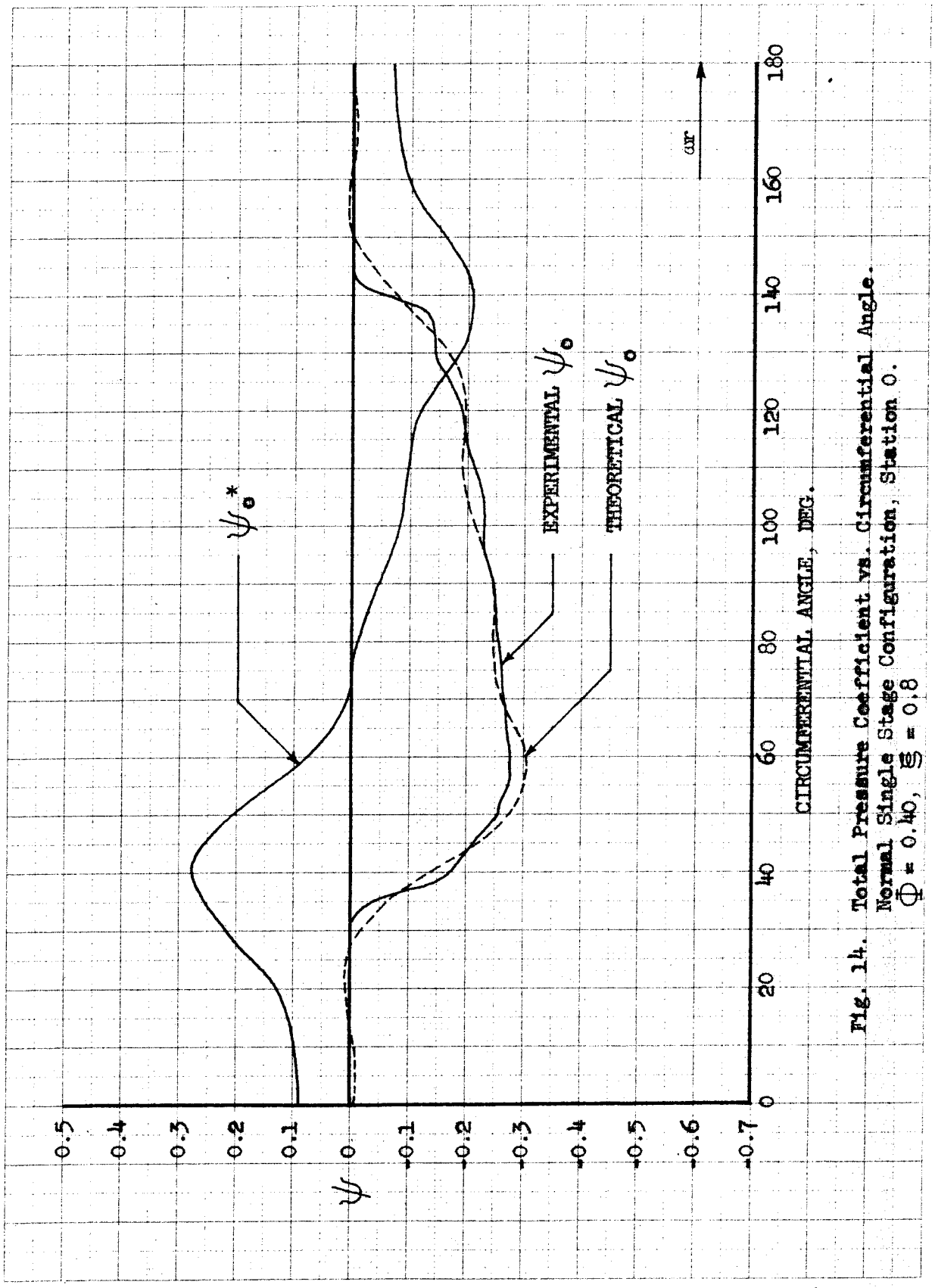

Fig. 14. Total Pressure Coefficient vs. Circumferential Angle.
Normal Single Stage Configuration, Station 0.
$\Phi = 0.40$, $\overline{\sigma} = 0.8$

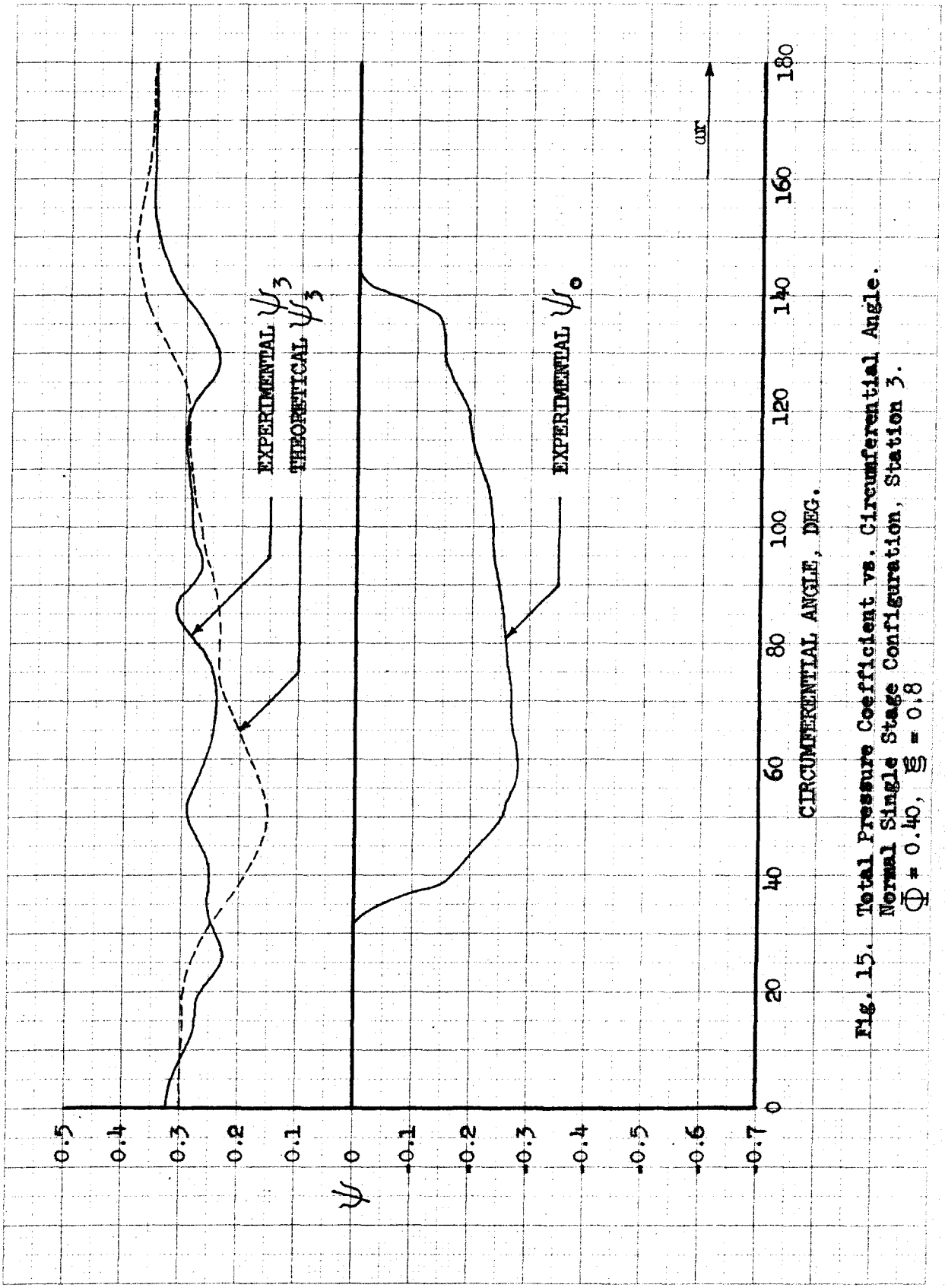

Fig. 15. Total Pressure Coefficient vs. Circumferential Angle.
Normal Single Stage Configuration, Station 3.
$\Phi = 0.40$, $\overline{\omega} = 0.8$

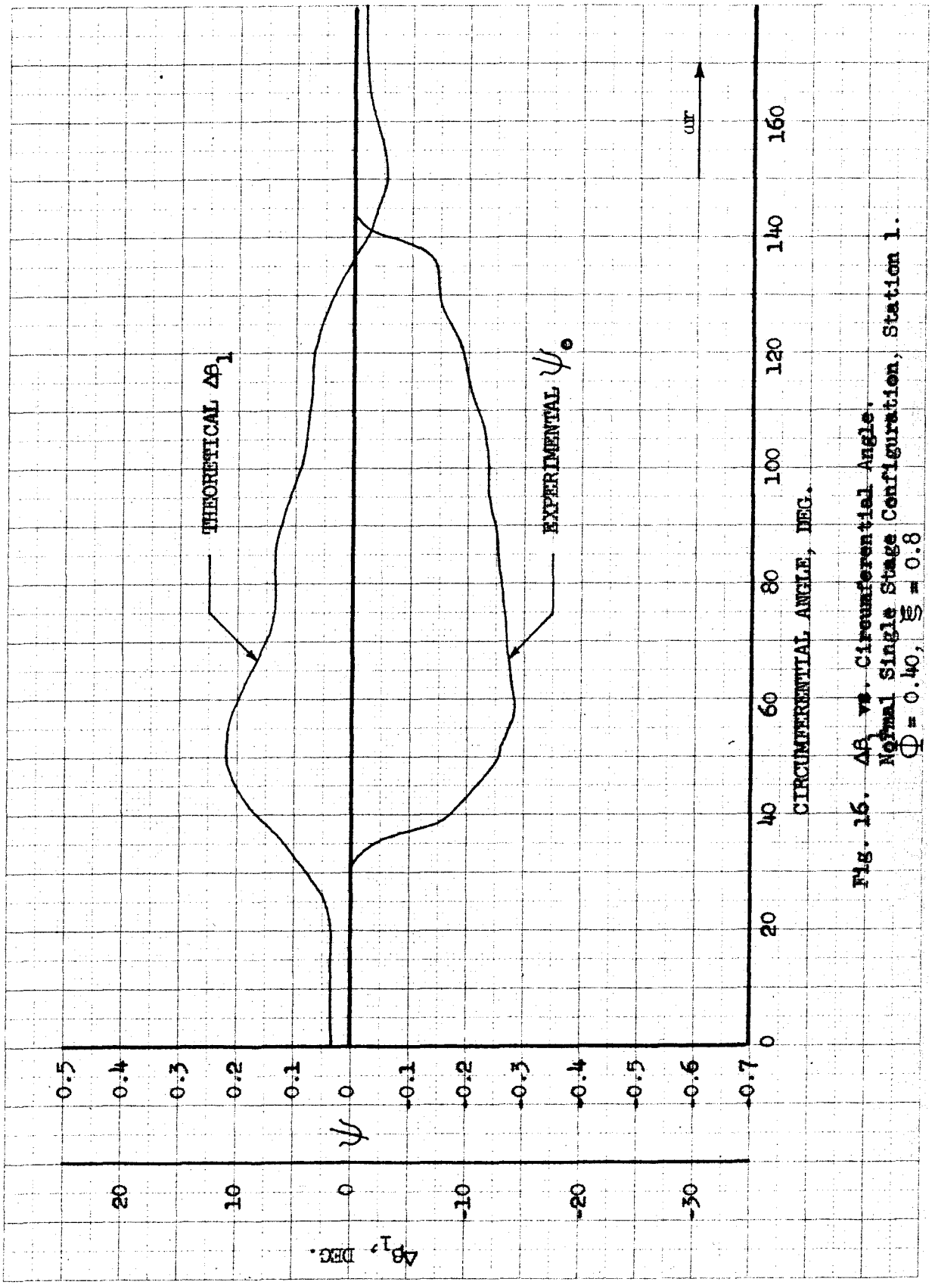

Fig. 16. $\Delta\beta_1$ vs. Circumferential Angle.
Normal Single Stage Configuration, Station 1.
$\Phi = 0.40$, $\bar{\Psi} = 0.8$

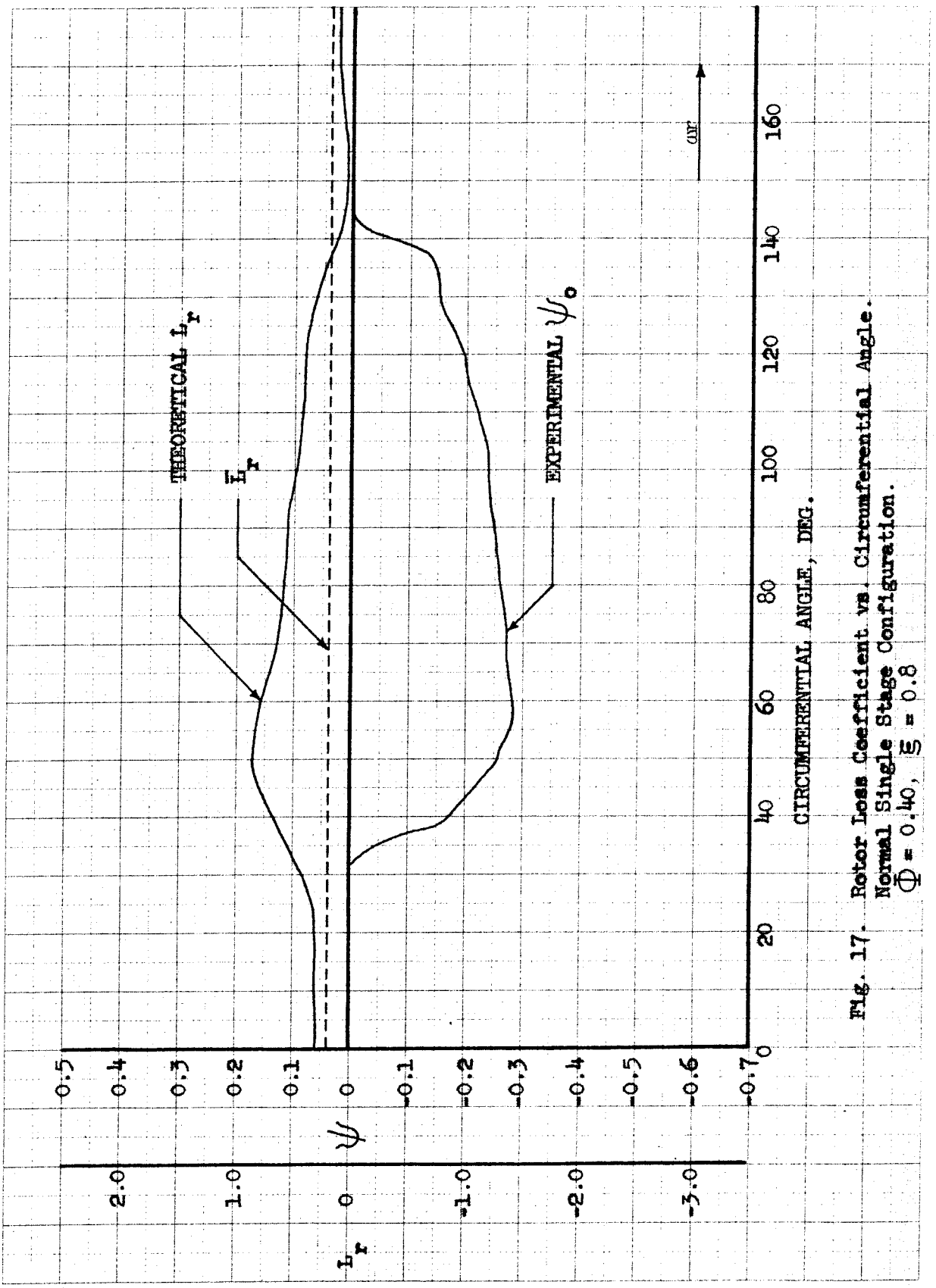

Fig. 17. Rotor Loss Coefficient vs. Circumferential Angle.
Normal Single Stage Configuration.
$\bar{\Phi} = 0.40$, $\bar{\Xi} = 0.8$

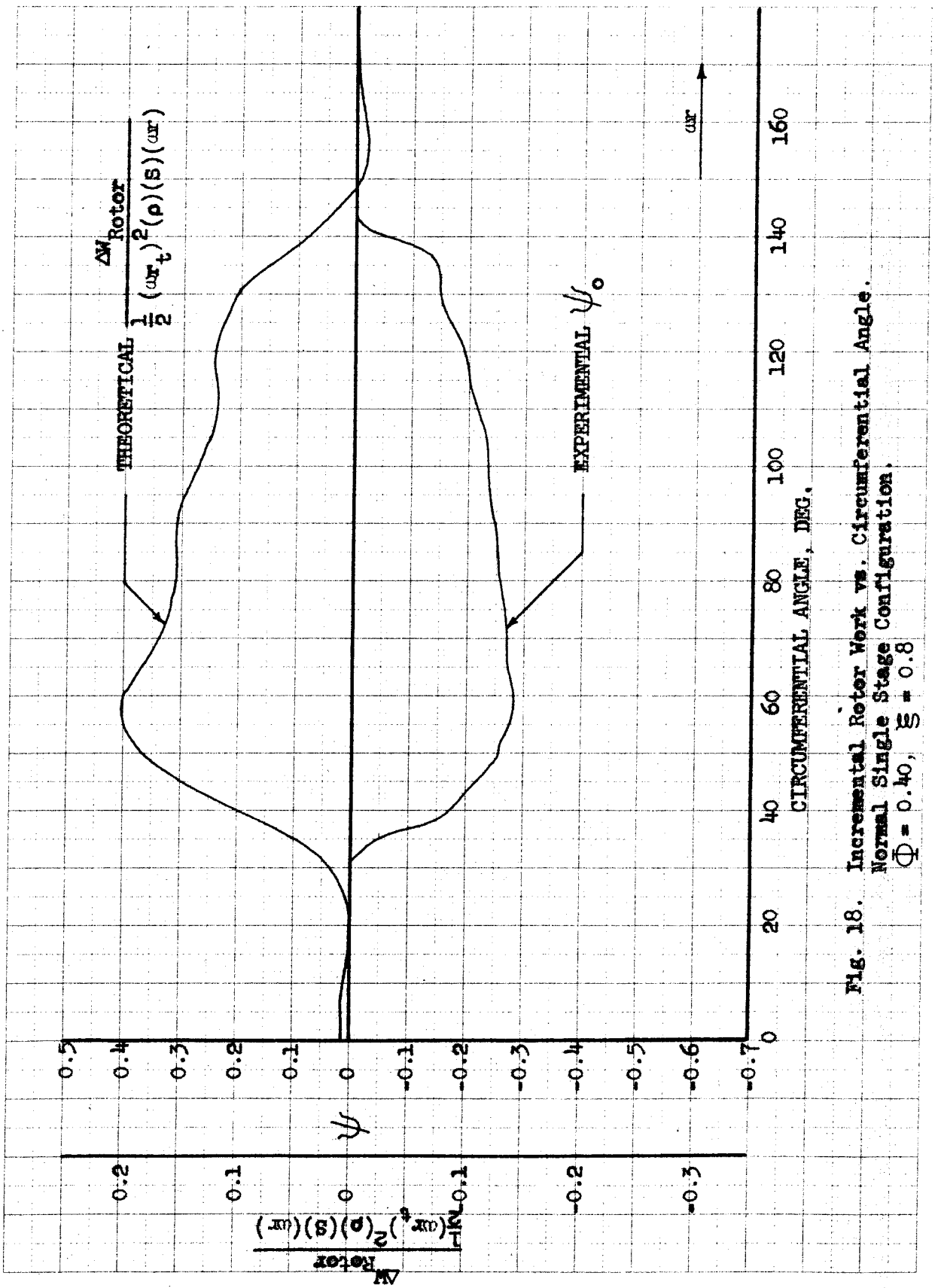

Fig. 18. Incremental Rotor Work vs. Circumferential Angle.
Normal Single Stage Configuration.
$\Phi = 0.40$, $\Sigma = 0.8$

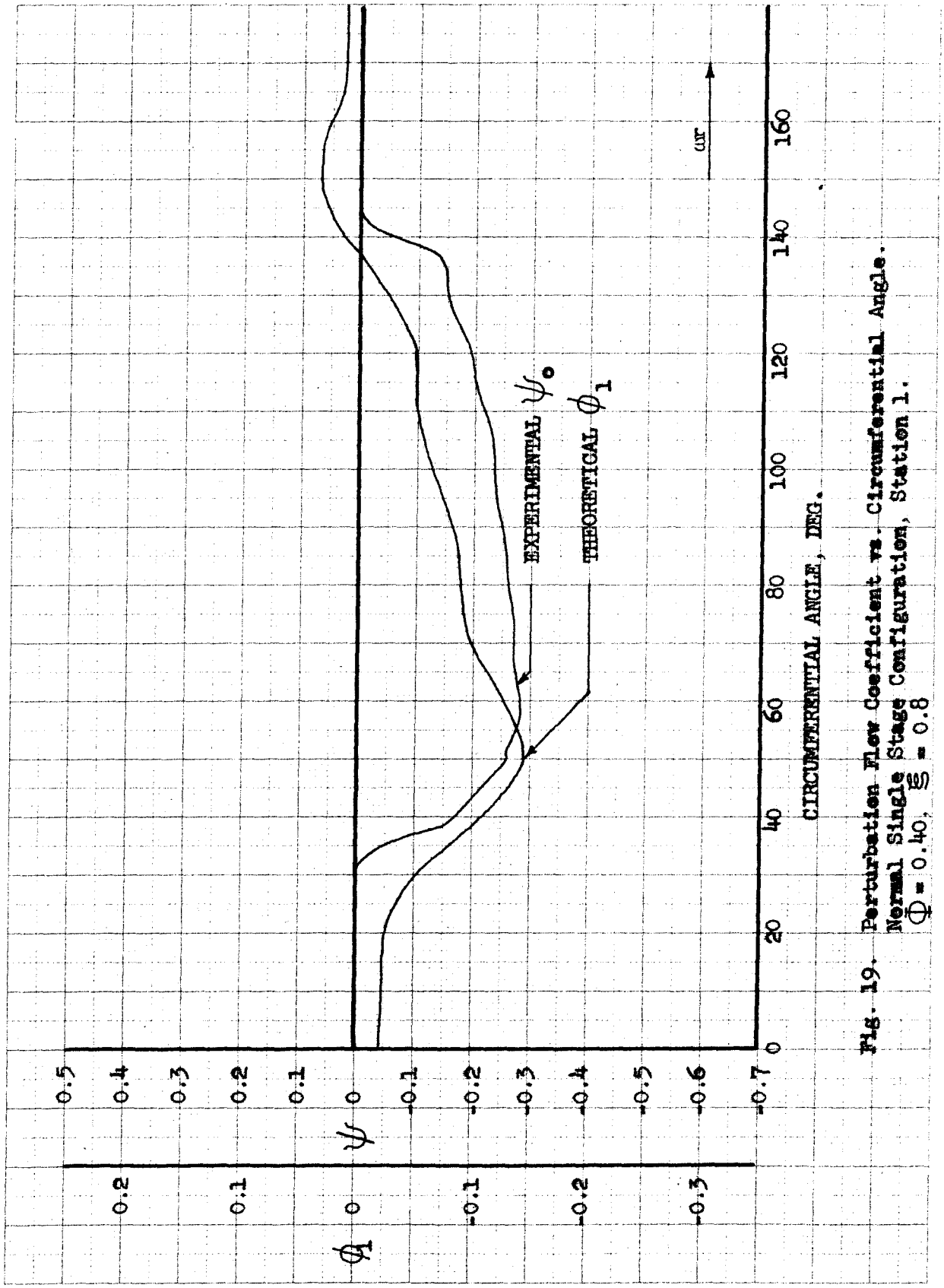

Fig. 19. Perturbation Flow Coefficient vs. Circumferential Angle.
Normal Single Stage Configuration, Station 1.
$\Phi = 0.40$, $\frac{\omega r}{a} = 0.8$

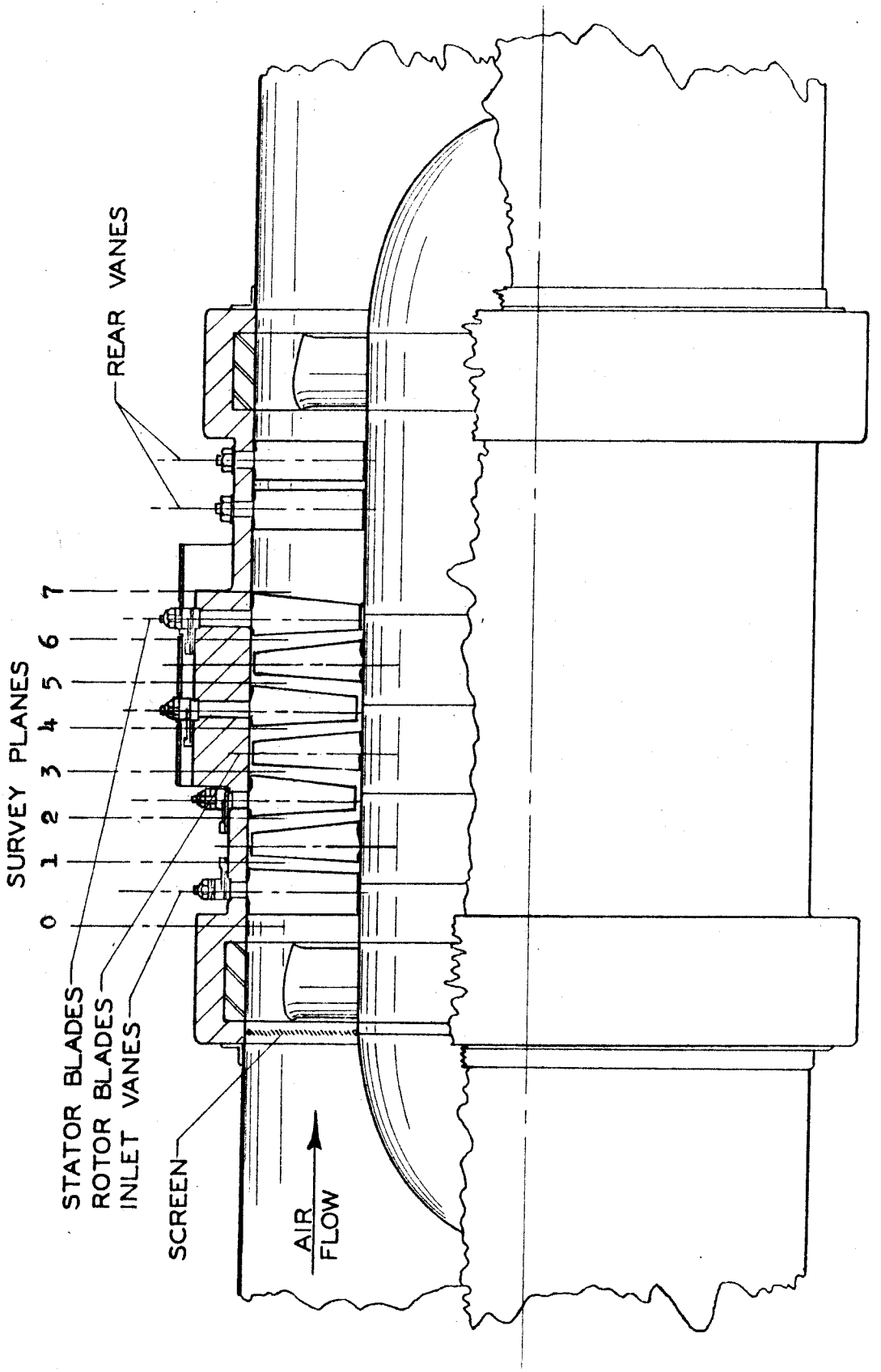

Fig. 20. Three Stage Configuration.

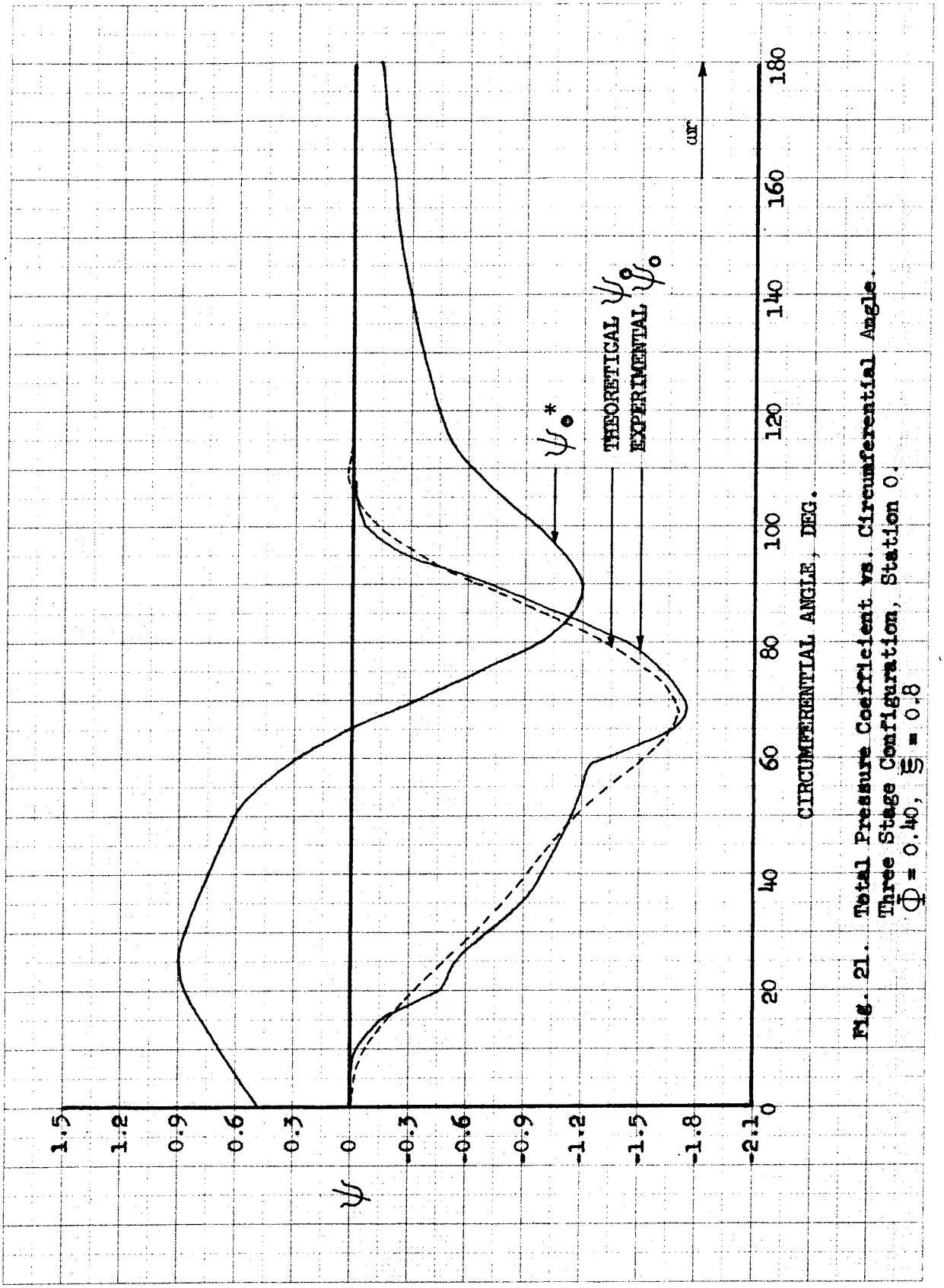

Fig. 21. Total Pressure Coefficient vs. Circumferential Angle.
Three Stage Configuration, Station 0.
$\Phi = 0.40$, $\overline{W} = 0.8$

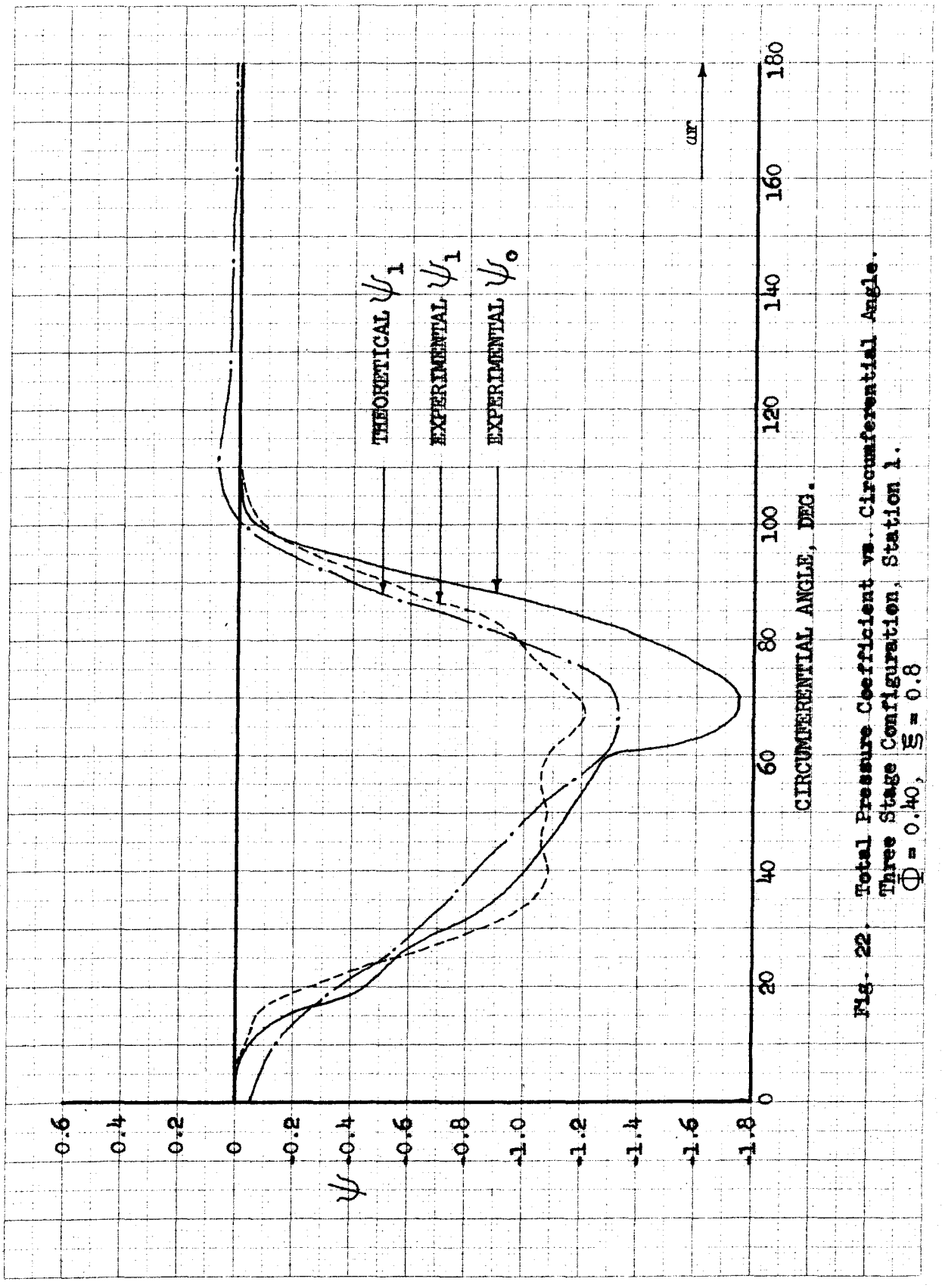

Fig. 22. Total Pressure Coefficient vs. Circumferential Angle.
Three Stage Configuration, Station 1.
$\Phi = 0.40$, $\Xi = 0.8$

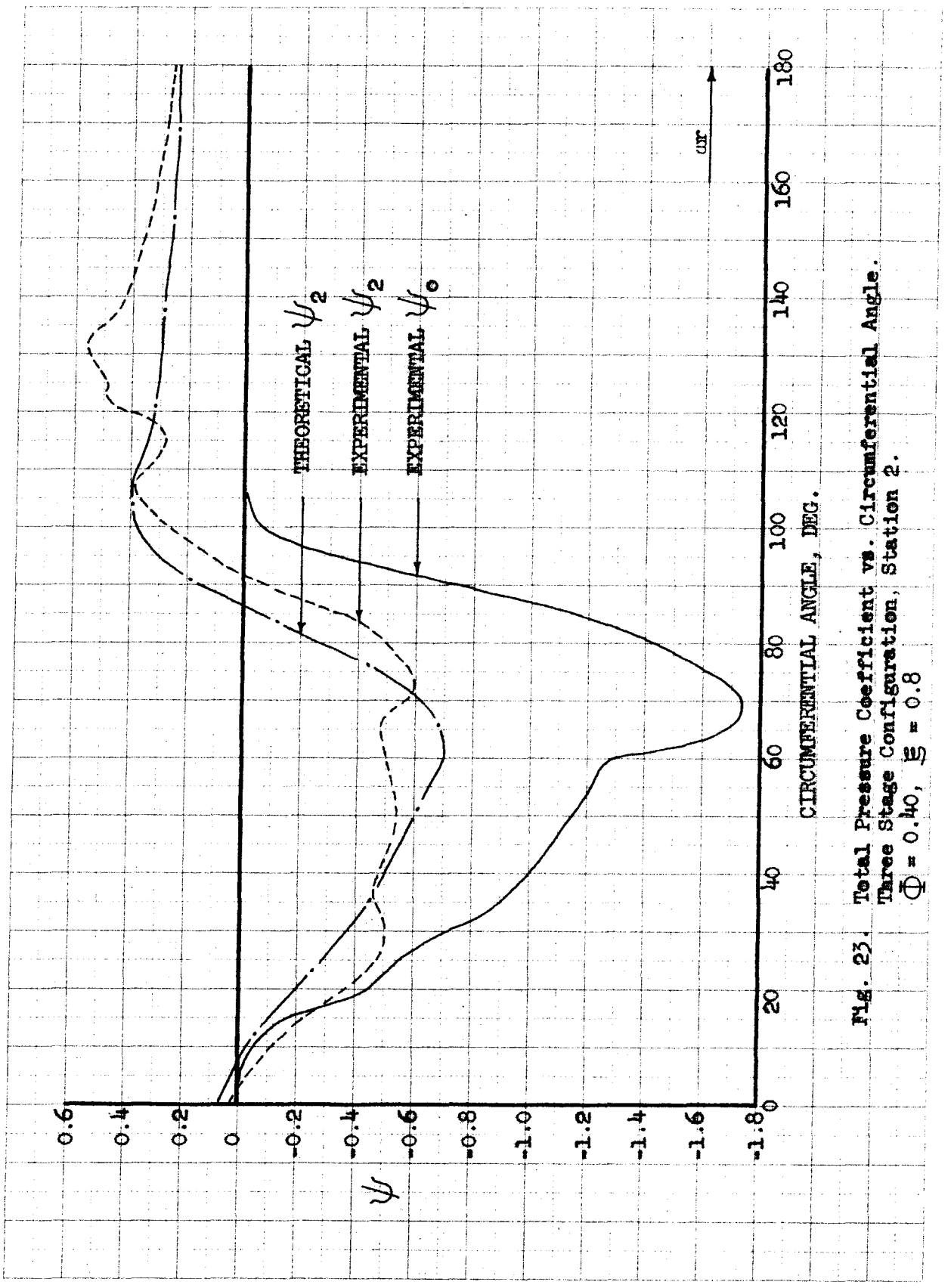

Fig. 23. Total Pressure Coefficient vs. Circumferential Angle. Three Stage Configuration, Station 2. $\Phi = 0.40$, $\bar{\omega} = 0.8$

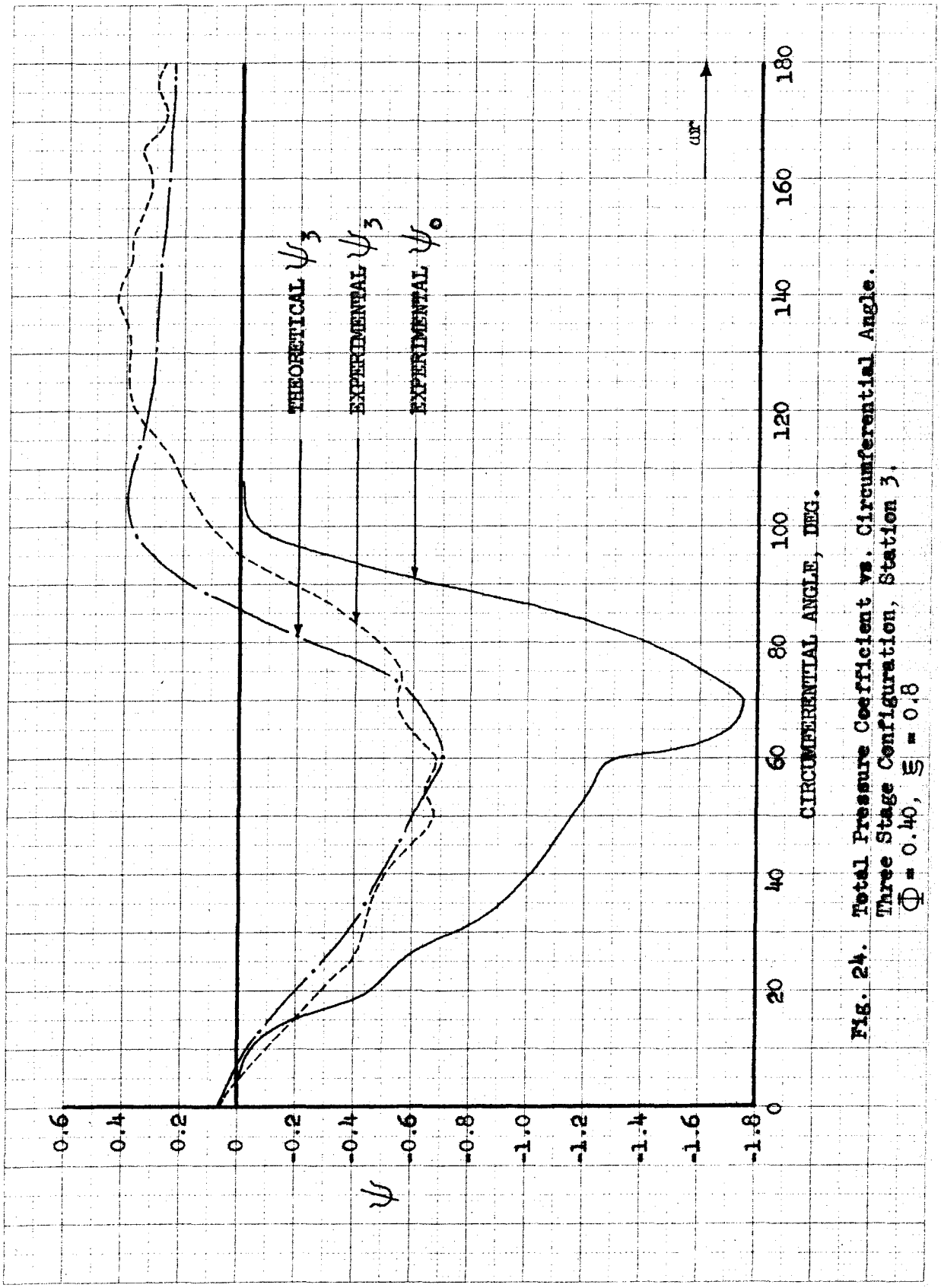

Fig. 24. Total Pressure Coefficient vs. Circumferential Angle.
Three Stage Configuration, Station 3.
$\Phi = 0.40$, $\Xi = 0.8$

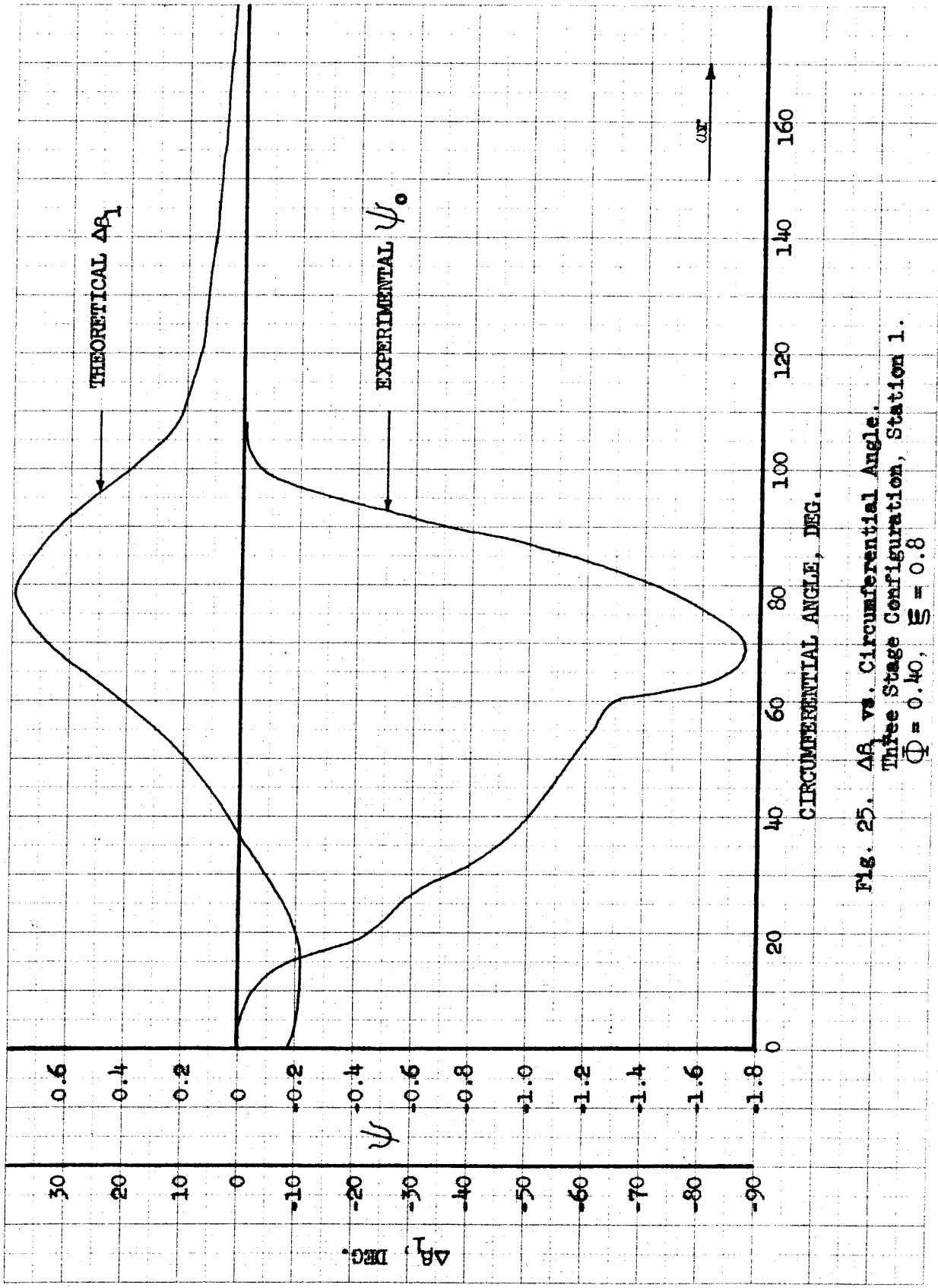

Fig. 25. $\Delta\beta_1$ vs. Circumferential Angle.
Three Stage Configuration, Station 1.
$\bar{\Phi} = 0.40$, $\bar{\Psi} = 0.8$

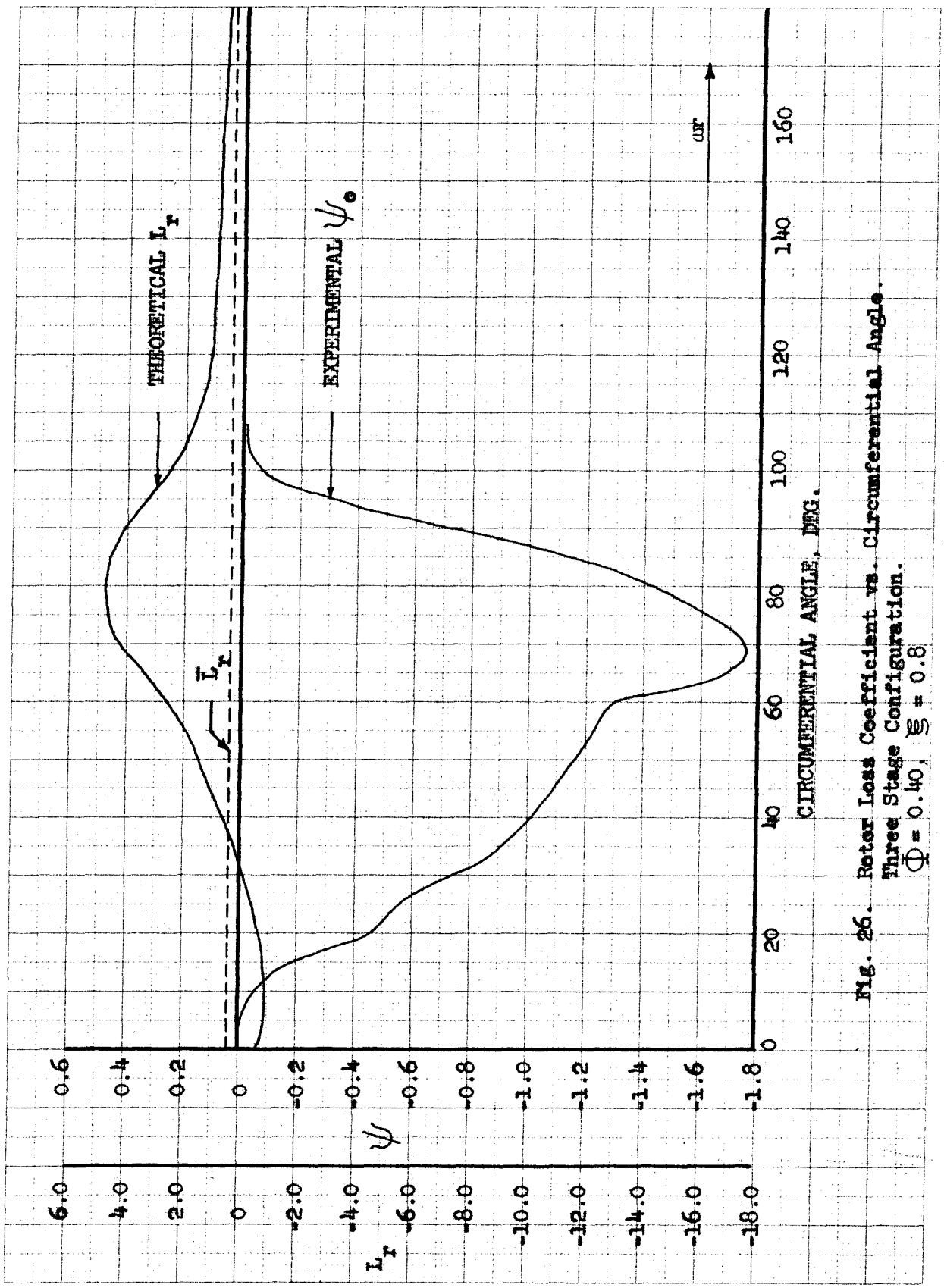

Fig. 26. Rotor Loss Coefficient vs. Circumferential Angle.
Three Stage Configuration.
$\bar{\Phi} = 0.40$, $\bar{\psi} = 0.8$

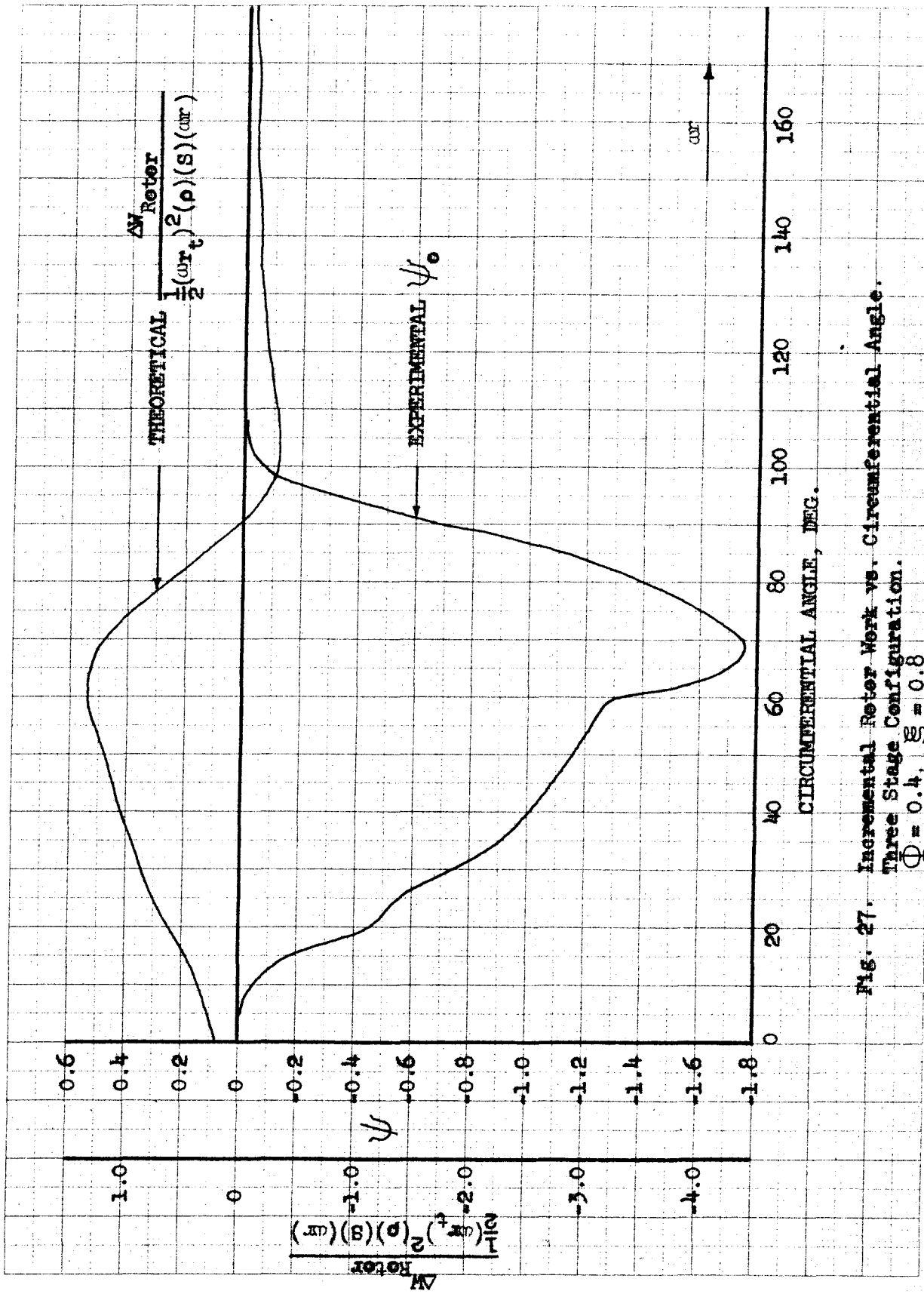

Fig. 27. Incremental Rotor Work vs. Circumferential Angle.
Three Stage Configuration.
$\Phi = 0.4$, $\mathfrak{B} = 0.8$

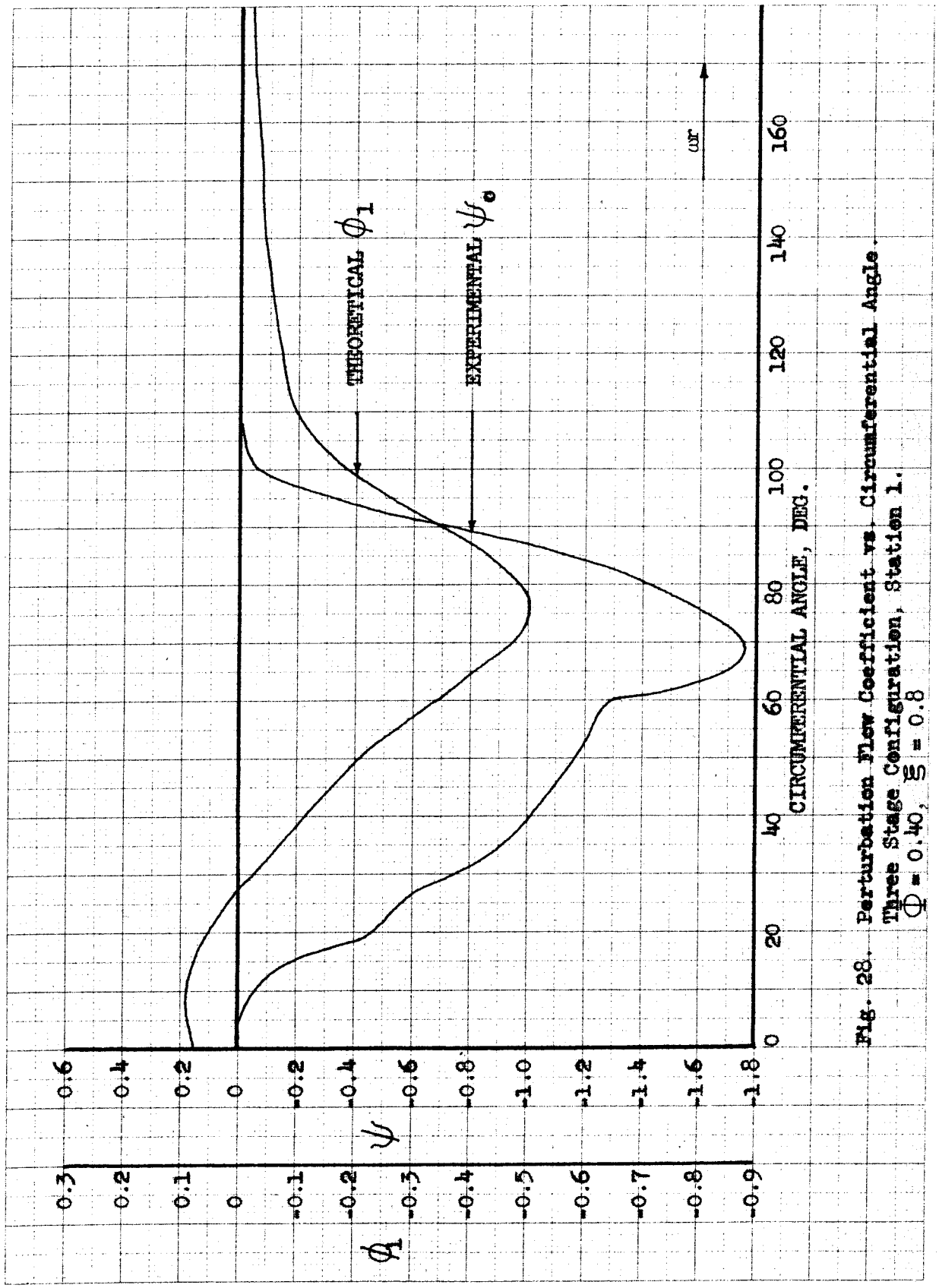

Fig. 28. Perturbation Flow Coefficient vs Circumferential Angle.
Three Stage Configuration, Station 1.
$\Phi = 0.40$, $\overline{\omega} = 0.8$

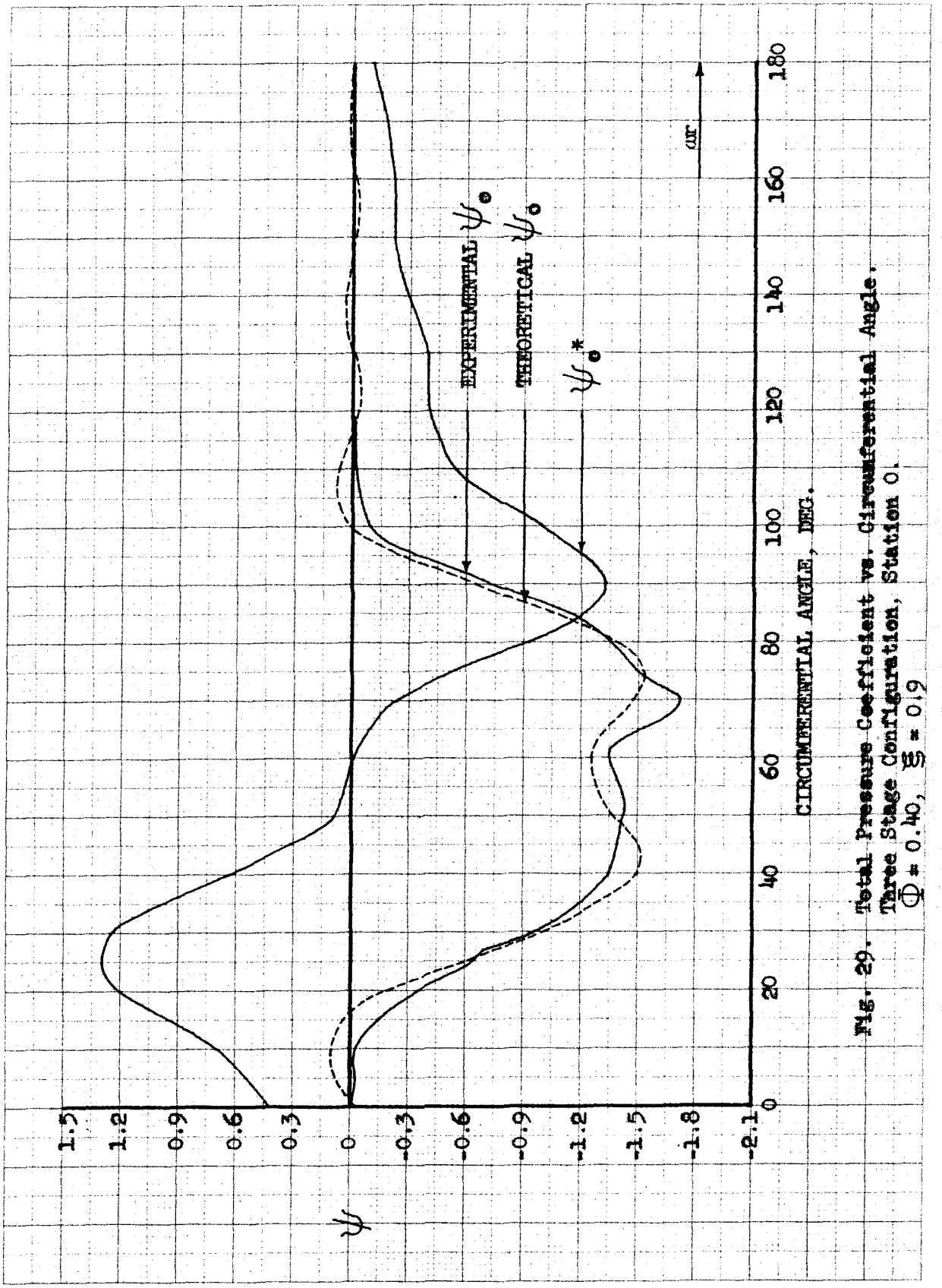

Fig. 29. Total Pressure Coefficient vs. Circumferential Angle, Three Stage Configuration, Station 0, $\Phi = 0.40$, $\overline{\Psi} = 0.9$

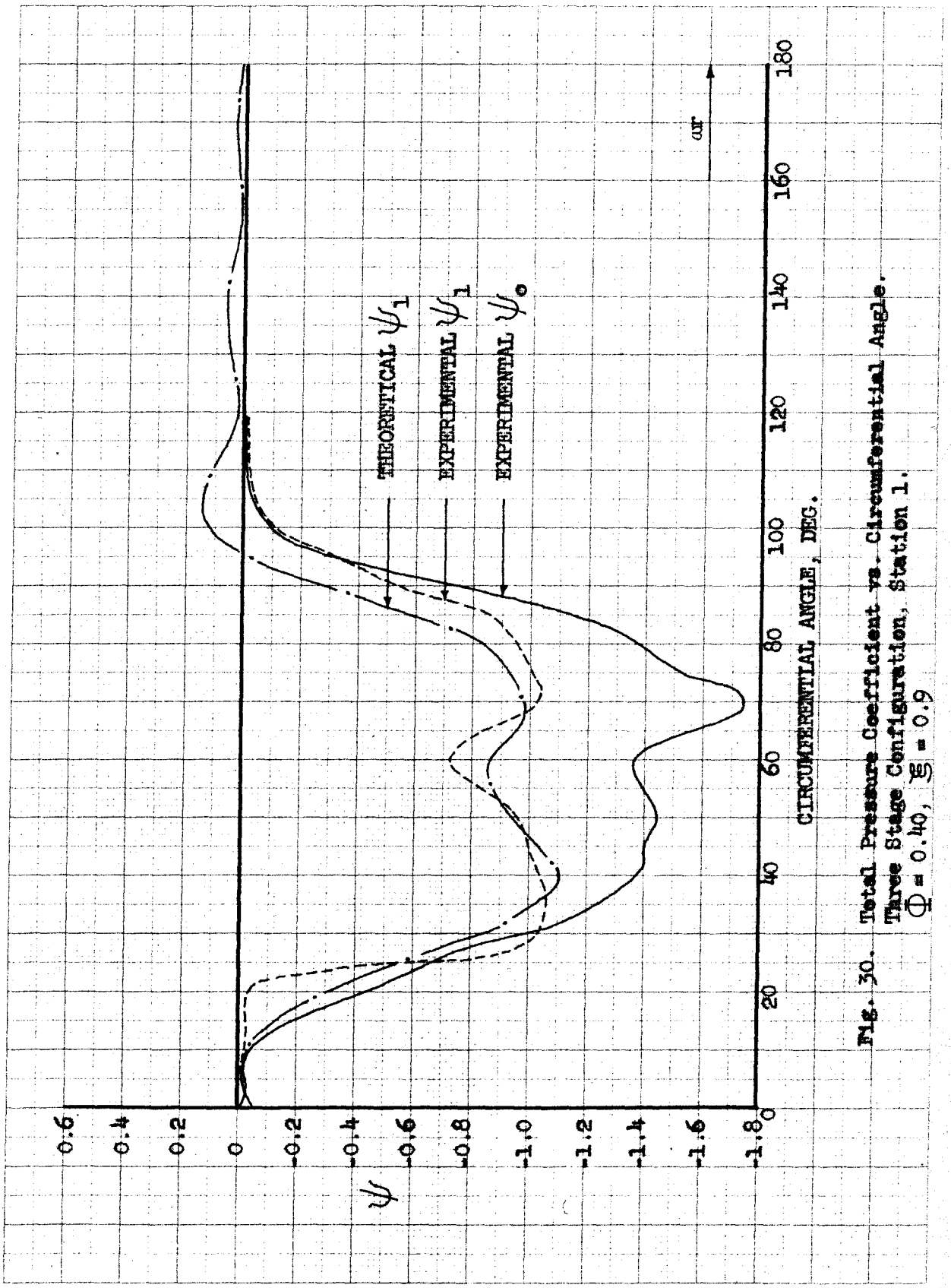

Fig. 30. Total Pressure Coefficient vs. Circumferential Angle.
Three Stage Configuration, Station 1.
$\Phi = 0.40$, $\overline{\omega} = 0.9$

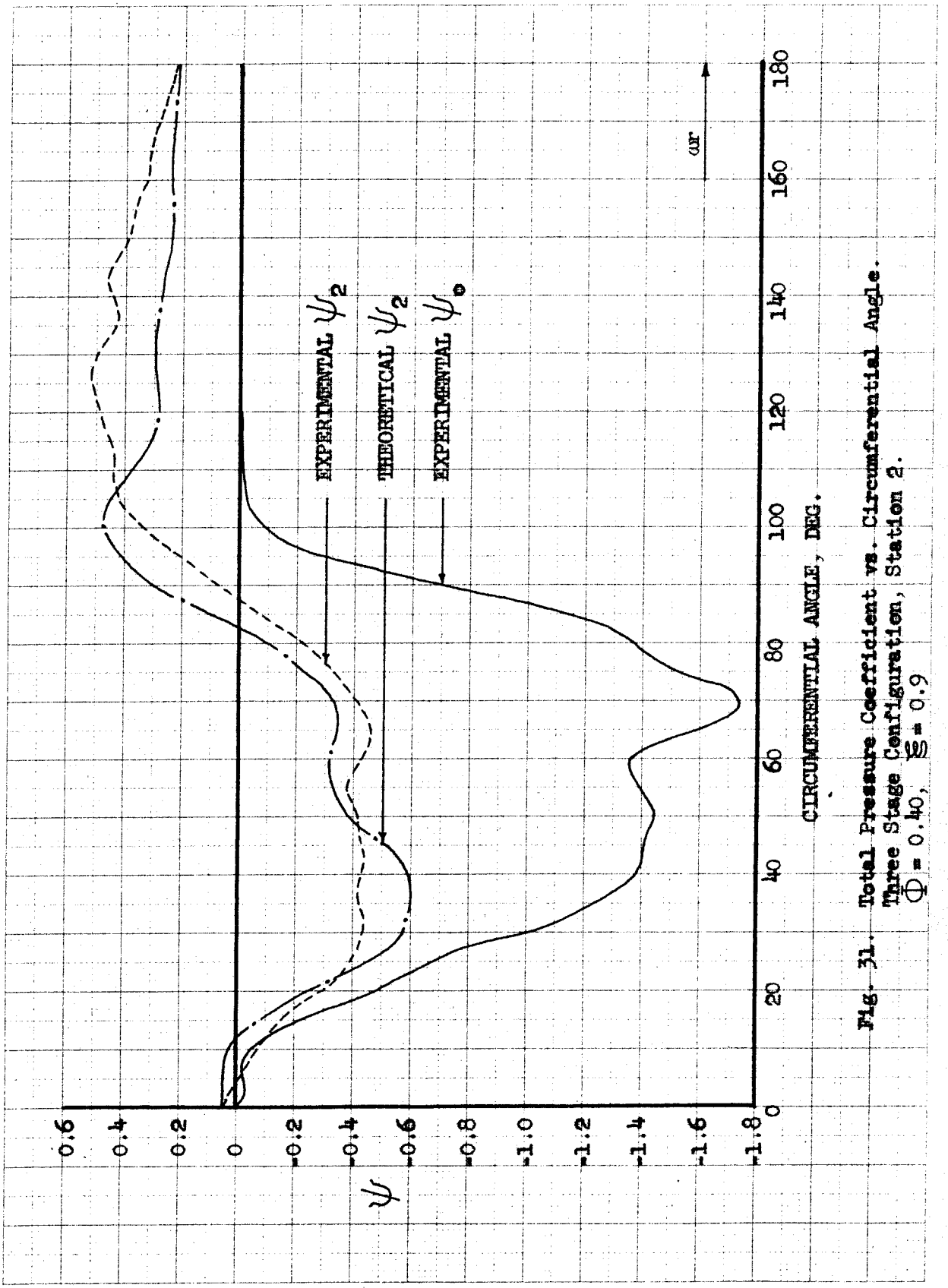

Fig. 31. Total Pressure Coefficient vs. Circumferential Angle. Three Stage Configuration, Station 2. $\Phi = 0.40$, $\Omega = 0.9$

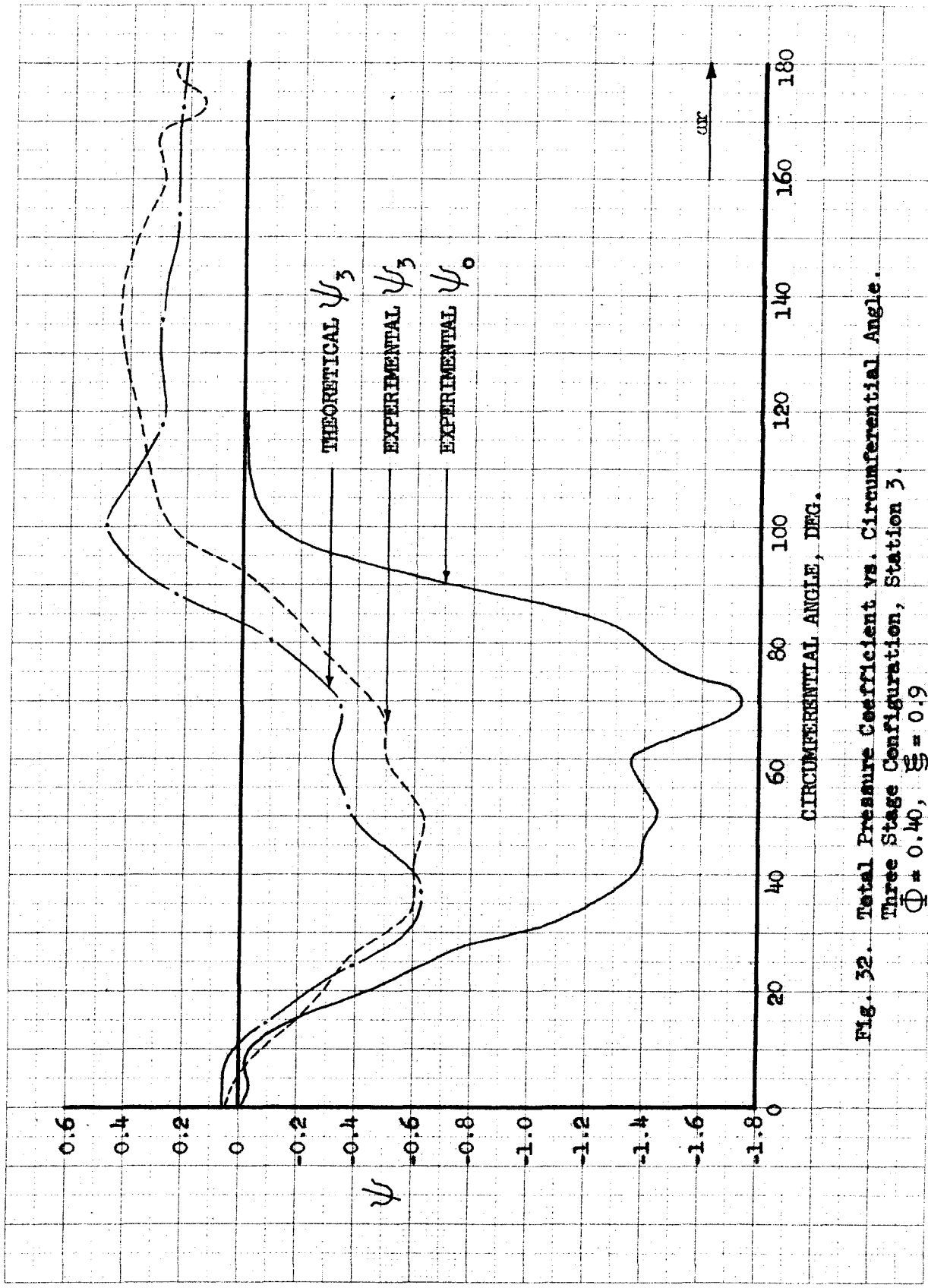

Fig. 32. Total Pressure Coefficient vs. Circumferential Angle. Three Stage Configuration, Station 3. $\Phi = 0.40$, $\bar{\Psi} = 0.9$

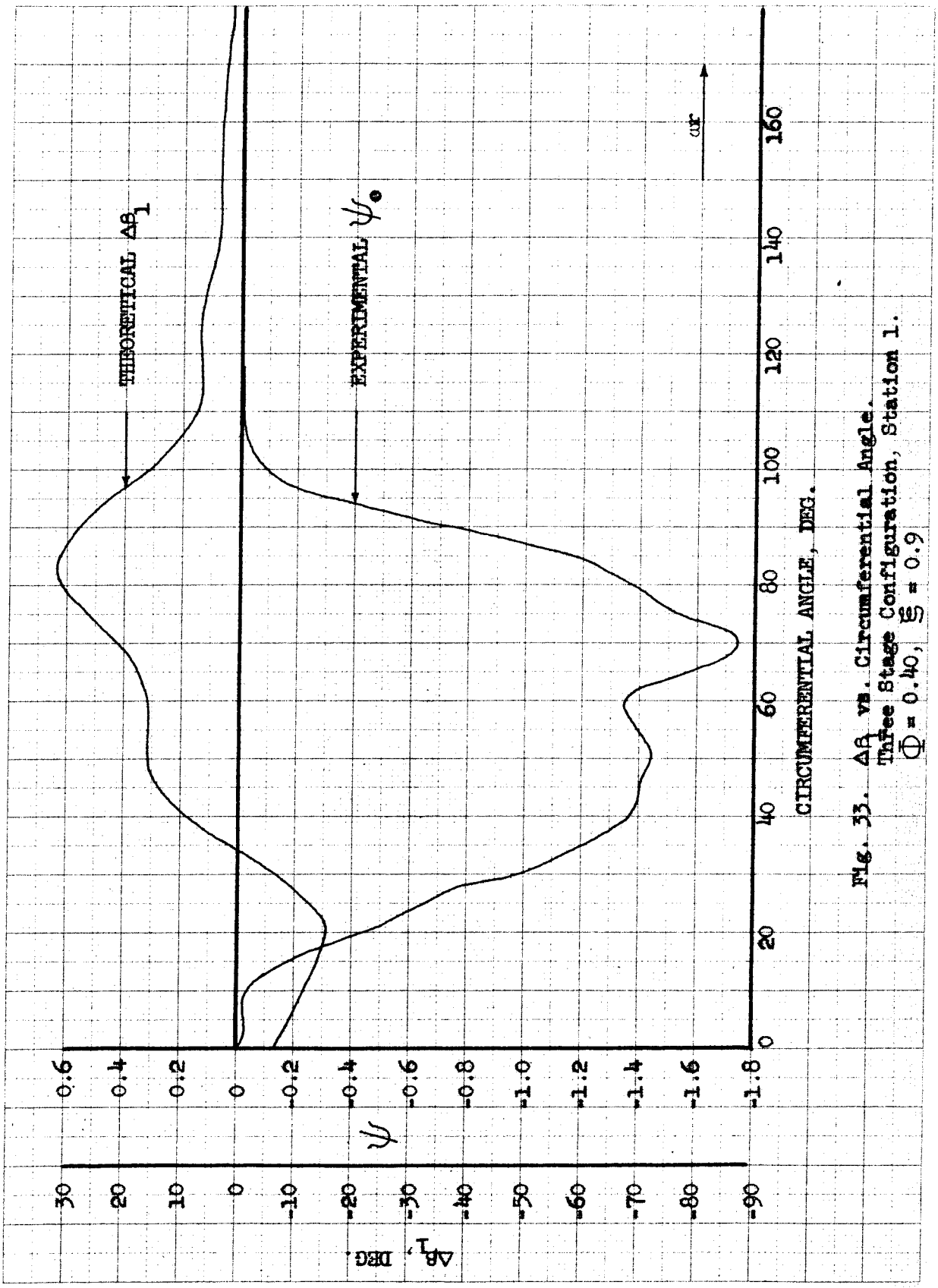

Fig. 33. $\Delta\beta_1$ vs. Circumferential Angle.
Three Stage Configuration, Station 1.
$\Phi = 0.40$, $\mathbb{S} = 0.9$

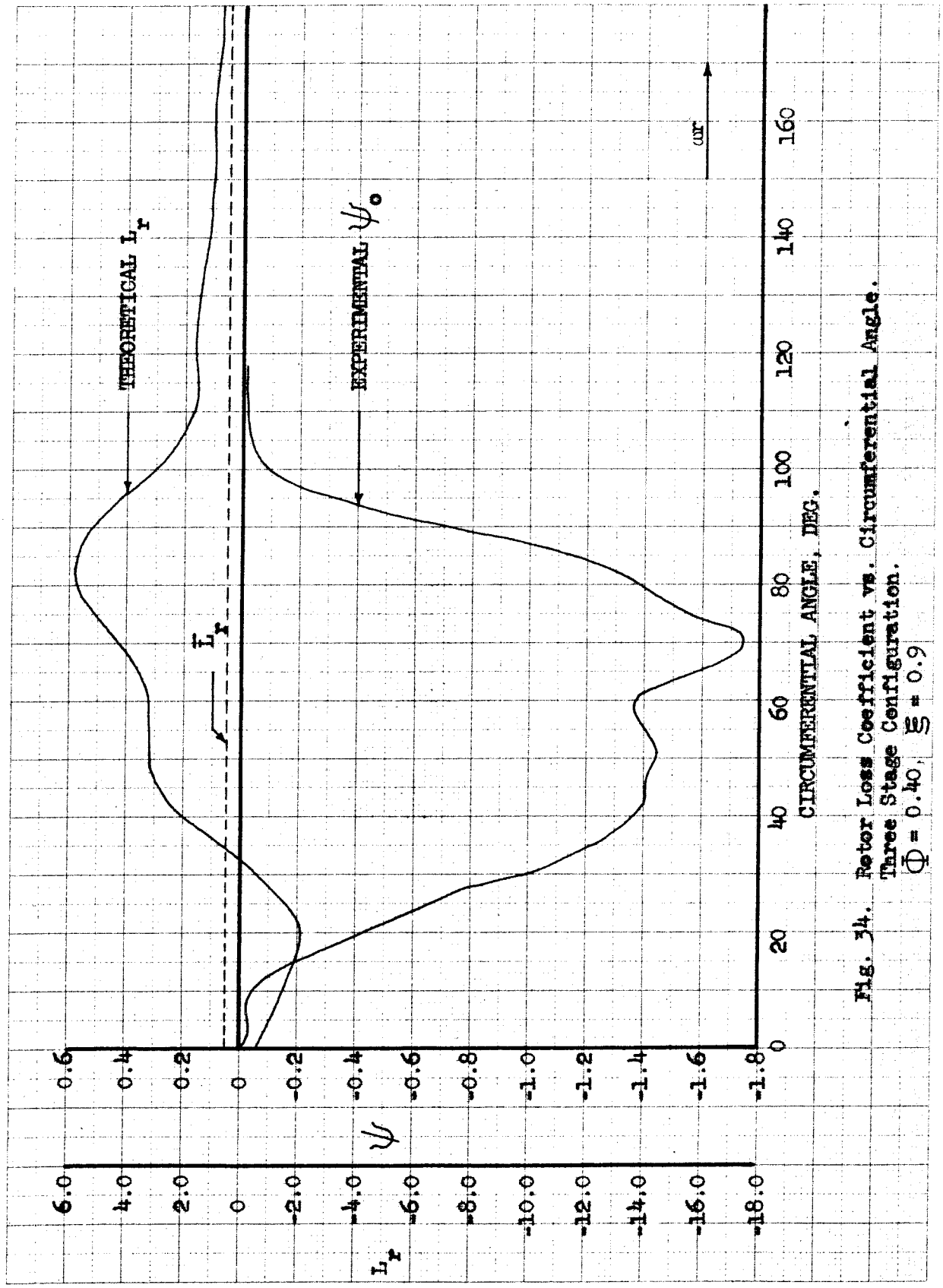

Fig. 34. Rotor Loss Coefficient vs. Circumferential Angle. Three Stage Configuration. $\bar{\Phi} = 0.40$, $\bar{\sigma} = 0.9$

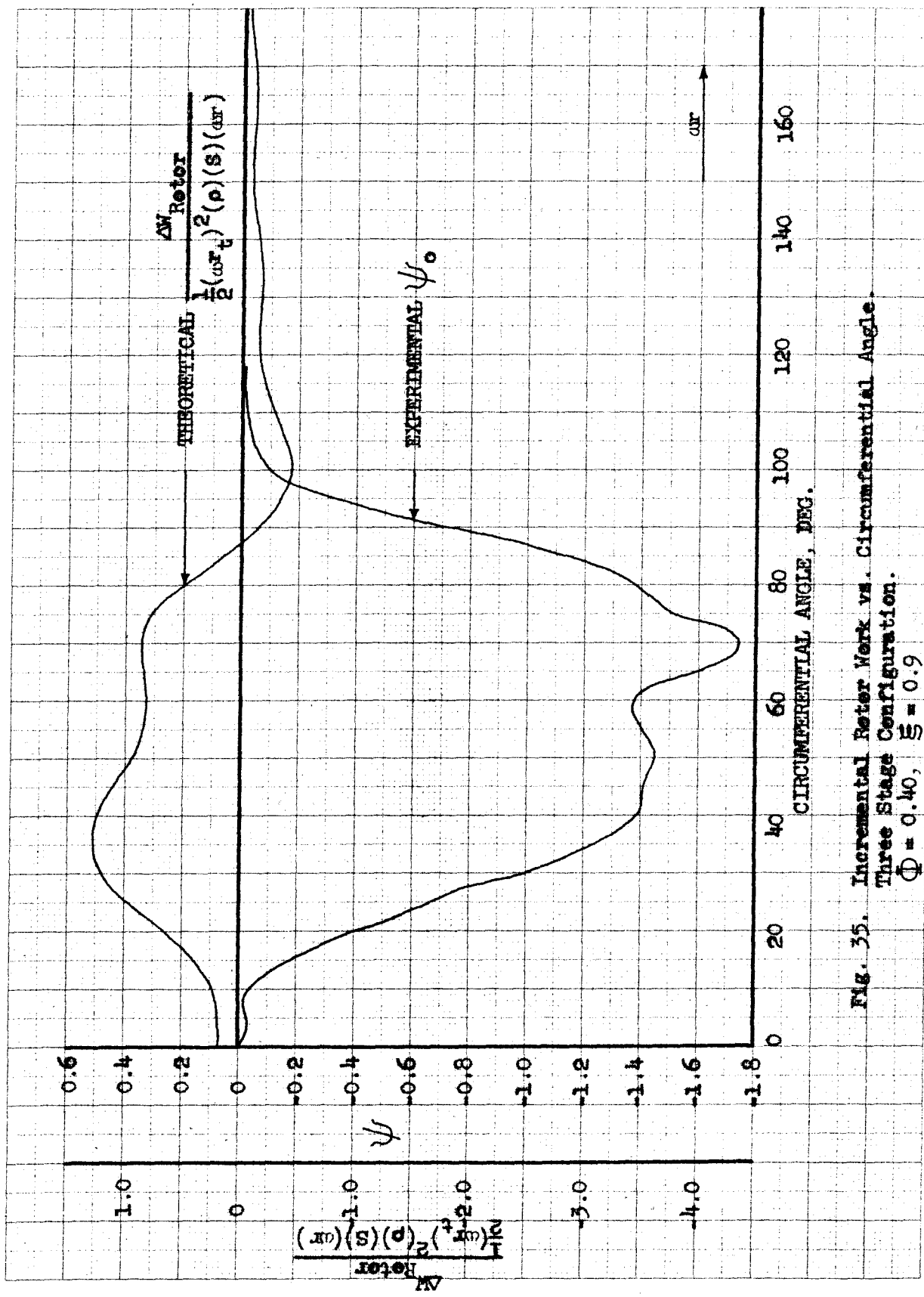

Fig. 35. Incremental Rotor Work vs. Circumferential Angle. Three Stage Configuration. $\Phi = 0.40$, $\overline{S} = 0.9$

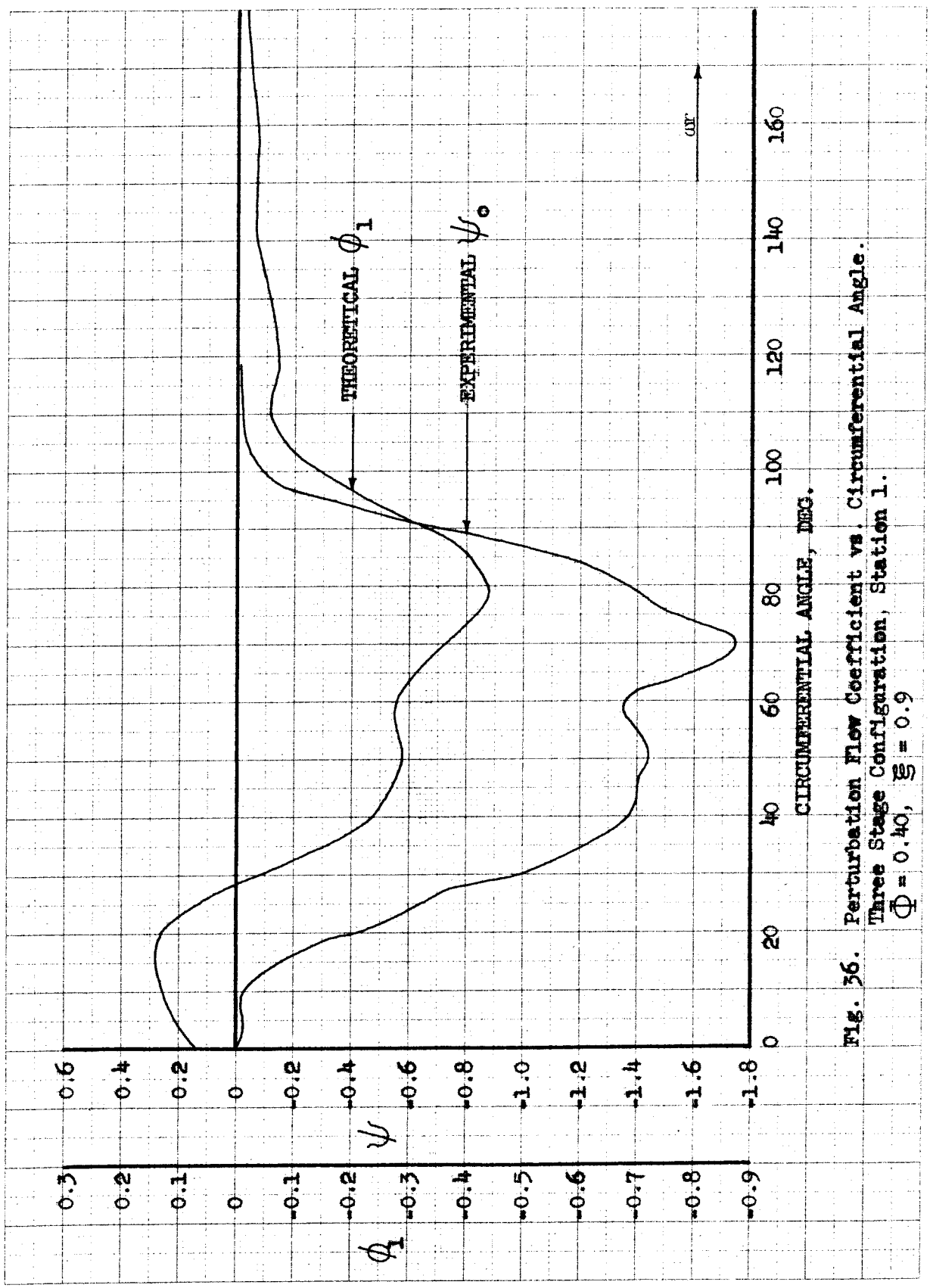

Fig. 36. Perturbation Flow Coefficient vs. Circumferential Angle.
Three Stage Configuration, Station 1.
$\Phi = 0.40$, $\overline{\omega} = 0.9$

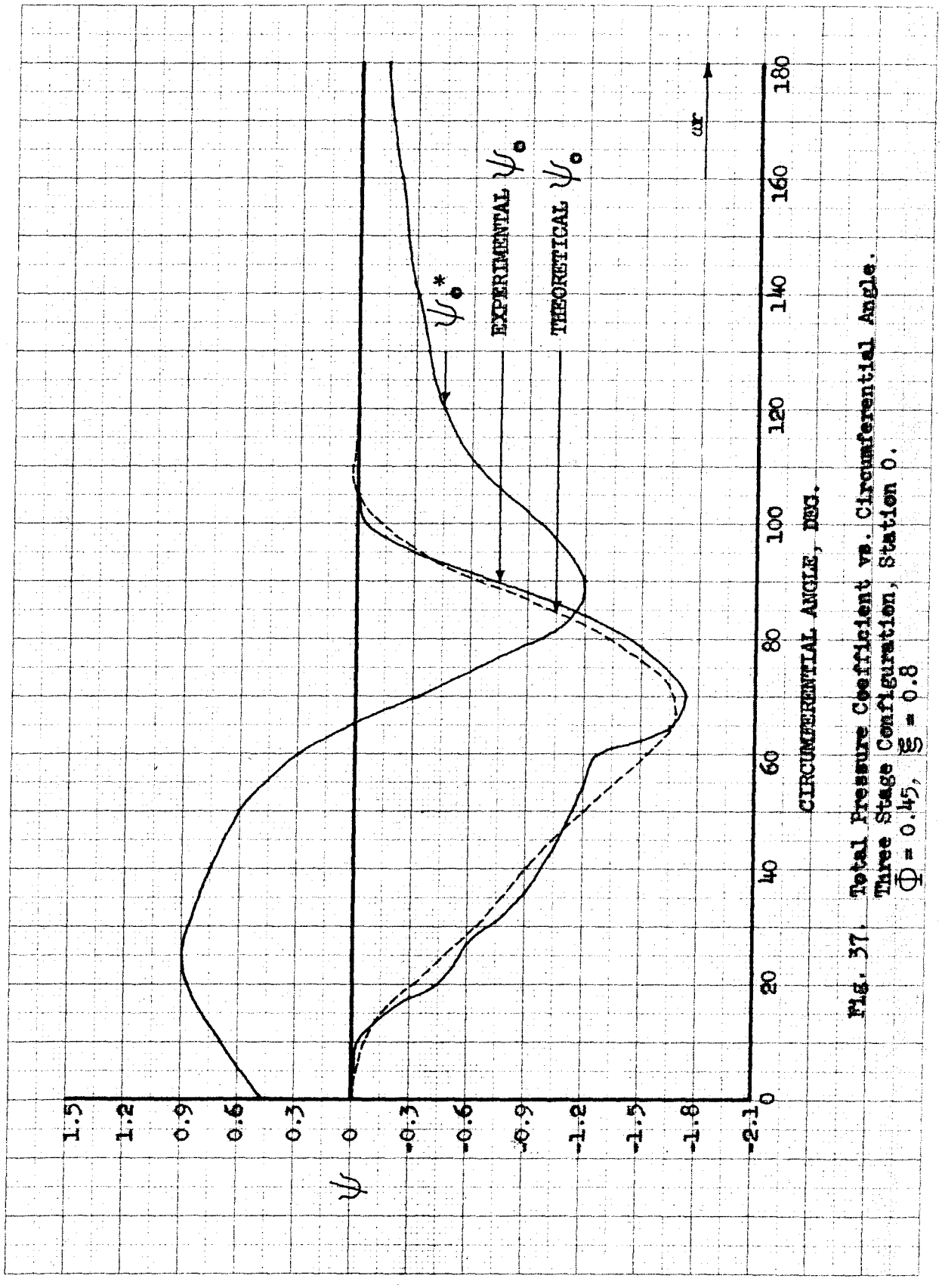

Fig. 37 Total Pressure Coefficient vs. Circumferential Angle.
Three Stage Configuration, Station 0.
$\Phi = 0.45$, $\Xi = 0.8$

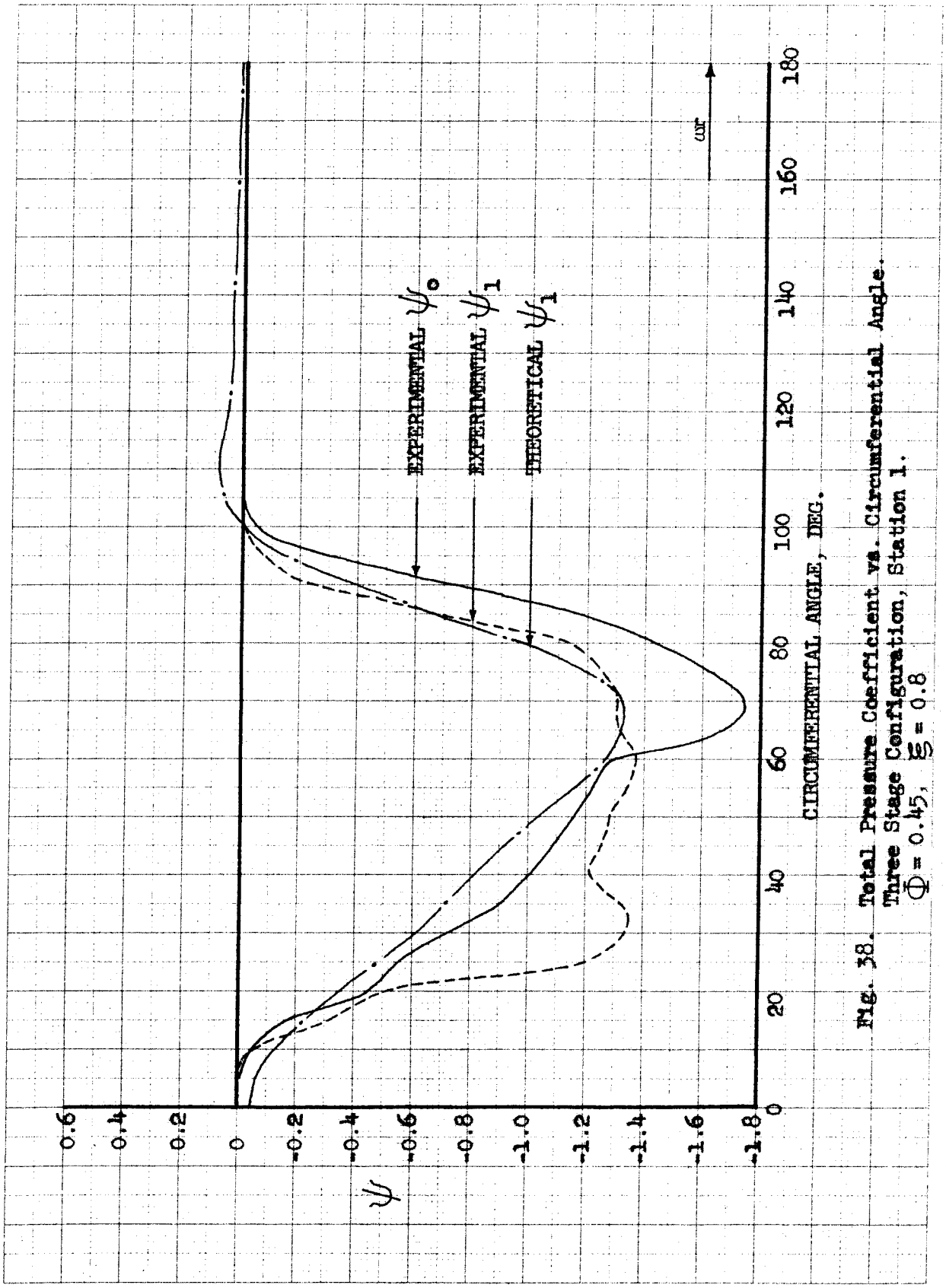

Fig. 38. Total Pressure Coefficient vs. Circumferential Angle. Three Stage Configuration, Station 1. $\bar{\Phi} = 0.45$, $\bar{\psi} = 0.8$

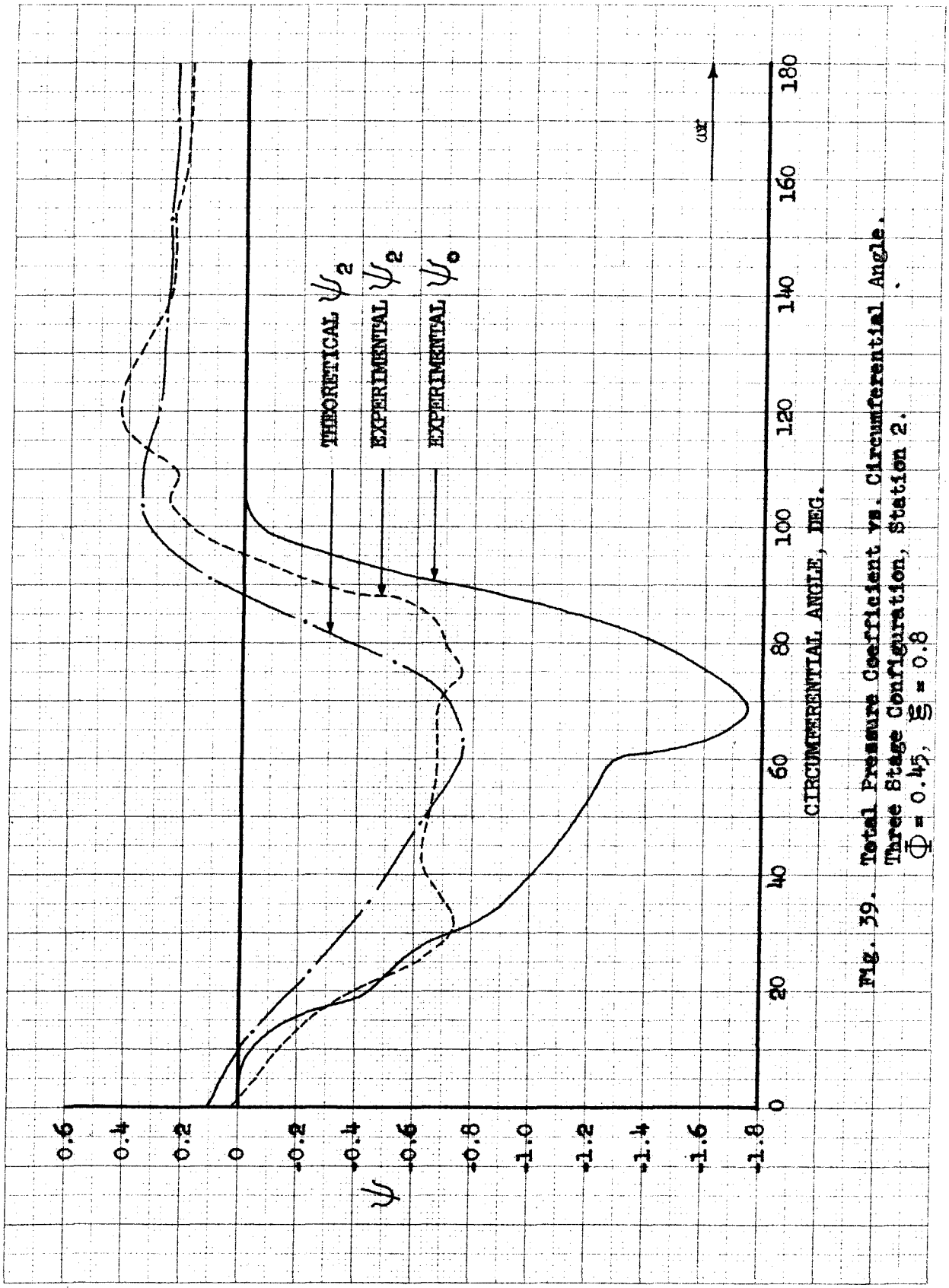

Fig. 39. Total Pressure Coefficient vs. Circumferential Angle.
Three Stage Configuration, Station 2.
$\Phi = 0.45$, $\Xi = 0.8$

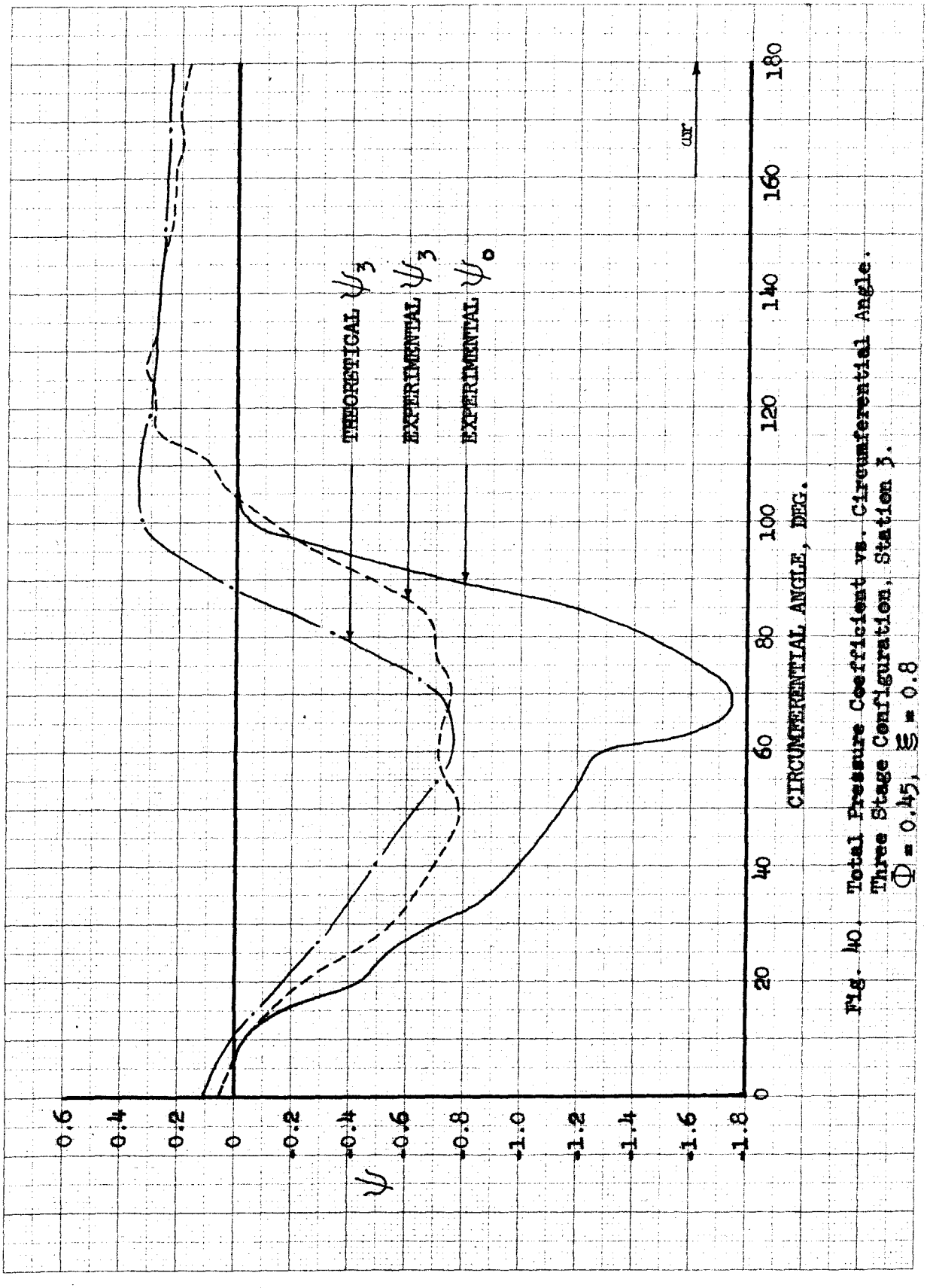

Fig. 40. Total Pressure Coefficient vs. Circumferential Angle. Three Stage Configuration, Station 3. $\Phi = 0.45$, $\bar{\omega} = 0.8$

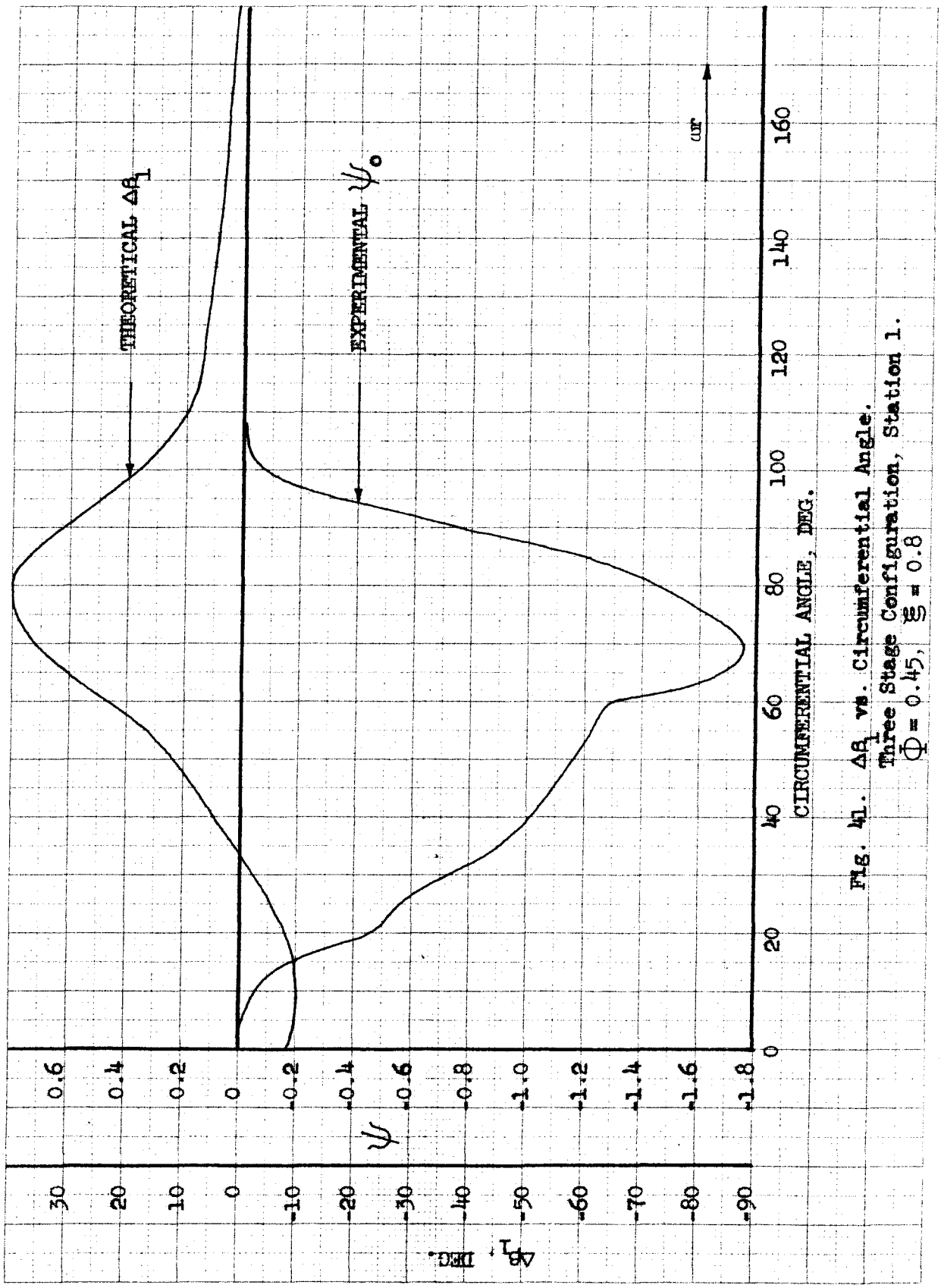

Fig. 41. $\Delta\beta_1$ vs. Circumferential Angle.
Three Stage Configuration, Station 1.
$\Phi = 0.45$, $\bar{\omega} = 0.8$

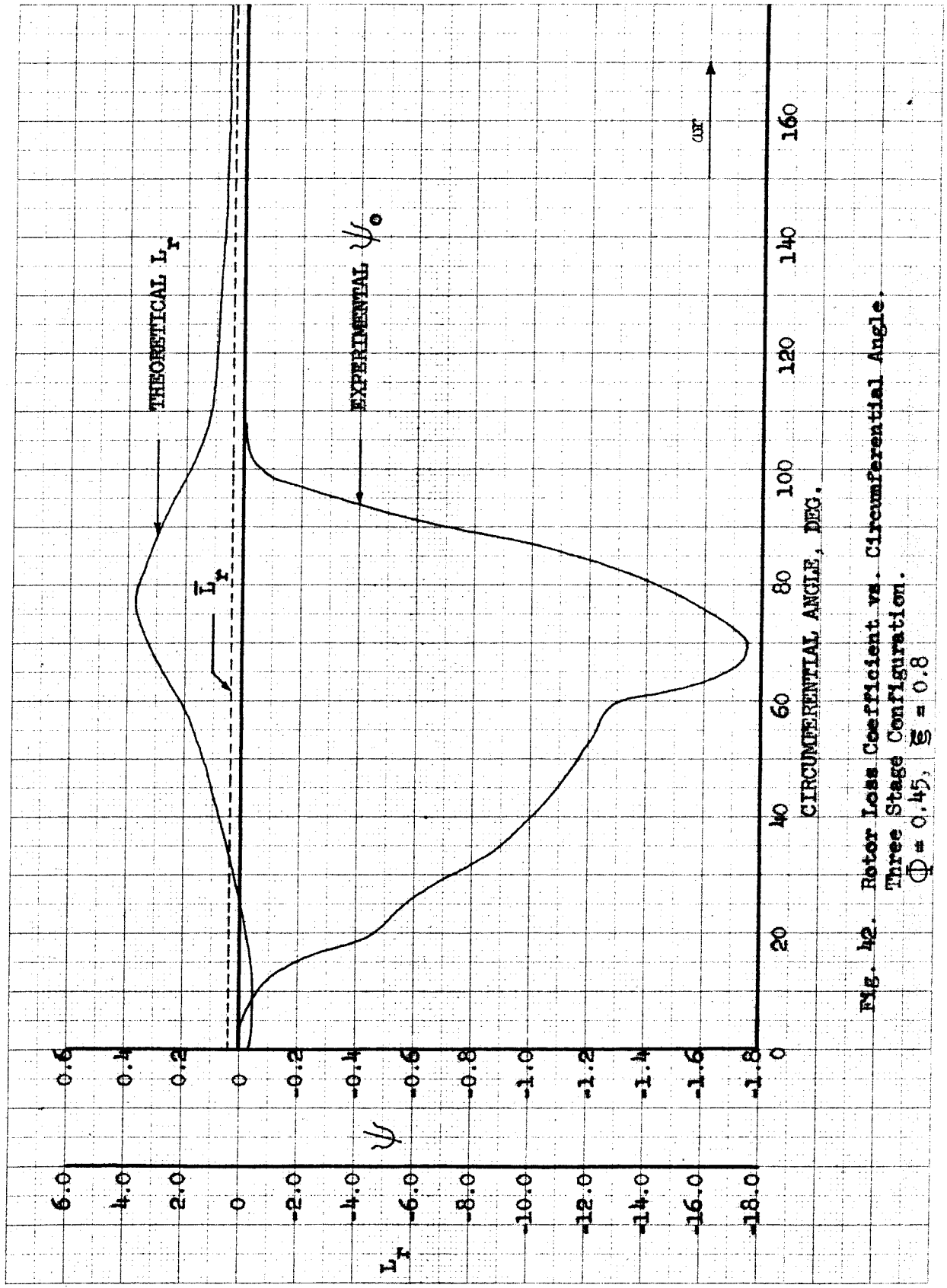

Fig. 42. Rotor Loss Coefficient vs. Circumferential Angle. Three Stage Configuration. $\Phi = 0.45$, $\mathfrak{S} = 0.8$

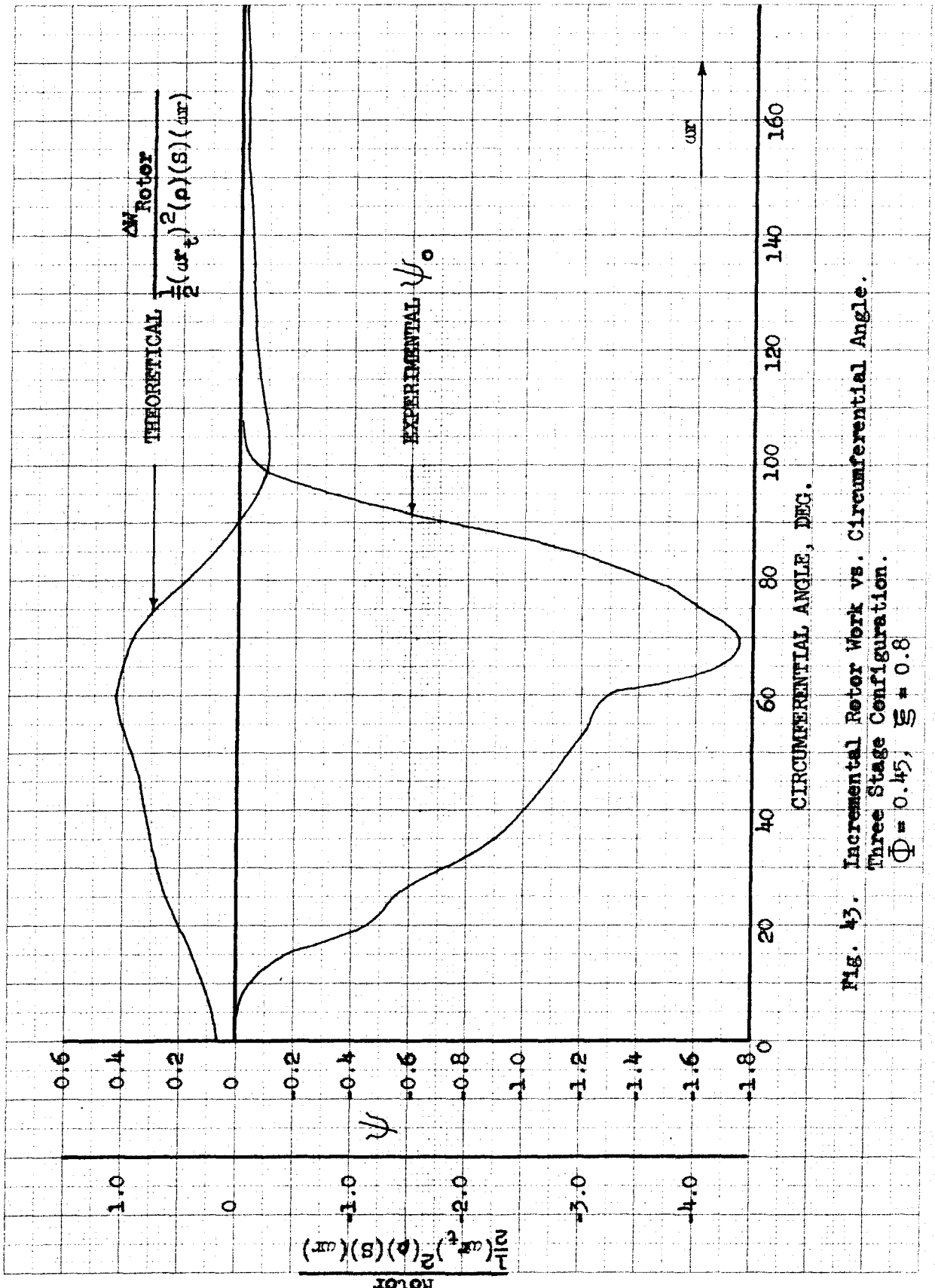

Fig. 43. Incremental Rotor Work vs. Circumferential Angle.
Three Stage Configuration.
$\Phi = 0.45$; $\overline{S} = 0.8$

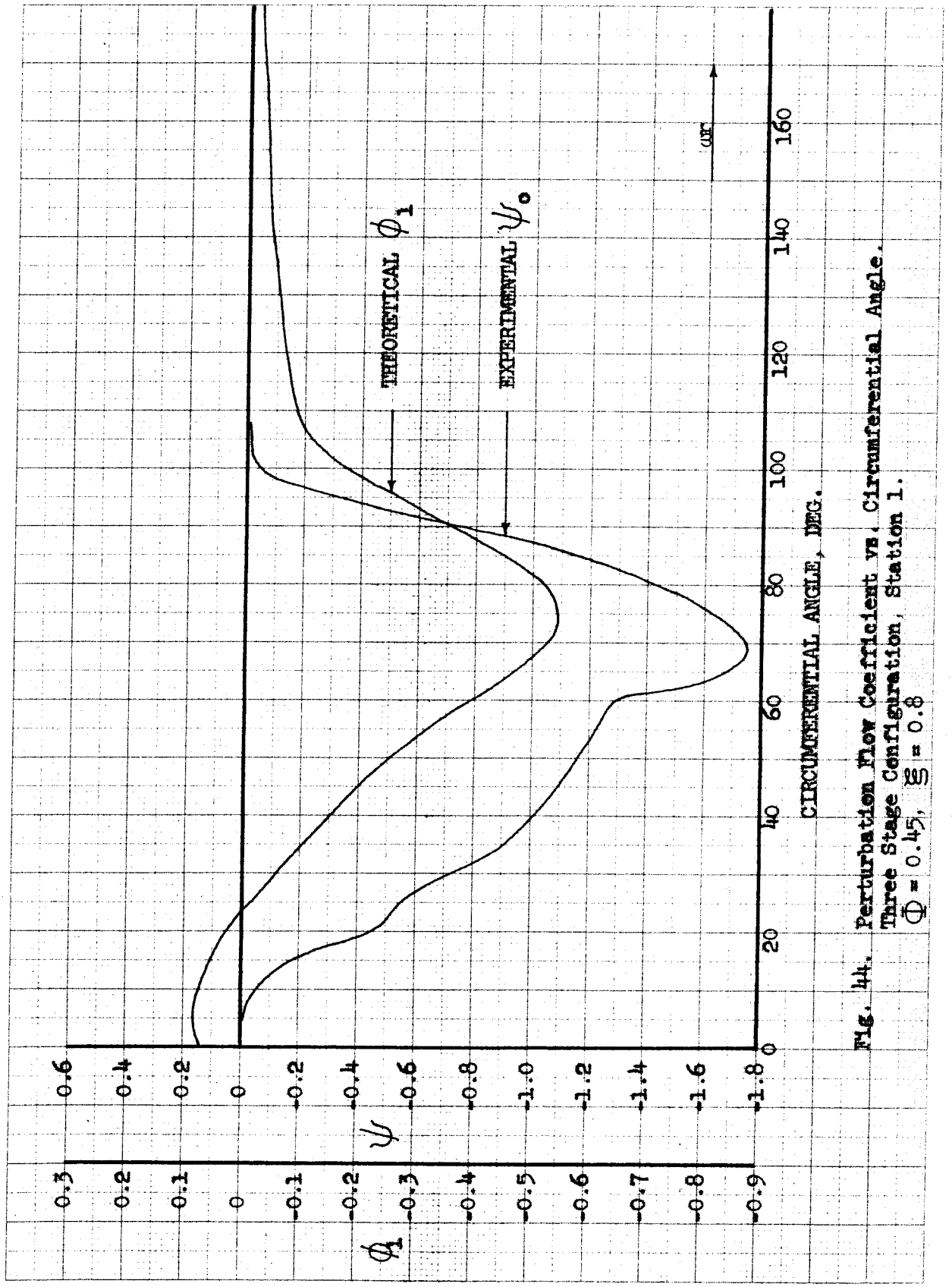

Fig. 44. Perturbation Flow Coefficient vs. Circumferential Angle.
Three Stage Configuration, Station 1.
$\Phi = 0.45$, $\frac{R}{S} = 0.8$

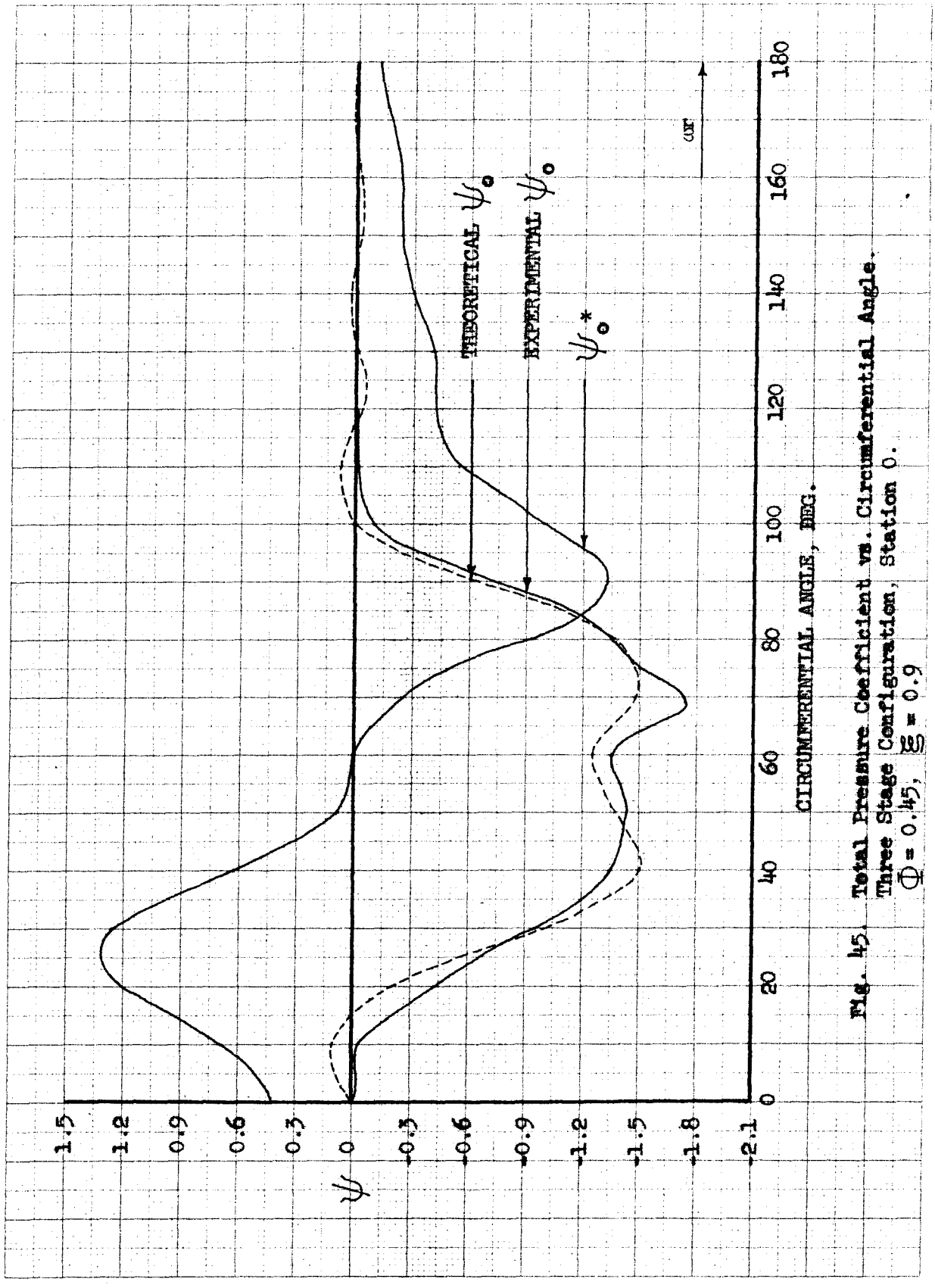

Fig. 45. Total Pressure Coefficient vs. Circumferential Angle.
Three Stage Configuration, Station 0.
$\Phi = 0.45$, $\Xi = 0.9$

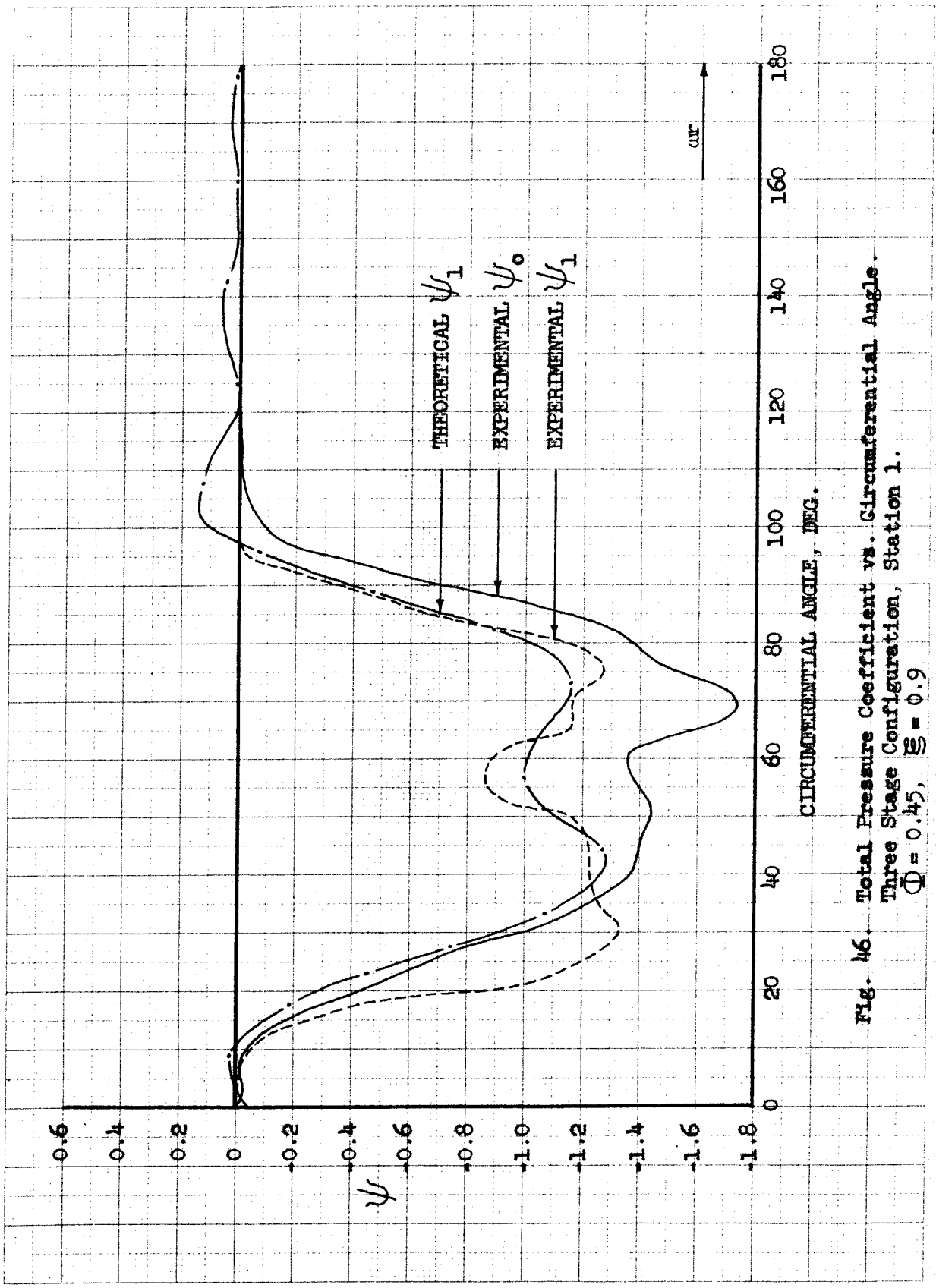

Fig. 46. Total Pressure Coefficient vs. Circumferential Angle.
Three Stage Configuration, Station 1.
$\Phi = 0.45$, $\overline{\omega} = 0.9$

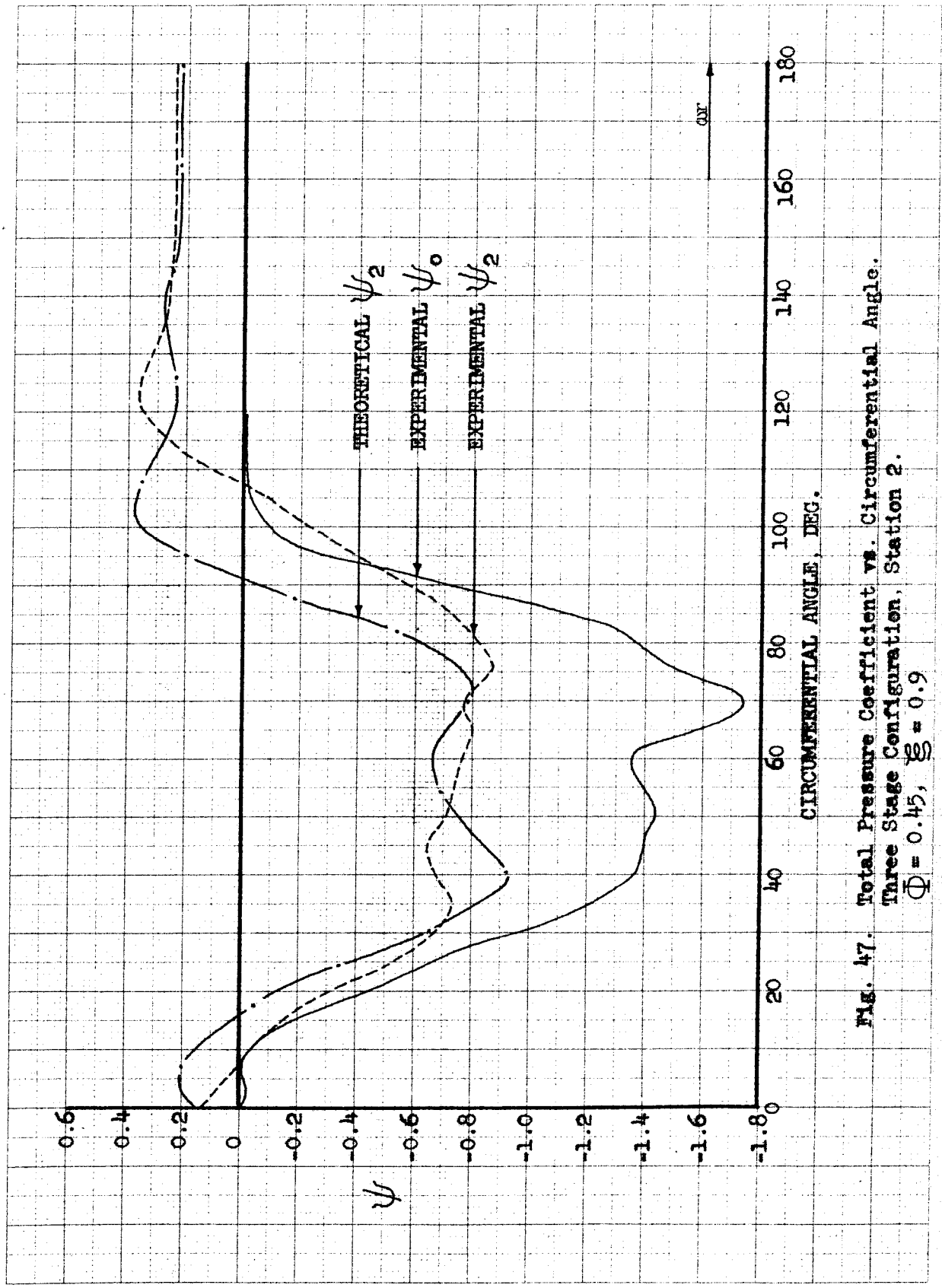

Fig. 47. Total Pressure Coefficient vs. Circumferential Angle.
Three Stage Configuration, Station 2.
$\Phi = 0.45$, $\overline{\text{gs}} = 0.9$

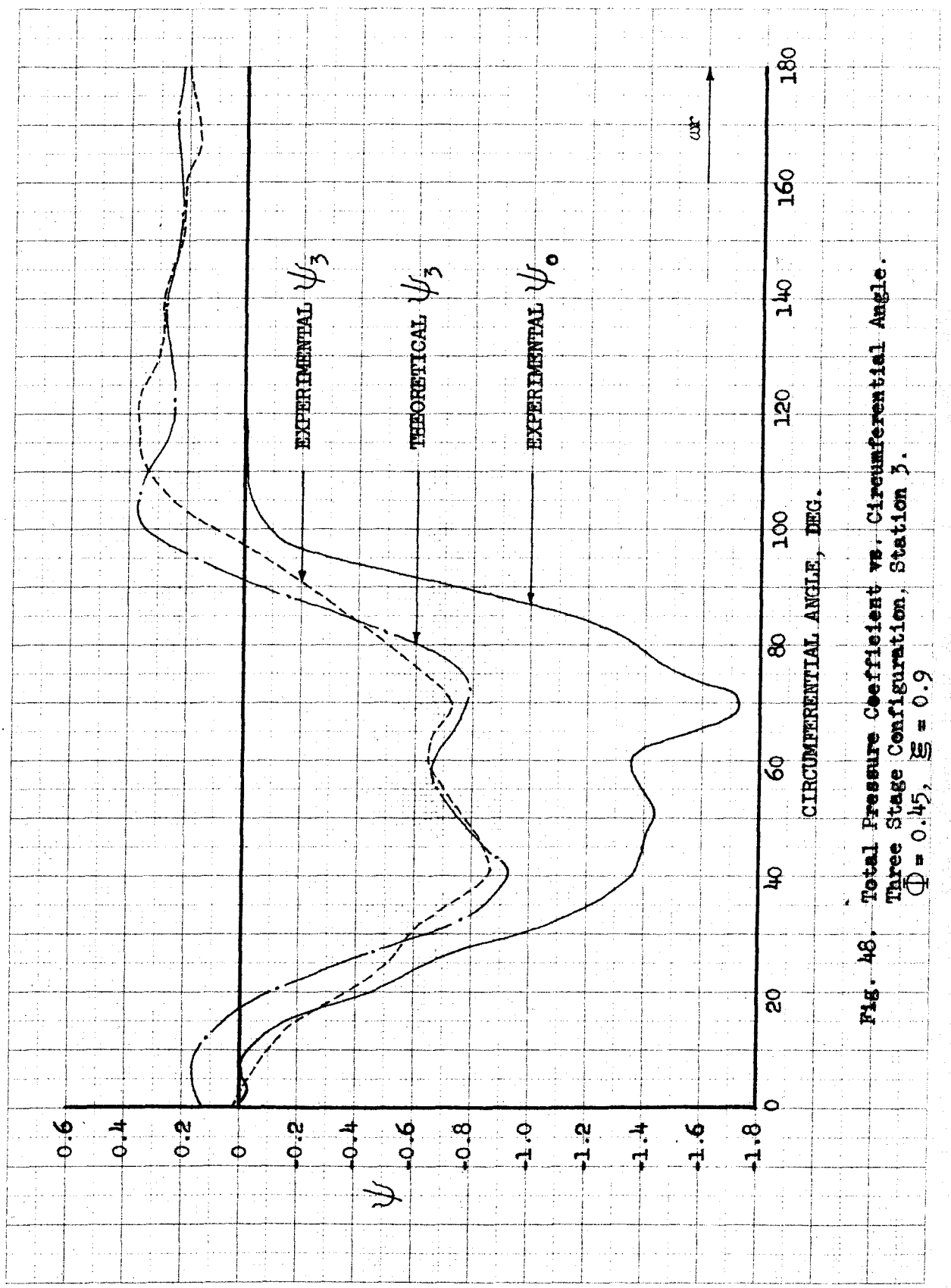

Fig. 48. Total Pressure Coefficient vs. Circumferential Angle.
Three Stage Configuration, Station 3.
$\Phi = 0.45$, $\overline{\omega} = 0.9$

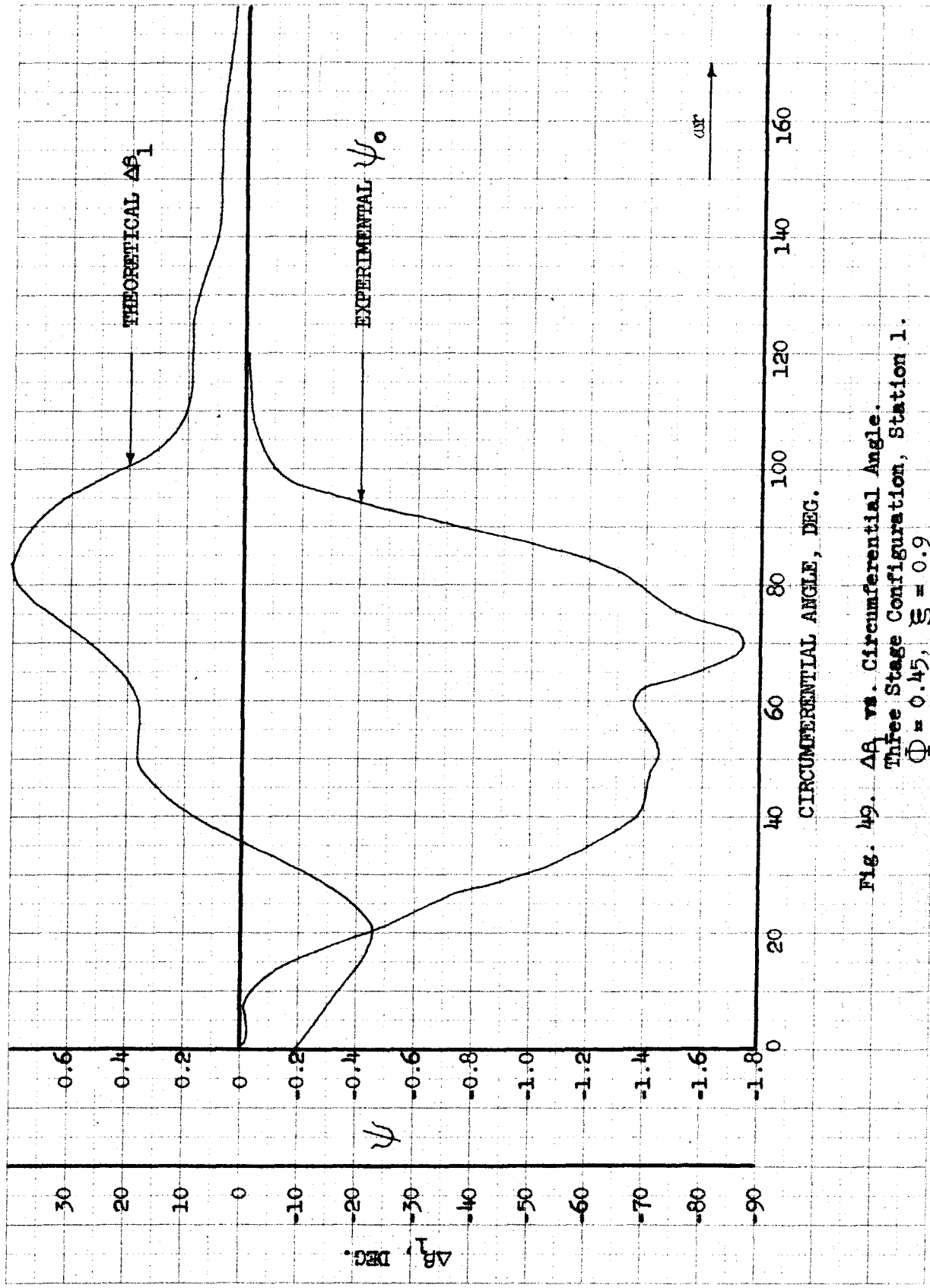

Fig. 49. $\Delta\beta_1$ vs. Circumferential Angle.
Three Stage Configuration, Station 1.
$\bar{\Phi} = 0.45$, $\bar{\Psi} = 0.9$

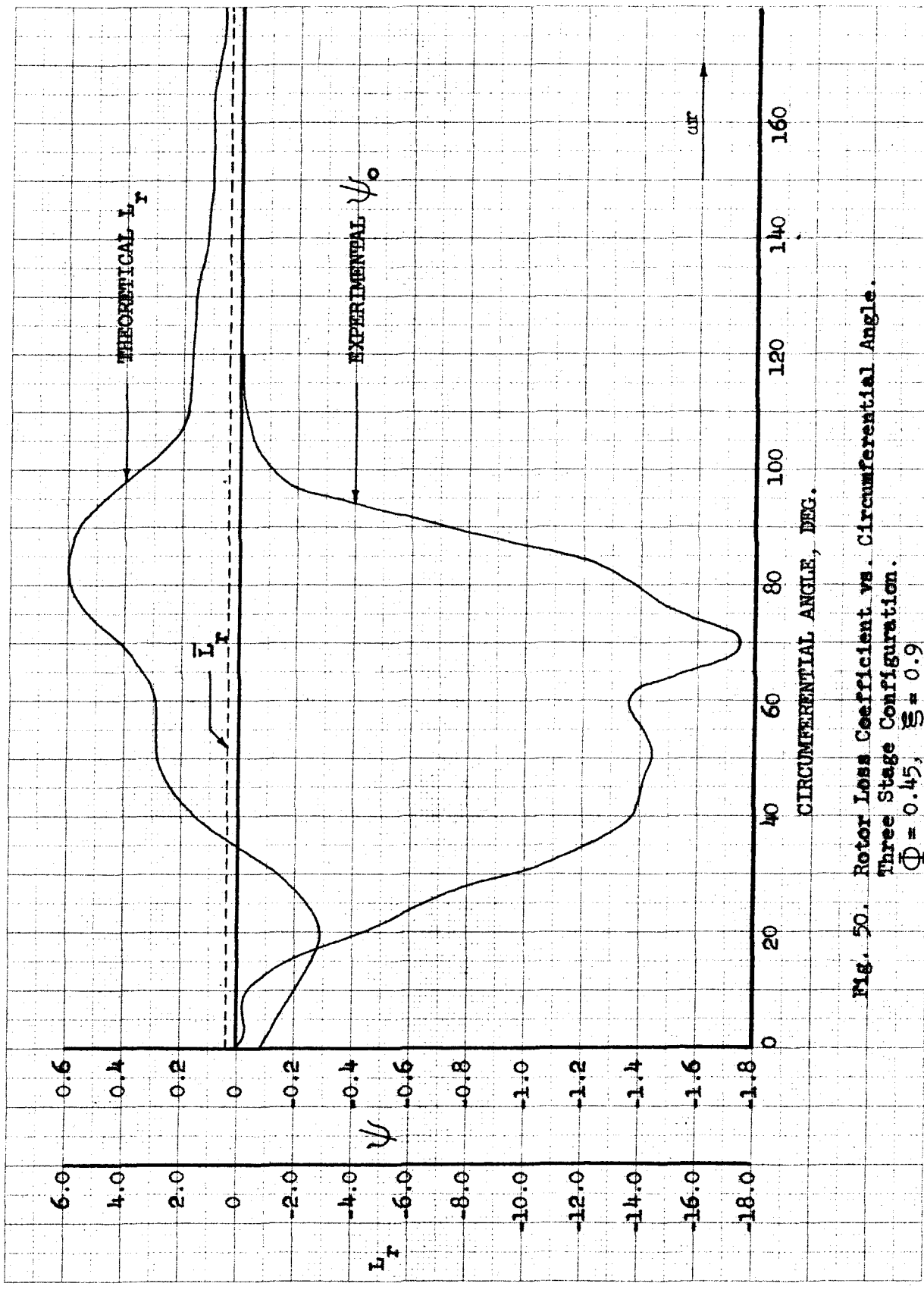

Fig. 50. Rotor Loss Coefficient vs. Circumferential Angle.
Three Stage Configuration.
$\Phi = 0.45$, $\overline{\psi} = 0.9$

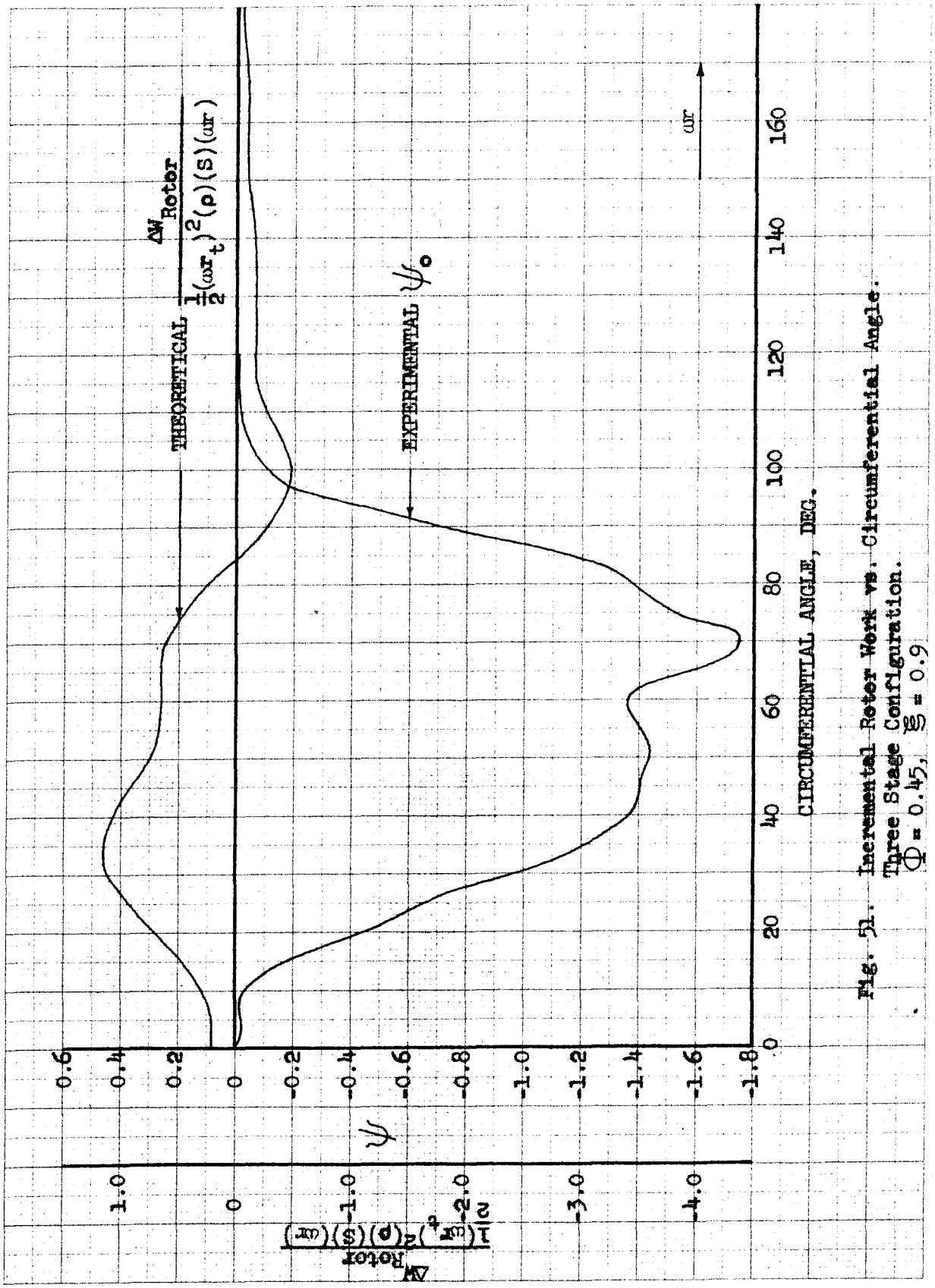

Fig. 51. Incremental Rotor Work vs. Circumferential Angle.
Three Stage Configuration.
$\Phi = 0.45$, $\overline{\omega} = 0.9$

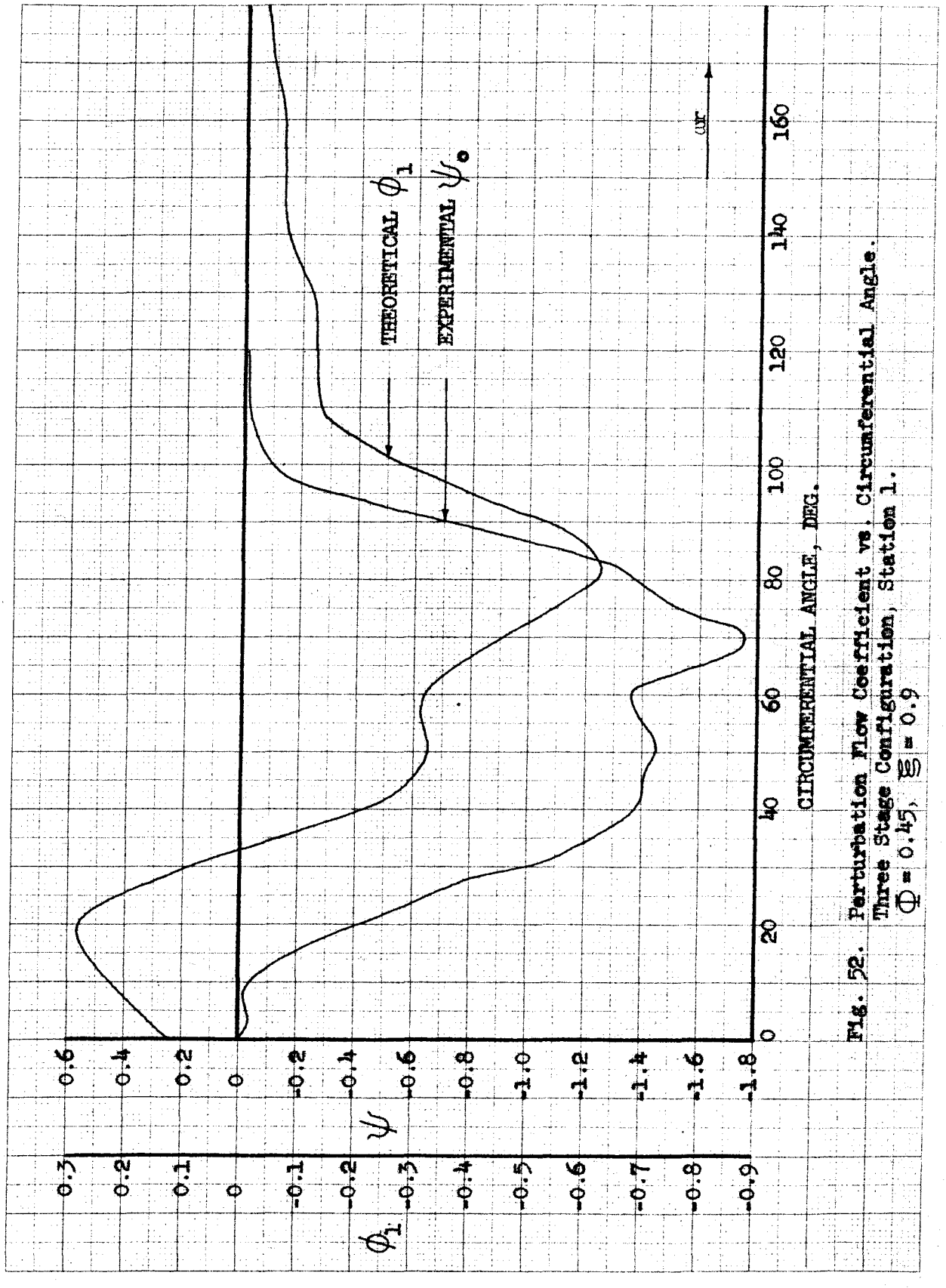

Fig. 52. Perturbation Flow Coefficient vs. Circumferential Angle.
Three Stage Configuration, Station 1.
$\Phi = 0.45$, $\overline{\omega} = 0.9$

APPENDIX

CONSTANTS IN THE MATCHING EQUATIONS

The constants listed below are required to obtain the analytical expressions listed in Part IV and are based on the mean flow parameters given in Part IV.

Expanded Single Stage, $\Phi = 0.35$, $\xi = 0.9$

$\lambda_1 = 1.082$	$\lambda_5 = 0.649$	$\lambda_9 = 1.931$	$\lambda_{15} = -0.106$
$\lambda_2 = 0$	$\lambda_6 = 0.200$	$\lambda_{10} = -0.282$	$\lambda_{16} = -0.298$
$\lambda_3 = 0$	$\lambda_7 = 0.500$	$\lambda_{11} = 0.174$	
$\lambda_4 = 0.287$	$\lambda_8 = -0.686$	$\lambda_{12} = 0.197$	

$L_r' = 1.0$

$\mu_1 = 0.570$	$\mu_5 = 1.796$	$\mu_9 = 0.915$	$\mu_{13} = -0.904$
$\mu_2 = 1.987$	$\mu_6 = 2.866$	$\mu_{10} = -1.843$	$\mu_{14} = 0.481$
$\mu_3 = 1.072$	$\mu_7 = 2.775$	$\mu_{11} = -2.954$	$\mu_{15} = -0.190$
$\mu_4 = 0.759$	$\mu_8 = 2.571$	$\mu_{12} = 2.663$	

$L_r' = 2.0$

$\mu_1 = 0.570$	$\mu_5 = 1.796$	$\mu_9 = 0.756$	$\mu_{13} = 0.284$
$\mu_2 = 1.987$	$\mu_6 = 2.707$	$\mu_{10} = -0.655$	$\mu_{14} = 0.308$
$\mu_3 = 1.072$	$\mu_7 = 3.963$	$\mu_{11} = -2.795$	$\mu_{15} = -0.072$
$\mu_4 = 0.759$	$\mu_8 = 2.571$	$\mu_{12} = 1.475$	

$L_r' = 3.0$

$\mu_1 = 0.570$	$\mu_5 = 1.796$	$\mu_9 = 0.596$	$\mu_{13} = 1.472$
$\mu_2 = 1.987$	$\mu_6 = 2.547$	$\mu_{10} = 0.533$	$\mu_{14} = 0.202$
$\mu_3 = 1.072$	$\mu_7 = 5.151$	$\mu_{11} = -2.635$	$\mu_{15} = 0.224$
$\mu_4 = 0.759$	$\mu_8 = 2.571$	$\mu_{12} = 0.287$	

$\nu_1 = 0.566$	$\nu_4 = 0.466$	$\nu_7 = 0$	$\nu_{10} = 0.434$
$\nu_2 = 1.072$	$\nu_5 = 0$	$\nu_8 = 0.608$	$\nu_{11} = 0$
$\nu_3 = 0.608$	$\nu_6 = 0$	$\nu_9 = 0.566$	$\nu_{12} = 0$

Normal Single Stage, $\Phi = 0.40$, $\xi = 0.8$

$\lambda_1 = 1.132$	$\lambda_5 = 0$	$\lambda_9 = 1.132$	$\lambda_{15} = 0$
$\lambda_2 = 0$	$\lambda_6 = 0$	$\lambda_{10} = -0.132$	$\lambda_{16} = 0$
$\lambda_3 = 0$	$\lambda_7 = 0$	$\lambda_{11} = 0$	
$\lambda_4 = 0.364$	$\lambda_8 = 0$	$\lambda_{12} = 0$	

$\mu_1 = 0.691$	$\mu_5 = 1.257$	$\mu_9 = 0.738$	$\mu_{13} = -0.197$
$\mu_2 = 1.899$	$\mu_6 = 2.230$	$\mu_{10} = -0.646$	$\mu_{14} = 0.342$
$\mu_3 = 1.072$	$\mu_7 = 1.868$	$\mu_{11} = -2.104$	$\mu_{15} = 0.009$
$\mu_4 = 0.746$	$\mu_8 = 2.000$	$\mu_{12} = 1.943$	$\mu_{18} = 0.106$
			$\mu_{19} = 0.499$

$\nu_1 = 0.566$	$\nu_4 = 0.466$	$\nu_7 = 0.350$	$\nu_{10} = 0.341$
$\nu_2 = 1.072$	$\nu_5 = 0.340$	$\nu_8 = 0.099$	$\nu_{11} = 0.058$
$\nu_3 = 0.607$	$\nu_6 = 0.093$	$\nu_9 = 0.999$	$\nu_{12} = 0.356$

Three-Stage Configuration, $\Phi = 0.4$, $\varepsilon = 0.8$

$\lambda_1 = 1.132$	$\lambda_5 = 0.679$	$\lambda_9 = 2.111$	$\lambda_{15} = -0.124$
$\lambda_2 = 0$	$\lambda_6 = 0.300$	$\lambda_{10} = -0.432$	$\lambda_{16} = -0.263$
$\lambda_3 = 0$	$\lambda_7 = 0.750$	$\lambda_{11} = 0.253$	
$\lambda_4 = 0.364$	$\lambda_8 = -0.977$	$\lambda_{12} = 0.236$	

$\mu_1 = 0.691$	$\mu_5 = 1.257$	$\mu_9 = 0.531$	$\mu_{13} = 0.333$
$\mu_2 = 1.899$	$\mu_6 = 2.023$	$\mu_{10} = -0.116$	$\mu_{14} = 0.209$
$\mu_3 = 1.072$	$\mu_7 = 2.398$	$\mu_{11} = -1.897$	$\mu_{15} = 0.095$
$\mu_4 = 0.746$	$\mu_8 = 2.000$	$\mu_{12} = 1.413$	$\mu_{18} = 0.065$
			$\mu_{19} = -0.615$

$\nu_1 = 0.566$	$\nu_4 = 0.466$	$\nu_7 = 0$	$\nu_{10} = 0.434$
$\nu_2 = 1.072$	$\nu_5 = 0$	$\nu_8 = 0.608$	$\nu_{11} = 0$
$\nu_3 = 0.607$	$\nu_6 = 0$	$\nu_9 = 0.566$	$\nu_{12} = 0$

Three-Stage Configuration, $\Phi = 0.4$, $\varepsilon = 0.9$

$\lambda_1 = 1.082$	$\lambda_5 = 0.649$	$\lambda_9 = 2.231$	$\lambda_{15} = -0.104$
$\lambda_2 = 0$	$\lambda_6 = 0.500$	$\lambda_{10} = -0.582$	$\lambda_{16} = -0.247$
$\lambda_3 = 0$	$\lambda_7 = 0.750$	$\lambda_{11} = 0.311$	
$\lambda_4 = 0.287$	$\lambda_8 = -0.936$	$\lambda_{12} = 0.206$	

$\mu_1 = 0.495$	$\mu_5 = 1.432$	$\mu_9 = 0.474$	$\mu_{13} = 0.347$
$\mu_2 = 1.727$	$\mu_6 = 2.102$	$\mu_{10} = -0.262$	$\mu_{14} = 0.216$
$\mu_3 = 0.933$	$\mu_7 = 2.963$	$\mu_{11} = -2.085$	$\mu_{15} = 0.017$
$\mu_4 = 0.723$	$\mu_8 = 2.252$	$\mu_{12} = 1.376$	$\mu_{18} = 0.074$
			$\mu_{19} = -0.638$

$\nu_1 = 0.622$ $\nu_4 = 0.404$ $\nu_7 = 0$ $\nu_{10} = 0.378$

$\nu_2 = 0.933$ $\nu_5 = 0$ $\nu_8 = 0.580$ $\nu_{11} = 0$

$\nu_3 = 0.580$ $\nu_6 = 0$ $\nu_9 = 0.622$ $\nu_{12} = 0$

Three-Stage Configuration, $\Phi = 0.45$, $\xi = 0.8$

$\lambda_1 = 1.132$ $\lambda_5 = 0.679$ $\lambda_9 = 2.111$ $\lambda_{15} = 0.124$

$\lambda_2 = 0$ $\lambda_6 = 0.300$ $\lambda_{10} = -0.432$ $\lambda_{16} = -0.263$

$\lambda_3 = 0$ $\lambda_7 = 0.750$ $\lambda_{11} = 0.253$

$\lambda_4 = 0.364$ $\lambda_8 = -0.997$ $\lambda_{12} = 0.236$

$\mu_1 = 0.601$ $\mu_5 = 1.041$ $\mu_9 = 0.380$ $\mu_{13} = 0.185$

$\mu_2 = 1.651$ $\mu_6 = 1.650$ $\mu_{10} = -0.135$ $\mu_{14} = 0.170$

$\mu_3 = 0.933$ $\mu_7 = 1.714$ $\mu_{11} = -1.487$ $\mu_{15} = 0.083$

$\mu_4 = 0.715$ $\mu_8 = 1.776$ $\mu_{12} = 1.530$ $\mu_{18} = 0.116$

$\mu_{19} = -0.580$

$\nu_1 = 0.631$ $\nu_4 = 0.425$ $\nu_7 = 0$ $\nu_{10} = 0.369$

$\nu_2 = 0.933$ $\nu_5 = 0$ $\nu_8 = 0.589$ $\nu_{11} = 0$

$\nu_3 = 0.589$ $\nu_6 = 0$ $\nu_9 = 0.631$ $\nu_{12} = 0$

Three-Stage Configuration, $\Phi = 0.45$, $\xi = 0.9$

$\lambda_1 = 1.082$ $\lambda_5 = 0.649$ $\lambda_9 = 2.031$ $\lambda_{15} = -0.121$

$\lambda_2 = 0$ $\lambda_6 = 0.300$ $\lambda_{10} = -0.382$ $\lambda_{16} = -0.264$

$\lambda_3 = 0$ $\lambda_7 = 0.750$ $\lambda_{11} = 0.262$

$\lambda_4 = 0.287$ $\lambda_8 = -0.936$ $\lambda_{12} = 0.248$

$\mu_1 = 0.427$ $\mu_4 = 0.701$ $\mu_7 = 2.393$ $\mu_{10} = 0.039$

$\mu_2 = 1.488$ $\mu_5 = 1.177$ $\mu_8 = 2.000$ $\mu_{11} = -1.581$

$\mu_3 = 0.781$ $\mu_6 = 1.686$ $\mu_9 = 0.284$ $\mu_{12} = 1.231$

$\mu_{13} = 0.470$ $\mu_{14} = 0.100$ $\mu_{15} = 0.103$ $\mu_{18} = 0.085$

$\mu_{19} = -0.678$

$\nu_1 = 0.712$ $\nu_4 = 0.384$ $\nu_7 = 0$ $\nu_{10} = 0.288$

$\nu_2 = 0.781$ $\nu_5 = 0$ $\nu_8 = 0.556$ $\nu_{11} = 0$

$\nu_3 = 0.556$ $\nu_6 = 0$ $\nu_9 = 0.712$ $\nu_{12} = 0$